INTELLIGENT REAL-TIME ENVIRONMENT AND PROCESS ADAPTIVE RADIO FREQUENCY FRONT-ENDS FOR ULTRA LOW POWER APPLICATIONS

A Thesis
Presented to
The Academic Faculty

by

Debashis Banerjee

In Partial Fulfillment
of the Requirements for the Degree
Doctor of Philosophy in the
School of Electrical and Computer Engineering

Georgia Institute of Technology
Aug 2015

INTELLIGENT REAL-TIME ENVIRONMENT AND PROCESS ADAPTIVE RADIO FREQUENCY FRONT-ENDS FOR ULTRA LOW POWER APPLICATIONS

Approved by:

Professor Abhijit Chatterjee, Advisor
School of Electrical and Computer Engineering
Georgia Institute of Technology

Professor Linda Milor
School of Electrical and Computer Engineering
Georgia Institute of Technology

Professor Hua Wang
School of Electrical and Computer Engineering
Georgia Institute of Technology

Professor Satish Kumar
The George W. Woodruff School of Mechanical Engineering
Georgia Institute of Technology

Professor John D. Cressler
School of Electrical and Computer Engineering
Georgia Institute of Technology

Date Approved: 23 April 2015

To my parents, my brother and my wife.

For always being there for me.

ACKNOWLEDGEMENTS

A PhD is a journey, a long and hard one, but yet so enjoyable and fulfilling. Such a journey is worth embarking on not only for the academic enrichment and self-development it brings to ones life but also for the guidance, friendship and company of teachers and friends. I have been extremely fortunate to have met many such individuals over the course of this journey. First and foremost I would like to thank my advisor Prof. Abhijit Chatterjee who has over the past few years guided, taught and helped me. His technical expertise and constant drive and excitement about the cutting edge of research inspired and will continue to inspire me. Additionally he has been a role model and a friend to his students and I hope I can imbibe some of his generosity, understanding, kindness in my personal life.

I would also like to thank my committee members Prof. Hua Wang, Prof. John D. Cressler, Prof. Linda Milor and Prof. Satish Kumar. Georgia Tech would not be the place it is without the many excellent faculty and I would like to thank all the faculty members whom I have been lucky to learn from.

I would like to mention all my friends at Georgia Tech and Atlanta who made these years such fun. A special thanks to Shreyas Sen & Shyam Devarakond for helping me immensely in my research. I owe a lot to the countless hours of discussion we had together. I am indebted to Debesh Bhatta for teaching me how to drive. A big thanks to all the members of my lab including Sehun Kook, Jayaram Natarajan, Aritra Banerjee, Sabyasachi Deyati, Suvadeep Banerjee, Nicholas Zhou, Thomas Moon, Xian Wang, Barry Muldrey & Joshua Wells for their help and co-operation. Life would have been a lot less fun without my friends in Atlanta: Ayan Chakraborty, Payel Chakraborty, Akash, Ananda Barua, Arindam Khan, Abhishek Banerjee and

Anshuman Goswami. An acknowledgement would be incomplete without mentioning the immense contribution of my family: my parents Ranu and Gautam Banerjee, my brother Debayan and my wife Nairwita. My parents sacrificed a lot to provide me a cushion from the harsh difficulties of life. Through my successes they relive the opportunities they were not given. I owe everything to them. My brother has been a friend to me and remains someone I can always talk freely if I need to. And last but not the least I am grateful to my wife Nairwita for being the perfect partner. When the going gets tough I know I can count on you. From technical discussions to actual drafting of this thesis and my publications, she has helped me in every possible way. I am proud to have you by my side.

TABLE OF CONTENTS

LIST OF TABLES

LIST OF FIGURES

SUMMARY

Modern communication systems are increasingly demanding better power vs. performance from the radio front-ends in order to meet the increasing throughput and battery-life demands of a growing consumer base. Today's RF transceivers must be designed to operate at high data rates over adverse channel conditions with ultra-low power consumption. To save energy per transmitted bit, modern wireless systems are designed to adapt to wireless channel quality by adjusting data transmission rates, adjusting the output power of the RF power amplifier in wireless transmitter and by automatic gain compensation in RF receiver subsystems. However, the wireless transceiver still consumes more power than necessary for a specified end-to-end bit-error-rate (BER) when the wireless channel is not the worst case channel corresponding to the date rate at which the transceiver is operating.

Previous work has focused on single-input single-output (SISO) communication systems for low-power adaptation. However a key technology that enables current systems to meet the stringent demands of the latest communication standards is multiple input multiple output (MIMO) communication. While MIMO systems provide higher bandwidth and increased range of operation, due to increased number of transceiver chains they must also be designed for low energy consumption across diverse operating conditions. However in current low-power adaptation front-end the nature of the application which is using the front-end to transmit/receive has no bearing on the adaptation strategy. Different applications have different throughput priorities when it comes to data reception/transmission. In this thesis, a channel-adaptive MIMO RF

front-end that can operate in multiple low-power modes depending upon the throughput and energy-per-bit needs of different end-user applications is demonstrated.

A key issue in devising such an adaptation strategy is that the control logic thus devised must depend upon the performance of the device under real process perturbations. This becomes especially important at lower technology nodes at which the front-end sub-blocks exhibit significant variation in key specifications (like gain, linearity, noise-figure etc.). It is almost impossible to simulate all possible process corners to provide an optimal control law for each process perturbed device. In this thesis, an elegant solution to this problem is provided by allowing the device to tailor the nominal control law during the intitial operational period of the device depending on the process corner it is at.

Previous research has proposed lookup table (LUT) based controller which suffers from the disadvantage of requiring extensive design phase optimization compounded even more by the presence of process variability. Moreover, the table must be m-dimensional, m being the dimensionality of channels. A better approach to the problem is to derive analytical expressions of the optimum performance parameters of the front-end in terms of the channel conditions. This would eliminate any off-line design phase optimization process. This work demonstrates that this becomes especially feasible in presence of front-end blocks whose key performance parameters are independently tunable. However, in general, deducing analytical expressions of the QoS metric (EVM or BER) in terms of the channel parameters and the front-end configuration may become computationally intractable. One way to alleviate this difficulty is to use a control logic which can mimic the decision making capabilities of a human being through a set of general operational rules. This research proposes a solution to this problem by designing fuzzy-logic based control systems which track the changes in channel conditions without requiring extensive characterization of the system.

CHAPTER 1

INTRODUCTION

The objective of the proposed research is the design of process tolerant radio frequency (RF) wireless communication systems which can adapt to changes in its environment to operate at the minimum possible power consumption levels while maintaining the minimum quality of service (QoS) desired for effective communication even in the presence of significant process variation.

In the past few years the amount of data consumed has increased exponentially due to connected business needs, social media, high fidelity video and audio transmission, cloud computing and storage. The rapid growth in the demand for connectivity has driven the development of communication infrastructure and equipments to make mobile connectivity ubiquitous, easy and cost-effective. Thus mobile communication devices having become an integral part of daily life. Two key desirable aspects in any such design are a small ergonomically attractive physical profile and the ability to transmit, receive and process data for a significantly long time between two re-charges of the battery. However, the requirement of having small physical dimensions imposes a restriction on the charge capacity of the battery. While the charge capacities of batteries have improved over the years, they have not been able to keep pace with the energy requirements of the modern day communication device. Thus a key emphasis has been there on the design of ultra-low power systems for wireless communication. Moreover with shrinking transistor geometries the performance of the designed circuits and systems vary widely from chip-to-chip due to uncertainties in the process parameters which are difficult to control. Thus the designed integrated circuits should be able to operate at low-power consumption levels with desired performance in the

presence of significant process variation.

Traditionally wireless systems have been designed to achieve minimum quality-of-service (QoS) for worst case channel conditions. When the channel is not at its worst case condition then the power consumption is more than required for achieving the minimum QoS. Because the worst case channel condition is not statistically prevalent the average power consumption of the system is significantly higher than the minimum possible average power consumption across channel conditions. Adaptive systems seek to solve this problem by dynamically modulating the performance of the system(through built-in control knobs or "tuning knobs") in real-time using a look-up table (LUT) based feedback loop to operate at the minimum QoS and the minimum power consumption possible across all channel conditions. Such adaptation can be performed in multiple different modes depending upon the throughput and energy-per-bit requirements of the device. Moreover, the system can learn the optimum configurations on-the-fly for the entire gamut of channel conditions it encounters. Since this is done on a per-chip basis the problem of process-resilient adaptation is resolved. All the above methods make use of look-up table (LUT) to store the optimum configurations. This research shows that, alternatively, with a proper understanding of the effect of different sub-circuit parameters across channel conditions on the QoS metric, a fuzzy logic or analytical expression based feedback systems can be formulated to achieve channel-adaptive low-power operation.

1.1 Origin and History of the problem

Since the invention and first successful demonstration of the integrated circuit by Jack Kilby in 1958, a recurring goal in the development of the semiconductor industry has been to shrink the physical dimensions of the transistors and passive devices. Shrinking transistors sizes have led the industry through small-scale integration (SSI),

medium-scale integration (MSI), large-scale integration(LSI), very large scale integration (VLSI) into the age of ultra-large scale integration (ULSI). The industry leaders are currently commercially producing chips at 28 nm, 20 nm & 14 nm with 10 nm chips in the pipeline. Such advances in circuit design and fabrication have been fuelled by rising demands of electronic consumer goods like laptops, phones and tablets. Each of these portable devices have radio-frequency (RF) front-ends for wireless communication and are powered by a battery. Analog and digital circuits designed at such small process nodes have their benefits in terms of more functionality & higher frequency of operation. However the power consumption per unit area has gone up significantly for the lower process nodes. Hence a key area of research has been in that of low-power RF front-end design. A major downside of having smaller process geometries is the effect of process variation becomes more apparent at the lower technology nodes. Thus circuits deviate from their expected or nominal performance by a larger degree at lower technology nodes due to the relatively larger uncertainties in the manufacturing process. Thus modern circuits must be designed to be process-variation tolerant.

1.2 Traditional static RF front-end design

Traditional RF front-ends are designed in a top-down fashion. In this design paradigm, the performance specifications of the front-end for the worst case channel specifications are first derived. Thereafter the individual sub-block specifications are apportioned from the front-end specifications. A few key sub-blocks of the modern front-end are shown in Figure 1. While deriving the sub-block specifications it is ensured that sufficient margin is kept to account for process, voltage and temperature (PVT) variations. The sub-blocks have little or no adaptivity built into them and as a result the entire system consumes the same power for all channel conditions.

Current systems try to maximize the throughput for a given channel by changing

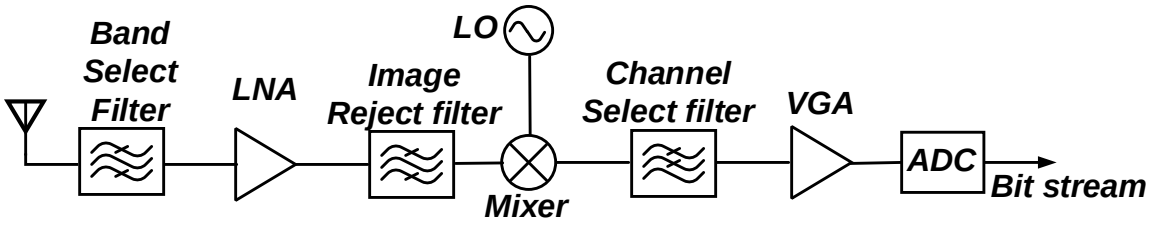

Figure 1: Simplified diagram of basic receiver front-end.

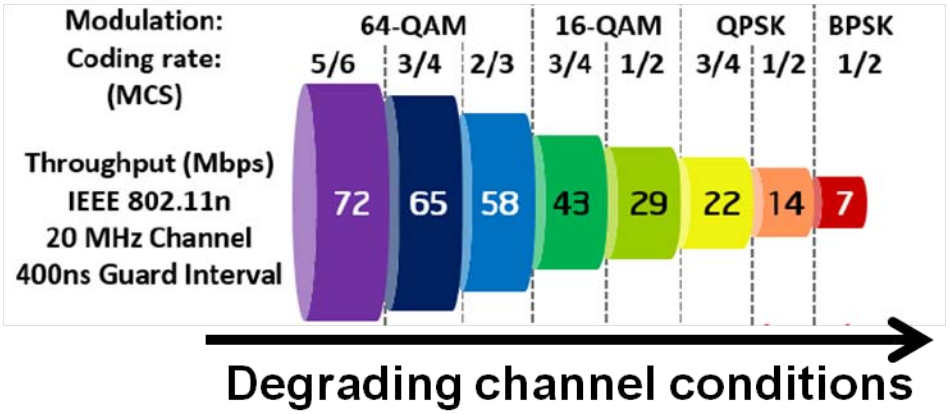

Figure 2: Traditional modulation and coding rate switching in 802.11n systems.

the modulation and coding rate as shown in Figure 2. While this does lead to a more optimized energy-per-bit such adaptation is coarse and there exists significant opportunity even within a fixed modulation and coding rate setting to trade-off power versus performance. Such front-end designs (with no adaptatation capability in the front-end blocks) can be referred to as *static* front-end designs.

RF front-ends can be classified broadly into two categories: single-input-single-output(SISO) and multiple-input-multiple-output(MIMO). SISO systems have a single RF front-end chain to up-convert/down-convert, amplify and digitize the signal. MIMO systems on the other hand accomplish the same task using multiple RF chains. While SISO has the advantage of having lower power consumption, MIMO can provide both extended coverage and higher data rates depending on the channel conditions and mode of use.

1.3 Adaptive RF front-end design

The discussion in Section 1.2 clearly points out an opportunity to reduce the power consumption when the channel is not at the worst case condition. To enable such power savings, the sub-blocks of the RF front-end (like LNA, mixer, PA , ADC word size etc.) must be designed to accommodate tuning knobs (for e.g. bias voltage,current etc.) which would allow them to trade-off their performance for power savings. The propagation of a transmitted signal through the channel can be described through the equation:

$$Y = HX + N + I \tag{1}$$

Here X and Y are transmitted and received signals. In our work they are modelled as OFDM waveforms. H encapsulates the path loss caused by the channel between the transmitter and the receiver. It can be subdivided into two major effects:

a) Propagation or Path Loss: This can be approximated by the equation $k.d^{-n}$ where k is a constant of proportionality, d is distance between the two antennas and n is an empirical constant which varies between 2.5 to 3 depending on atmospheric conditions.

b) Fading: Fading is caused by the transmitted signal arriving at the receiver using multiple paths(and hence having different delays and attenuations) and adding up. For urban environments with no direct line of sight path between the transmitter and receiver the strength of received signal can be approximated by a Rayleigh distribution.

N represents the noise floor of the channel and can be represented by additive white gaussian noise (AWGN). I represents the interferers present in the channel. Interferers can be of many types for e.g. adjacent OFDM channels or narrowband signals. In our discussions we will assume they are adjacent OFDM channels. The system must be able to sense when to adapt and how much to change the tuning knobs to achieve

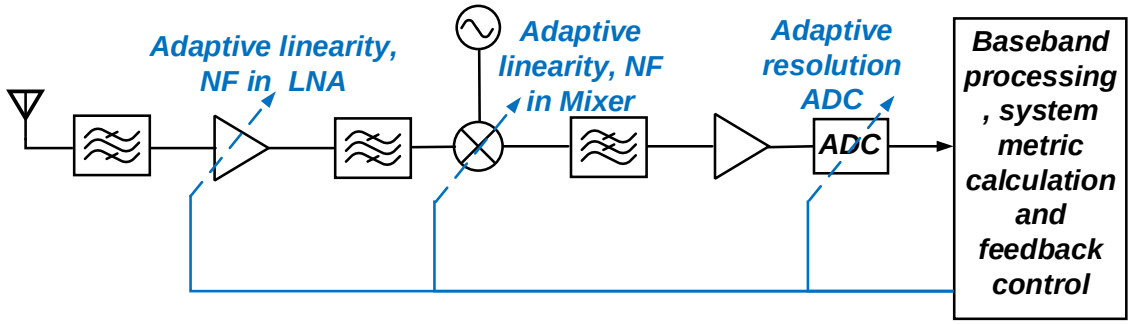

Figure 3: Illustration of possible RF receiver adaptation architecture

minimum required QoS for any given channel. This can be achieved through directly sensing the channel parameters (like signal and interferer strength) or by observing a system level metric which measures the quality of the received signal. In either case a feedback loop (as shown in Figure 3 can use the system level metric or the channel parameters to set the appropriate pre-configured settings for the tuning knobs. The pre-configured settings are calculated during the design phase and may be stored in an LUT on-chip.

Thus from the above discussion the key requirements for designing an adaptive transceiver front-end can be illustrated in Figure 4. As shown, an adaptive system requires sensors to determine the channel condition and the quality of the received signal. The sensors may be implemented in baseband or as additional sensors on the front-end. Similarly, the adaptive front-end requires sub-blocks like LNA, Mixer and ADC to be capable of trading-off performance versus power. the third requirement for the design of the system is to devise a strategy to change the front-end performance as a function of channel conditions. The simplest implementation of this can be the deployment of an on-chip LUT which contains the set of optimized front-end tuning knob values as a function of different channel conditions.

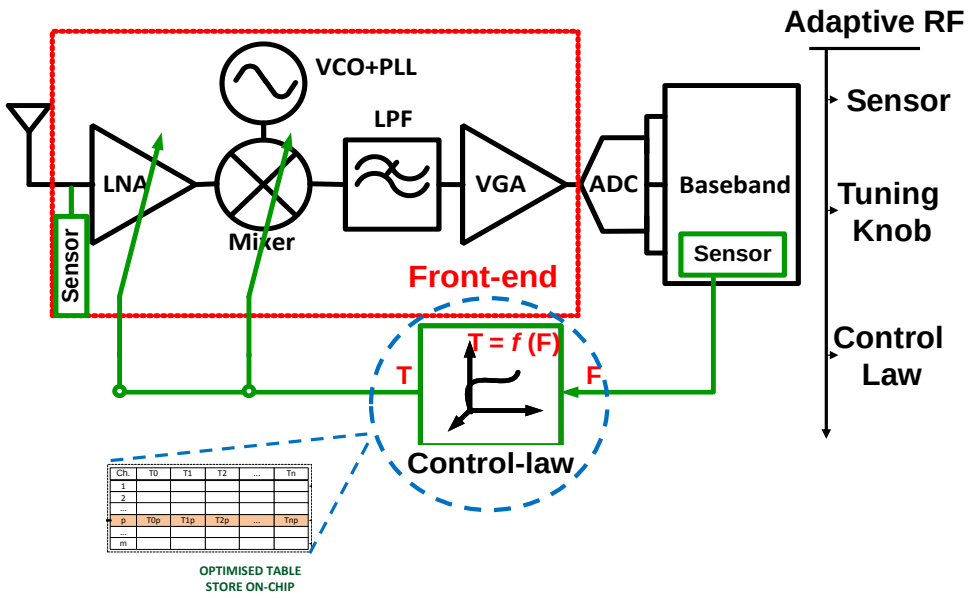

Figure 4: Key requirements for designing adaptive system

1.4 Need for use-aware adaptive MIMO front-end design

In prior work, adaptive systems have been proposed to adapt to channel conditions while achieving lowest power consumption. Thus the goal for the optimization problem traditionally has been to minimize the power consumption of the system. However depending upon the applications accessing the front-end to transmit and receive data, the optimization goal may be different. For example in certain real-time applications like video/audio streaming the data throughput may be of primary importance. Once a minimum data throughput is achieved, any additional signal-to-noise ratio (SNR) may be traded off for power savings. However in certain other applications like (background downloads and uploads), throughput may not be of primary importance. Here the emphasis is to achieve the minimum energy-per-bit. Thus while the first case corresponds to minimizing power consumption, in the latter case the goal is to minimize the energy-per-bit. So, it can be seen that depending on the nature of application the optimum tuning knob configuration for a particular channel would be different. Such use-aware low-power operation is specially critical for MIMO front-ends which due

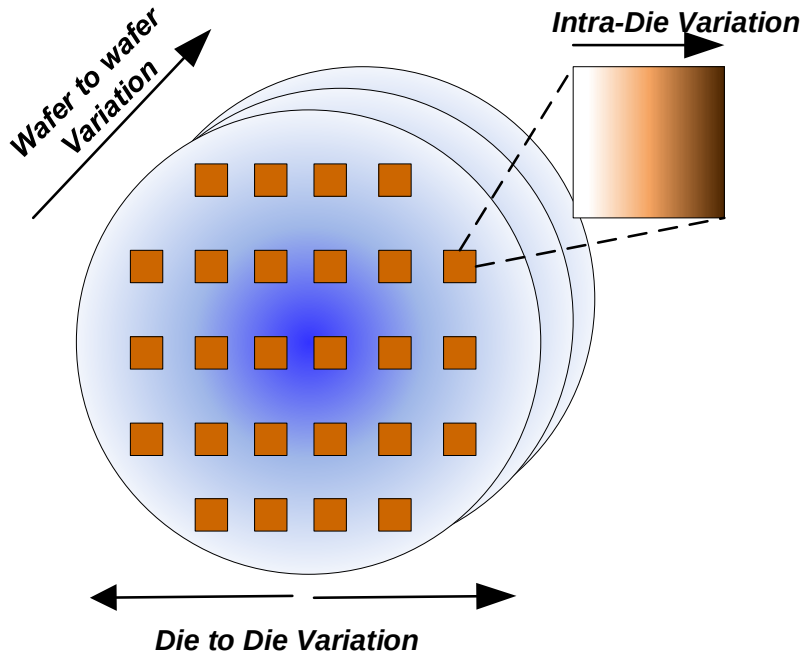

Figure 5: Illustration of inter-chip and intra-chip process variation

to the presence of multiple RF chains for a single transceiver consume significantly higher power than a SISO front-end. A use-aware MIMO front-end would provide the flexibility of choosing to minimize energy-per-bit whenever possible while reaping the benfits of additional throughput and resiliency provided by the MIMO system.

1.5 Need for process-resilient self-learning front-end design

Due to process scaling the parameter variations in the manufactured chips become significantly large at nanometer nodes. This leads to significant variations in front-end performance from one chip to the other. These variations can be inter-chip (wafer-to-wafer and die-to-die on the same wafer) and intra-chip as shown in Figure 5. This poses a significant challenge to RF front-end design in general and adaptive RF front-end in particular. Firstly, due to performance deviations a certain fraction of the manufactured chips do not lie within the desired specification bounds. This leads to significant yield loss, more so at the lowest process nodes. The yield loss

in turn translates to reduced profitability and thus is extremely undesirable. These variations are even more critical in adaptive system since they operate at the boundary of acceptable operation and leave little or no margin for error. Thus for any such adaptive RF front-end the reconfiguration settings across channel conditions must be a function of the process corner it is at. Thus this requires multitude of pre-computed LUTs, one for each process corner. It also requires the test phase detection of the correct process corner a chip is at. Both of these are significant challenges. However, if a system can learn its performance characteristics across channel and tuning knob space on-the-fly then a customized adaptation law can be devised which is immune to process variations, ageing etc. Such a system can learn their entire adaptation strategy on-line by generating maps of the power consumption and QoS (or EVM) versus the different configuration modes and channel conditions during real-time operation. The system can use these maps to incrementally build a LUT of optimum configuration settings across the entire gamut of channel conditions. Such architecture would automatically eliminate the problem of devising control laws under process variability.

1.6 Alternate control strategies for adaptive front-end design

Previous research has proposed LUT based controller which suffers from the disadvantage of requiring extensive characterization of the QoS across channel and tuning knob space. Such a control strategy has been demonstrated to work adequately when the channel conditions can be arranged in a linear fashion fron "Good" channel to "Bad" channel. This is only possible for a uni-dimensional channel. However channel conditions are a multi-dimensional space , for e.g. having signal strength(or equivalently signal attenuation) and interferer strength as channel parameters. A better approach to the problem is to try to derive analytical expressions of the optimum performance parameters of the front-end in terms of the channel conditions for the

minimum QoS. These relationships could be used to directly predict the optimum settings once the channel is estimated resulting in a feed-forward adaptation system. This is especially feasible if the key specifications of the front-end(linearity, gain, noise-figure) can be controlled independent to one another. However in general deducing such analytical expressions may become computationally intractable. One way to alleviate this difficulty is to use a control logic which can mimic the decision making capabilities of a human being through a set of general operational rules. In this research we try to solve this problem by designing fuzzy-logic based control systems which track the changes in channel conditions without requiring extensive QoS characterization of the system across tuning knob space.

1.7 Prior Work

1.7.1 Traditional low-power RF front-end design techniques

Traditional low-power front-end design approaches can be broadly classified into circuit level & system level techniques.

Circuit level techniques: Several circuit level techniques have been proposed to achieve low-power in the sub-blocks of the RF front-end, for e.g. in LNA, PA, ADC etc. In prior literature [2] active and passive g-m boosting has been used to achieve low NF and large gain, both of which are stable across process variations. In [3] an active resistor is used to achieve the desired linearity at low-power consumption. Similarly in PAs several circuit level techniques have been devised to achieve high efficiency even while attaining the desired gain, linearity etc. Similarly other analog/RF systems [4, 5] have been studied extensively for low-power performance while operating satisfactorily in the worst case channel conditions and for the worst case process variability and thermal effects. In PAs the supply voltage can be changed to track the envelope of the output signal, thereby achieving high efficiency [6]. This can

be done in one of three ways: slow-tracking, envelope modulation and polar tracking. In slow-tracking [7] PAs the supply is kept just above the maxiumum amplitude of the PA output envelope. In envelope modulation [8, 9, 10] the supply voltage tracks the PA output envelope providing optimum power consumption. Polar tracking [11] is an alternate way to achieve envelope modulation in which the amplitude and phase of the output waveform is first separated. The phase information is used by the oscillator to do produce a phase modulated waveform. The phase modulated waveform passes through a non-linear amplifier whose supply is modulated by the envelope information. Thus the output of the amplifier has both phase and amplitude modulation.

System level techniques: While circuit level techniques can significantly reduce power consumption, in many cases system level techniques can be equally or more effective. For example output power of a power amplifier is varied according to the distance between the communicating transmitter and receiver. The output power control information can be used at a system level to reduce the power consumption of the PA when the average output power is not at its peak [12, 13, 14]. Similarly in case of sigma-delta ADC proposed in [15], the order of the loop filter is varied depending upon the signal to interferer ratio. In this ADC when the signal to interferer ratio rises the dynamic range requirements can be relaxed to operate at a reduced power consumption.

1.7.2 Low-power multiple input multiple output (MIMO) transceiver systems

In todays harsh radio propagation environments providing high bit rates (for data-hungry applications) and extended range of mobile signal coverage has become increasingly challenging. Higher data rates demand higher power or larger bandwidth, both of which are at a premium in modern systems. Since the cell size determines the number of base stations required to cover a target population or area, the range of

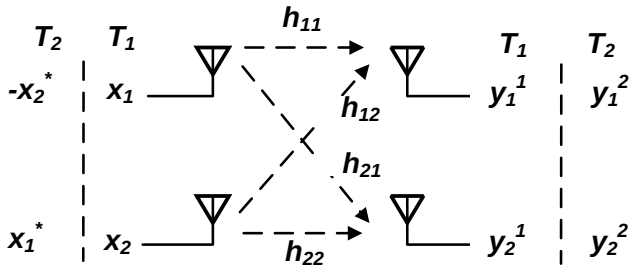

Figure 6: Illustration of Spatial Diversity mode of operation

coverage is intricately tied to the economics of network deployment. A key technology that enables current systems to meet the stringent demands of the latest communication standards is multiple input multiple output (MIMO) communication.

MIMO systems can transmit/receive multiple parallel streams of data within the same channel bandwidth. With the same RF front-end a MIMO system could be configured to operate in spatial multiplexing(SM)[16] mode for greater data rates or in spatial diversity(SD) modes for greater reliability and coverage[17].

Spatial Diversity (SD) Mode: In this mode the goal is to combine the SNRs from multiple MIMO chains (front-end+antenna) to achieve a higher effective SNR for the received signal. This leads to a more robust communication system which can operate over more degraded channel conditions as compared to a SISO system. The operation of SD mode is demonstrated in Figure 6. In this thesis SD mode combines signals using Alamouti's technique [17]. To explain how the system works let us consider two time slots T_1 and T_2 in which the system is transmitting and receiving symbols. In slot T_1 the system transmits symbols x_1 and x_2 from antenna 1 and 2 respectively. In time slot T_2 the system transmits symbols $-x_2^*$ and x_1^* from antennas 1 and 2 respectively. The channel can be modelled as a 2x2 matrix (for this 2x2 system) which encompasses all path loss and fading effects.

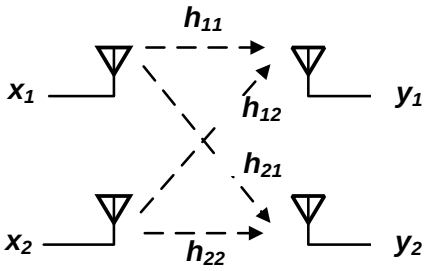

Figure 7: Illustration of Spatial Multiplexing mode of operation

$$Channel\ matrix = \begin{bmatrix} h_{11} & h_{12} \\ h_{21} & h_{22} \end{bmatrix} \tag{2}$$

The symbols received in time slot I by antenna J is denoted as y_J^I in Figure 6. It has been shown that the best way to combine the two received symbols in two time slots is as follows:

$$\begin{bmatrix} \hat{x_1} \\ \hat{x_2^*} \end{bmatrix} = (H^H H)^{-1} H^H \begin{bmatrix} y_1^1 \\ y_2^2 \\ y_1^{2*} \\ y_2^{2*} \end{bmatrix} \tag{3}$$

where H is defined as follows:

$$H = \begin{bmatrix} h_{11} & h_{12} \\ h_{21} & h_{22} \\ h_{12}^* & -h_{11}^* \\ h_{21}^* & -h_{22}^* \end{bmatrix} \tag{4}$$

Thus SD mode allows for communication over degraded channels while providing the same throughput as a SISO system.

Spatial Multiplexing (SM) Mode: In this mode the 2x2 MIMO system tries behave as two parallel chains of data. This is shown in Figure 7. The transmitted

symbols can be estimated using a zero-forcing equalizer as follows:

$$\begin{bmatrix} \hat{x_1} \\ \hat{x_2} \end{bmatrix} = (H^H H)^{-1} H^H \begin{bmatrix} y_1 \\ y_2 \end{bmatrix} \tag{5}$$

where

$$H = \begin{bmatrix} h_{11} & h_{12} \\ h_{21} & h_{22} \end{bmatrix} \tag{6}$$

SM mode provides increased throughput over a SISO system (ideally 2x if the modulation and coding rates are same). However since there is no SNR combination(like in SD mode) it requires a higher minimum SNR to operate in a particular modulation as compared to SD mode. While MIMO systems provide higher data bandwidth and increased range of operation, due to increased number of transceiver chains they must also be designed for low energy consumption across diverse operating conditions. Current standards allow for support of up to 8 chains on a single chip demanding high performance requirements from on-chip battery. Prior work in this domain end has been reported in [18, 19, 20, 21, 22]. In [18] the power consumption has been optimized at the transmitter for several Power Amplifiers (PA) topologies through intelligent power allocation schemes. [19, 20] discuss low-power baseband techniques for MIMO transceivers. In [21] the system is optimized to maintain a constant throughput across various channel conditions by switching between SISO, SIMO and MIMO configurations. [22] optimizes the power consumption of the system across channel conditions by switching between antenna modes and encoding schemes. Hence, all of the RF front-ends discussed are static in nature, power being saved by switching the number of chains. Prior work[23, 24] has also attempted to design static MIMO front-ends which can adapt itself to ro process variations through post-manufacture tuning to bring device performance back as close to nominal as possible.

However unlike SISO systems, the presence of multiple-modes of operation in

MIMO RF systems results in different non-monotonically varying performance margins across different points of operation of a MIMO transceiver system. As illustrated in [25] the maximum benefit can be derived from a MIMO system if it is used in Spatial Multiplexing(SM) mode when the wireless channel is good and in Spatial Diversity (SD) mode when the channel is bad. Depending on wireless channel conditions, current MIMO systems switch across different operational modes and signal modulation rates in real time to maximize the wireless data transmission rate for any given channel condition. However, fine-grained co-modulation of the RF circuit level performance along with the operational modes and signal modulation rates for MIMO systems has not been fully exploited by prior research.

1.7.3 Channel-adaptive wireless system design

For wireless systems, the probability of encountering the worst case channel conditions is very small. As a result, for most of the time(or for majority of operating conditions) the wireless device is over-designed for performance and hence consumes a greater power than necessary. The solution to this problem is to design systems(RF front-end, baseband and digital circuits) which can dynamically adapt to changing channel conditions while maintaining its operation at the minimum acceptable performance or threshold BER. In the digital domain, physical layer based design methodologies [26, 27] which modulate the power consumption and frequency of the digital circuitry depending on throughput requirements have been studied in the past. RF systems working at a maximum threshold BER have been discussed in detail in [28, 29, 30]. At the media access control(MAC) and network layer power management schemes have been proposed[31] which estimate the channel quality from training symbols and adapt the modulation and coding rates to conserve power while maintaining an acceptable performance. Modern wireless systems also have the option to switch

between high-power, low-power and shut-down states depending on the channel conditions and usage. However all the above techniques allow only a small number of discrete steps in adaptation and do not completely exploit the design margins. For the most optimal power consumption a fine-grained system-level adaptation is required. This design philosophy was explored in [32], which proposed an energy scalable RF transmitter, where the front-end is dynamically tuned (supply, bias, resistances) for each data rate modulation set by the higher-level link layer protocol. The tuning is driven by channel quality as determined by channel estimation metrics and relies on simulation of a large number of channel and RF front-end settings. Along with the above approaches several attempts have been made to holistically design environment adaptive RF front-end which react to changes in channel conditions in real-time to reconfigure the device for optimally low-power operation. In [1, 33, 34] an adaptive power management strategy is discussed which tunes the front-end to maintain the system at or below the maximum acceptable BER. This technique exploits the built-in margins in the wireless systems through continuous adaptation based on an optimal look up table based control law that is computed apriori. The look-up table (LUT) based adaptation strategy is depicted in Figure 8. Here, the entire gamut of channel conditions is partitioned into a finite number (say m) of representative channels. In the design and characterization phase of the system a combination of tuning knob settings is found for each of the m channels such that, the Error Vector Magnitude (EVM) is maintained at threshold (EVM_{th}) of acceptable operation while the power is minimized. These combinations are stored in the form of a $m \times n$ table (where n is the number of tuning knobs). The channels are ordered such that the first row represents the best channel (and hence minimum power consumption) and the last row represents the worst case channel (maximum power consumption). This optimization can be done with a multi-dimensional constrained optimization algorithm (e.g. gradient search). The table is then stored on-chip. During real time operation the EVM of

the system is constantly monitored and a control algorithm running on the baseband processor continuously attempts to maintain the EVM at EVM_{th} by changing the tuning knob settings using the stored LUT. Such a strategy can be implemented both at the receiver as well as the transmitter. At the receiver tunable LNA, Mixer etc. could be used to trade-off power vs. performance [35]. Using the same philosophy [36, 37] describes a low power multimode transmitter which employs channel dependent dynamic digital PAR reduction in conjunction with adaptive rebiasing of the Power Amplifier (PA).

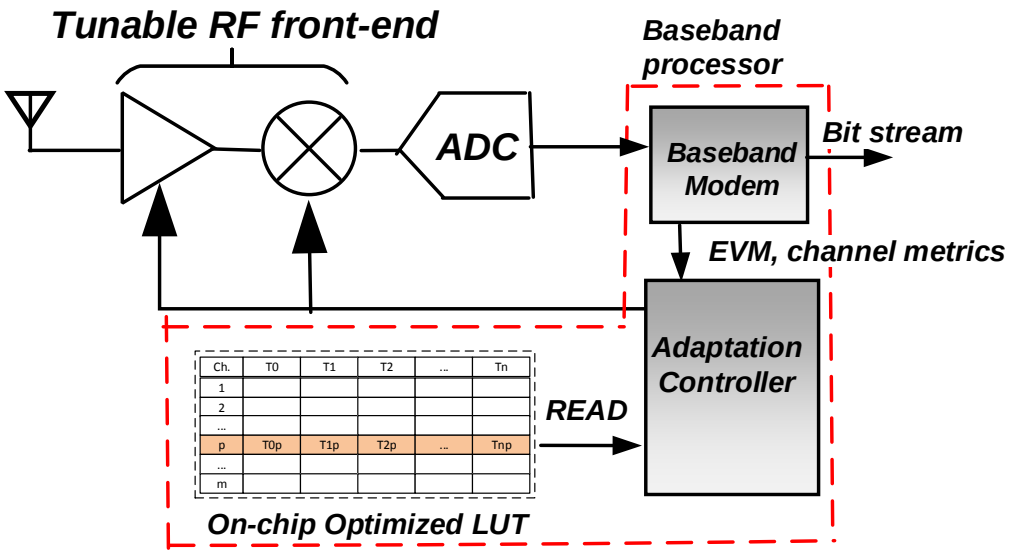

Figure 8: LUT based channel adaptation

1.7.4 Process tolerant channel-adaptive wireless systems

Besides power dissipation, process variations also pose a major design concern with technology scaling. To compensate for such variations, several built-in RF calibration techniques have been proposed in the past [38, 39, 40]. The capabilities of Design for Manufacturability (DFM) is demosntrated for analog/RF circuits in [41]. In [42], a VCO is demonstrated with a worst case specification variation of 43% and the authors present optimisation techniques in the design flow to correct these process variations.

Further design centering[43] can be used to reduce the effect of process variation on the performance of the device. However despite these measures process variations might cause the device to deviate from the nominal specifications to a large degree, specially at the lower technology nodes.Thus these manufacturing variations lead to a reduced Quality of Service(QoS) in wireless systems.

Specification prediction and tuning of low-speed devices has been discussed in [44, 45, 46]. Prior work has also explored the tuning of RF specifications through hardware "tuning knobs" or digital compensation [47, 48, 49, 50, 51, 52, 53, 54, 55]. Tuning of digitally assisted RF/ analog circuits and systems like PLL, frequency synthesizers and digital radio has also been implemented [56, 57, 58, 59]. Techniques to simultaneously tune multiple tuning knob parameters to counter small and large parameter variations in RF systems for yield enhancement are discussed in [60, 61, 62, 63]. However, except for work presented in [64], existing test and tune techniques are not targeted towards channel-dependent dynamic transceiver power management and tuning.

Preliminary experiments have shown [64] that the most power-optimal manner in which an RF transceiver can be dynamically tuned for changing wireless channel conditions is a direct function of the process corner to which the specific manufactured wireless IC corresponds to.

The technique proposed in [64] tries to discretize the multi- dimensional process variation space into finite number of states. As shown in Figure 9, for each of these states or process condition, [64] proposes a design phase optimization to generate a reconfiguration table that dictates how the circuit and algorithmic level tuning knobs should be modulated according to changing channel conditions using closed loop feedback to minimize power consumption. Prior to system deployment, a built-in test procedure is invoked to determine the process corner the RF device corresponds to. The appropriate table that best matches the diagnosed process corner for the

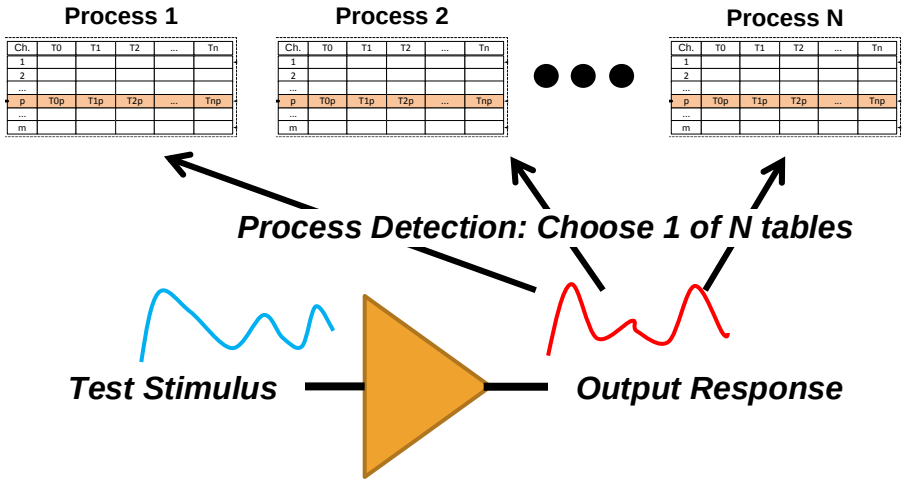

Figure 9: Illustration of prior process-resilience approach

RF device is then programmed into the device for real-time RF front end adaptation. The problem with the above technique is that this might lead to very coarse approximations and require a huge amount of design phase computation based on approximate models. Moreover, the process space is multi-dimensional and a set of process instances spanning this space is hard to construct.

1.8 Key Contributions of this work

In light of the prior discussions, several key aspects of channel-adaptive low-power front-ends need to be addressed for its successful adoption and implementation in modern mobile wireless devices. This thesis adresses each of the following areas in detail:

First The prior techniques focus on LUT based feedback control which requires extensive design phase characterization and only works for uni-dimensional channel space. This thesis proposes alternate fuzzy logic based and analytical equation based control strategies for RF front-ends. The proposed adaptation control methodologies are able to accommodate and adjust the front-end for multiple

independently varying channel parameters (e.g. signal strength and interference).

Second Prior discussion on channel-adaptive front-ends has focussed on minimizing power while always operating at the highest throughput for SISO systems only. In this thesis it is shown that such an approach does not guarantee the minimum energy-per-bit. Depending upon the throughput requirements of the application accessing the front-end one of two modes of low-power adaption can be adopted: one optimizing power in presence of highest throughput, the other sacrificing throughput to get the minimum energy-per-bit. Moreover such a use-aware adaptation methodology is implemented, for the first time, on a MIMO system for both the receiver and transmitter to demonstrate the benefits and trade-offs of the multiple low-power modes and compare it versus the existing technology.

Third Process-tolerance is an essential feature for adoption of channel-adaptive low-power front-ends. In this thesis self-learning front-ends are proposed which can learn the optimum configuration across channel conditions during the initial stages of its real-time operation to provide a customized reconfiguration settings on a per-chip basis (eliminating the problem of inter-chip process variation).

The contributions of the thesis have been summarized in Figure 10

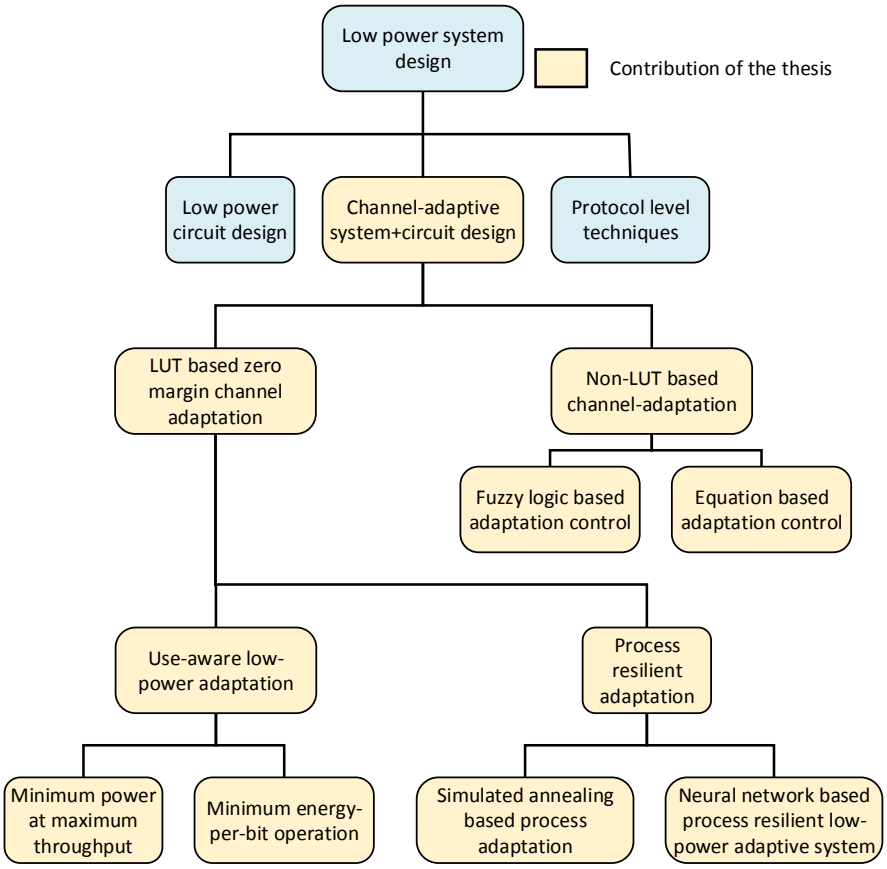

Figure 10: Key contributions of the thesis

CHAPTER 2

FUZZY LOGIC AND ANALYTICAL EXPRESSION BASED NOISE-DISTORTION CONTROL TECHNIQUES

2.1 Motivation

In prior literature it has been demonstrated that the power in a RF front-end can be traded off for performance in real-time to operate at the threshold of acceptable operation using a lookup table driven controller. LUT based feedback control works well with uni-dimensional channel models. For uni-dimensional channels, the channels can be arranged from "Good" to "Bad" in a linear fashion. While this approach leads to a simplified controller design, this assumption fails for most practical channels which have more than one independent variable. For example, both the received signal strength and interferer strength are independent quantities in practical communication channels. Additionally, the LUT based approach requires extensive design phase simulation and characterization of the front-end using approximate models to find the optimum "tuning-knob" combinations for each sub-block of the front end across a large range of channel conditions. In this work[65] we propose the design of an adaptive RF front end that can adapt to changes in channel conditions by modulation of the noise-distortion characteristics of embedded RF modules. As opposed to prior designs, a new fuzzy logic based system level control mechanism is proposed that, for the first time, facilitates RF front end adaptation without a pre-characterized LUT. A simple control strategy is proposed that alleviates the need for extensive characterization of the RF system while ensuring good control and performance for multiple independently varying channel parameters. It must be noted that RF architectures, like super-regenerative receivers, have demonstrated low power operation but they

are limited in their scope and may not be suitable for many wireless standards. However this work demonstrates low-power operation for existing architectures without compromising on receiver performance. Further, it is also shown that an analytical expression based prediction of the values of the tuning knob settings for a certain channel condition and target SNR may be possible. The advantage of this technique is that it would do away with the necessity to have a feedback loop and the values of the tuning knobs can be directly set based upon the values of the channel impairments and the relationship of the analytically derivable front-end performance to tuning knob settings.

2.2 Adaptation Metric and Reconfiguration Strategy

2.2.1 EVM based adaptation

From experiments we can determine that for a BER of 10^{-4} the maximum threshold EVM (EVM_{th}) is 35% for QPSK and is 14% for 16-QAM.To overcome the inherent uncertainty in calculation of a metric like EVM we can put a guardband of δ to get EVM_{gbd}. In LUT based approach a much larger guardband over and above this δ is required due to system oscillations. In our case:

$$EVM_{gbd} = EVM_{th} - \delta \tag{7}$$

2.2.2 Reconfiguration strategy

The two major specifications that are important in a modern radio receiver are its linearity and the input referred noise added by the receiver. These two are measured by the IIP3 and Noise Figure (NF)/Gain of the receiver. Static radio designs optimize the IIP3 and NF for the worst case channel conditions. In this work, both these specifications are changed dynamically based on the fidelity of the received signal.

For receiver adaptation, we are interested in determining the received signal SNR and the strengths of in-band and out-of-band interferers. Interferers cause signal

degradation in the receiver due to receiver saturation. This results in significant intermodulation distortion and the resulting intermodulation components raise the noise floor of the received signal. On the other hand if the received signal has low signal power then the NF and gain specifications of the receiver become critical due to the fact that any noise contributed to the received signal by the receiver circuitry can significantly decrease the SNR of the received signal. In modern receivers, both received signal power and the signal strength of interferers are estimated by embedded RF detectors (see Section 2.4.1). These detectors can be used to aid system level adaptation. We now discuss practical constraints on the linearity and NF of a receiver. These are used later to formulate the control law for dynamic adaptation of the RF front-end.

2.2.2.1 Linearity (IIP3) constraints

The linearity of a receiver becomes critical when either the signal or the interferer strength becomes high. One of the key goals of the adaptation law is to ensure that the $IIP3(\approx P1dB + 9.6dB)$ of the signal should be high enough so that in the presence of a strong signal or strong interferer, gain compression or intermodulation components do not push the EVM (and BER) above the maximum allowable level. Thus we can say that

$$IIP3 = f(SignalStrength, InterfererStrength) \tag{8}$$

More specifically if the signal or interferer is sufficiently below the IIP3 of the receiver then it has very little effect on the EVM. In dBm scale this means that for IIP3 to have an effect on the EVM:

$$Signal\ Strength > IIP3 - \Delta_1 \tag{9}$$

$$Interferer\ Strength > IIP3 - \Delta_2 \tag{10}$$

Since a high signal strength causes saturation only and a high interferer strength causes both saturation and intermodulation the margins Δ_1 and Δ_2 are different. They are constants (in dBm) whose values are system specific and can be determined from very simple system simulations.

2.2.2.2 Noise figure (NF) Constraints

The NF of the system becomes critical when the signal strength is close to the noise floor (SNR is low). In this case the goal is to demodulate the signal without any further significant addition of noise from the receiver. The NF of a system is given by:

$$NF = NF_1 + \frac{NF_2 - 1}{G_1} + \frac{NF_3 - 1}{G_1 G_2} + ... \tag{11}$$

Here NF_i and G_i are the Noise Figure and gain of the i^{th} stages in the RF chain. Thus the NF and Gain of the Low Noise Amplifier (LNA) becomes critical in this case. However the noise added by the system has very little effect on the EVM of the system when the signal strength is high. Only when the signal falls below certain strength, will we start seeing an appreciable effect of NF on the system performance. So assuming a fixed channel thermal noise floor we can say that NF of the system becomes critical when

$$Signal\ Strength < \Delta_3 \tag{12}$$

Again Δ_3 is a constant (for a particular system) and can be determined from the system design through simple simulations.

Table 1: Heuristics for Noise-Distortion Modulation

S_0	I_0	$(EVM_{gbd} - EVM)$	IIP3	NF
$> IIP3_0 - \Delta_1$	X	-ve +ve	$\uparrow$ $\uparrow$	$\uparrow$ $\downarrow$
X	$> IIP3_0 - \Delta_2$	-ve +ve	$\uparrow$ $\downarrow$	$-$ $\uparrow$
$< \Delta_3$	X	-ve +ve	$-$ $\downarrow$	$\downarrow$ $\uparrow$

2.2.2.3 Control Strategy

Based on the discussion in Sections 2.2.2.1 and 2.2.2.2 we can now formulate certain heuristics for modulating the noise and distortion in the front-end so as to power-optimally operate at the threshold of acceptable operation (i.e. at guard-banded EVM threshold EVM_{gbd}). Let us take a snapshot of the system at a time instant T_0 and formulate the strategy as to how to change the IIP3 and NF of the system. Let IIP3_0 and NF_0 be the IIP3 and NF of the system at this instant and let the signal and interferer strengths be S_0 and I_0 respectively. We formulate this strategy in the form of a rule table shown in Table 1. Here an $'X'$ denotes a *Don't-Care condition* while a $'-'$ means that decision regarding the variable cannot be taken based on that piece of information. When taking a decision, all the rows of the table are evaluated and a decision is taken regarding as to how to change the IIP3 and the NF of the system. Another goal of the control system is to make the transitions in IIP3 and NF dependent on the difference between the current EVM and the desired one (EVM_{gbd}). We have assumed that NF and gain of the sub-blocks are correlated (as is usually the case). An increase in NF is linked with a decrease in gain and vice versa.

2.3 Fuzzy Control Formulation

We can visualize the RF receiver system as a control system as shown in Figure 11.

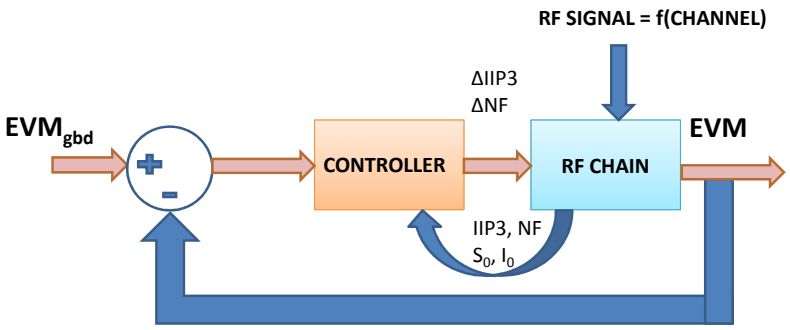

Figure 11: A Control Perspective of the RF chain and feedback controller.

One of the disadvantages of the control strategy formulated in section 2.2.2.3 is that it is essentially based on decisions taken depending on the relationship between the input variables (Signal Strength, Interferer Strength and EVM) and their decision boundaries($IIP3_0 - \Delta_1$, $IIP3_0 - \Delta_2$, Δ_3 and EVM_{gbd}). This leads to a "Yes" or "No" decision as to changing the IIP3 and NF and the amount of their change is also fixed. The disadvantage of such a control is that the system keeps on oscillating around the desired value like in a thermostat based room heater(bang-bang control). Moreover the choice of decision boundary becomes very critical in system performance. A more desirable feature of the control algorithm should be that the increment in IIP3 and NF for the next interval (T_1) should be a function of the deviation of the input variables from their decision boundaries.

$$\Delta IIP3 = g(\Omega) \tag{13}$$

$$\Delta NF = h(\Omega) \tag{14}$$

Here Ω is the set of deviations of input variables from their boundaries i.e.

$$\Omega = \{IIP3_0 - \Delta_1 - S_0, S_0 - \Delta_3, IIP3_0 - \Delta_2 - I_0, EVM_{margin}\} \tag{15}$$

$$EVM_{margin} = EVM_{gbd} - EVM \tag{16}$$

This would ensure that the system rapidly corrects any deviation from the desired steady position (i.e. $EVM \approx EVM_{gbd}$) quickly and settles down to a steady state. This type of control is known as proportional control. In this case the choice of decision boundaries becomes less critical than in "Bang-bang control".

In the field of control theory such problems are dealt with by designing a Proportional controller for optimum performance. However to design such a "controller" one needs to know the transfer function governing the "plant" (which in our case is the RF front-end) and hence the exact input-output relation i.e. we need to know the equation k where:

$$EVM = k(Channel, IIP3, NF) \tag{17}$$

However in this case the relationship is highly non-linear and difficult to formulate. Hence we cannot design a Proportional control using traditional techniques. This problem can be solved by the use of intelligent control algorithms like Fuzzy Controller[66, 67]. A Fuzzy controller "attempts to mimic human control logic" and creates a robust control logic which is very easy to implement and is computationally simple and it corrects the problems with the "bang-bang control". A schematic of a Fuzzy controller is shown in Figure 12.

The basic chain of fuzzy control starts with the fuzzification of the input. A group of membership functions is constructed which gives the grade, or degree, of "membership" within the set, of any element of the universe of discourse. The membership function maps the elements of the universe onto numerical values in the interval $[0, 1]$. Fuzzification is the process of decomposing a system input into one or more fuzzy sets. For example a decision making question "Is $S_0 < \Delta_3$?" no longer yields a binary value of 0 or 1(as in bang-bang control) but can be anything in the interval [01]. Thus they

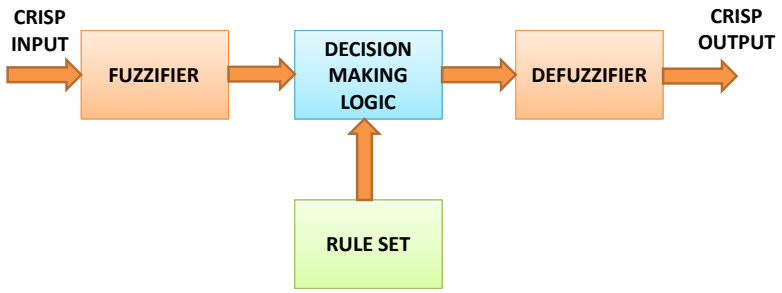

Figure 12: Block Diagram of a Fuzzy Controller.

convert the input a "Fuzzy value". The process of fuzzification allows the system inputs to be expressed in linguistic terms so that rules can be applied in a simple manner to express a complex system. The next step is to evaluate the rules of the system using the fuzzified inputs. All the rules that apply are invoked and using the membership functions and truth values obtained from the inputs the result of the rule is determined. This result in turn will be mapped into an output membership function and truth value controlling the output variable. The final step is to combine the fuzzy output of each output rule into a "crisp" value which is the output of the controller.

2.4 System Simulation

In order to demonstrate the concepts discussed in previous sections we consider the test vehicle of a 2.4 GHz OFDM WLAN direct conversion receiver. The block diagram of the receiver is shown in Figure 13.

2.4.1 Signal and Interferer Strength Estimation

In order to adapt to channel conditions the receiver must first estimate the quality of signal it receives. Modern radio front-ends already have sophisticated sensors and baseband algorithms built-in which sense the signal and interferer power.

One such widely-used metric is Received Signal Strength Indicator (RSSI), which

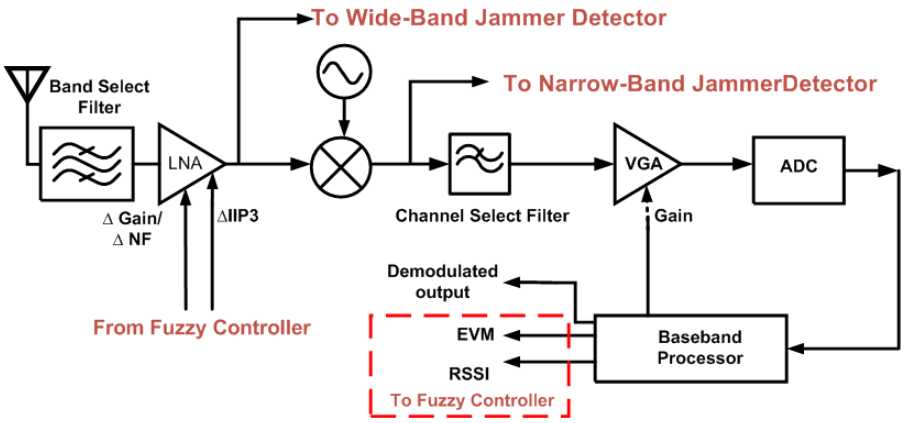

Figure 13: Detailed schematic of the proposed RF chain and baseband circuit showing signal and interferer estimation points.

gives an estimate of the in-channel power received. [68] discusses a method of detecting the power of in-band interferers. This is done by sensing the total in-band power by using a power detector between the mixer and the channel-select filter. The RSSI can then be subtracted from the in-band power to get the in-band interferer power. [69] discusses the design of a wide-band jammer detector which can be used to sense the total power received at the receiver. Thus combining both the outputs of interferer power detectors one can get the idea about the total interferer power at the input of the LNA.

It must be noted that if interferer power is estimated to be X dBm it could mean that there is one or more interferers causing this effect. However the worst case can occur when there are 2 interferers of $(X - 3)$ dBm each causing saturation and 3rd order intermodulation products which can fall in-channel corrupting the desired signal and increasing the noise floor. We shall always adapt the system for this worst case interferer combination for a particular interferer power.

2.4.2 Orthogonally tunable LNA

One of the most important components of the front-end described is the LNA. The NF of the system is dominated by the NF of the LNA and the linearity of the LNA

must be sufficient to allow strong input saturation and intermodulation components from corrupting the signal of interest. [35] demonstrate the design of an orthogonally tunable LNA where the Gain/NF and the IIP3 of the LNA can be tuned independent of each other. The NF can tune from 2 dB to 8 dB, while the Gain tunes from 6 dB to 17 dB. At the same time the IIP3 can be varied from -9 dBm to nearly -28 dBm. The schematic and the NF, OIP3 and current consumption variation with tuning knob voltages for the LNA are demonstrated in Figure 14. In the circuit shown in Figure 14, due to the orthogonal nature of tuning knobs, we can say with high confidence that NF is a function of V_{Gain} and IIP3 is a function of V_{IIP3}. So we can approximate these functions by polynomials. Given a desired value of NF and IIP3 we can then solve these equations on the baseband processor to get the required value of tuning knob voltages. Henceforth, in we would discuss about NF and IIP3 tuning directly. However, actually we are changing the tuning knob voltages to produce these changes. In our system we attempt to dynamically vary the NF/Gain and IIP3 of the LNA. As opposed to [1, 37] we want to preclude the locus based adaptation approach which requires extensive characterization and a bang-bang control algorithm. [70] discusses adaptation at Variable Gain Amplifier(VGA) and filters keeping the power in RF blocks (LNA, Mixer) unchanged. Our approach fills in this void by tuning the power in the RF blocks and along with [70] provides a complete tuning solution for low-power RF receiver.

2.4.3 System Characteristics

In order to formulate the control law we need to exercise the circuit so as to get an intuition about its behavior. Using the result of a few simple experiments we can determine the values of the constants discussed in Section 2.2.

To estimate value of Δ_1 we sweep the value of the signal strength over the entire Spurious Free Dynamic Range (SFDR) of the receiver and observe the system EVM

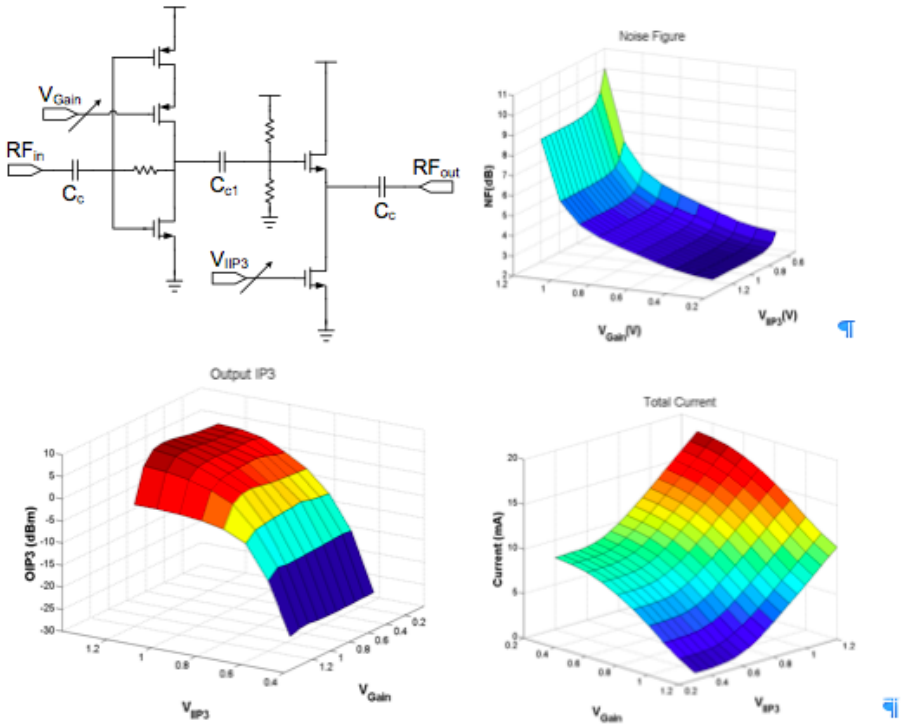

Figure 14: Orthogonally tunable LNA and variation of NF, OIP3 and Current with tuning knobs.

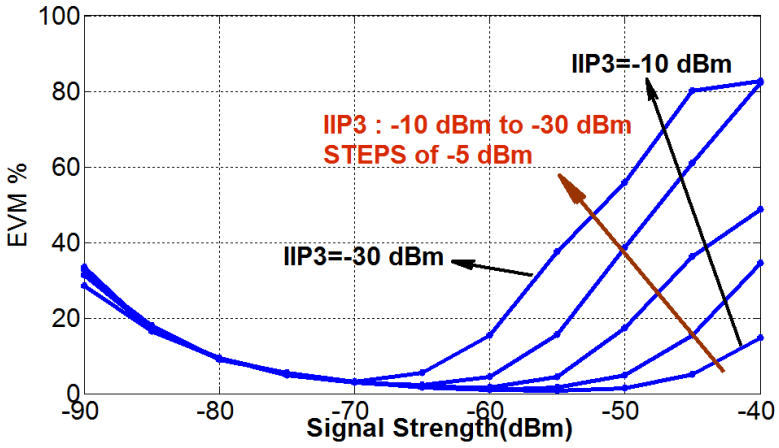

Figure 15: EVM variation with Signal Strength for different IIP3 values.

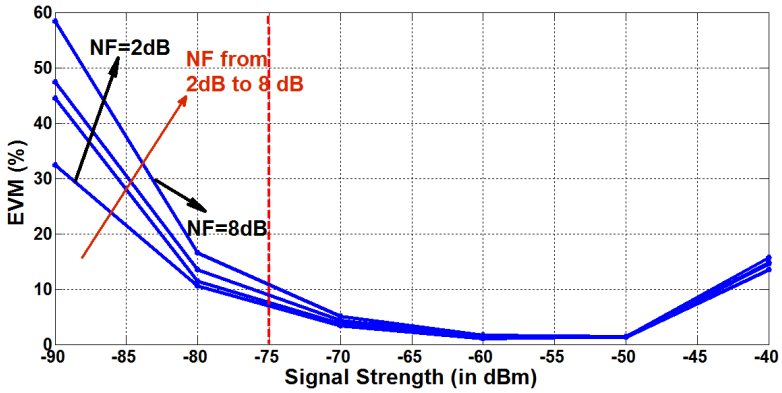

Figure 16: EVM variation with signal strength for varying NF.

for different values of LNA IIP3. It can be seen that non-linearity effects start to assume significant proportions once the signal crosses the level (IIP3-35) dBm. Hence $\Delta_1 = 35$ dB. Since interferers behave similarly but also have the added effect of intermodulation components we can keep $\Delta_2 = 50$ dB. In order to determine Δ_3 we sweep the signal over the entire SFDR for various Noise Figures of the system. It can be seen from Figure 6 that noise figure really starts affecting the signal below $\Delta_3 = -75$ dBm. The amount of system simulation required to find these constants is significantly less than gradient based search for optimum knob setting for each channel condition in a LUT based approach.

2.5 Fuzzy Controller Design

Using the heuristics formulated in Table 1 and estimating the values of the system parameters from Section 2.4.3 we formulate input and output membership functions for the controller (Figure 17). Each input/output membership function is constructed to have considerable overlap with the adjacent functions in order to prevent abrupt step changes in the output of the Fuzzy controller. Here PVL, PL, PS, NL, NVL and NS stand for Positive Very Large , Positive Large, Positive Small, Negative Large, Negative Very Large and Negative Small. Given a value of S_0, I_0 the Fuzzy controller uses the rule set and membership functions to calculate the desired change in IIP3(

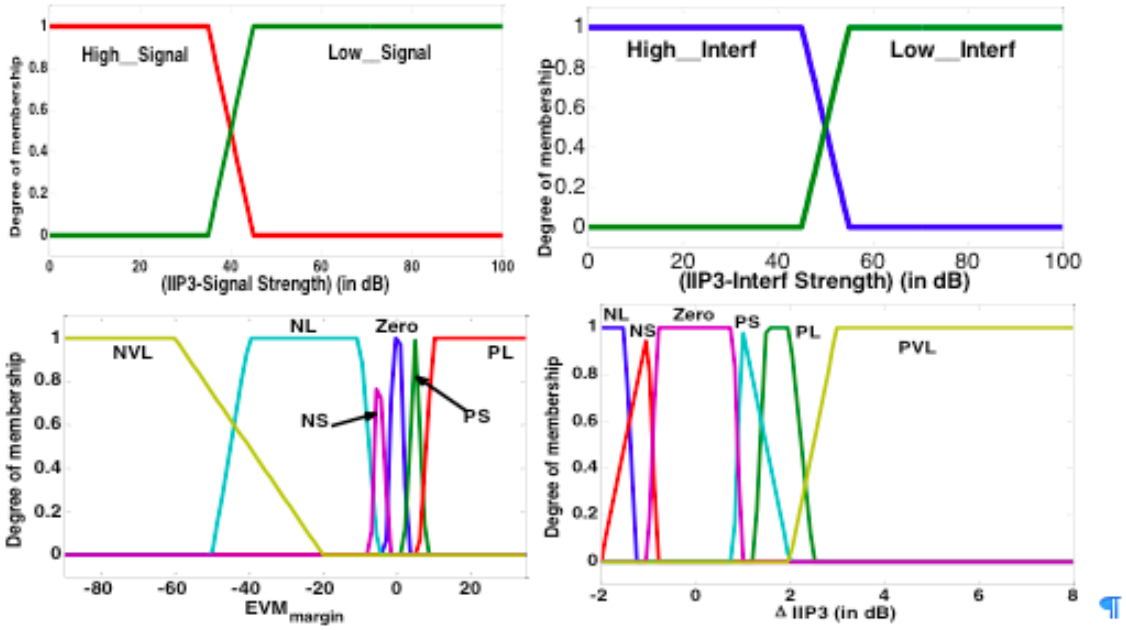

Figure 17: Input and Output Membership Function for IIP3 controller.

i.e. ΔIIP3). Here ΔIIP3 is a function of (IIP3$-I_0$), (IIP3$-S_0$) and EVM$_{margin}$. The surface for $\Delta IIP3$ at EVM$_{margin}$ = 3% is shown in Figure 18. The use of a Fuzzy controller has ensured the smooth transition of ΔIIP3 across the range of input variables instead of a step jump at hard decision boundaries (as is for "bang-bang" control). As there are no hard boundaries (and hence discrete switching points), hysteresis need not be implemented in the system. Similarly, input and output membership functions are constructed for NF controller as a function of signal strength and EVM$_{margin}$.

For the sake of brevity, we do not show the membership functions of the NF controller. Figure 19 shows the ΔNF surface as a function of signal strength and EVM. Given an input vector (set of signal strengths, current LNA specifications and EVM), the controller maps the vector to a particular point on the surface. This corresponds to the desired change in IIP3 and NF over the next cycle. One must remember that this fuzzy controller is computationally inexpensive and can run as software on the baseband processor. Thus no additional hardware overhead is required. Moreover

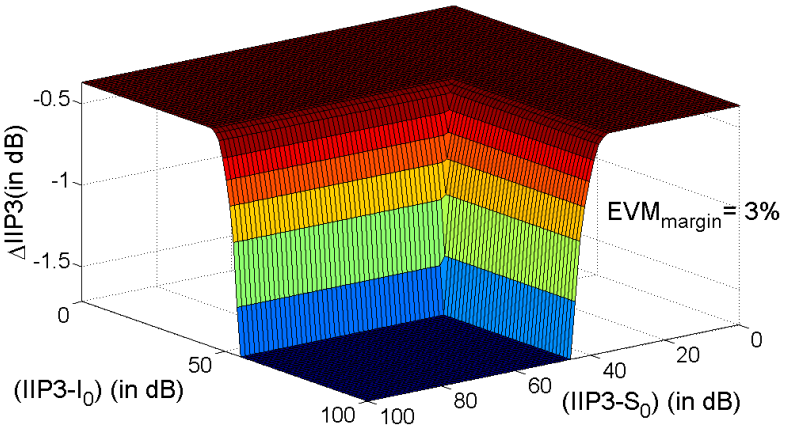

Figure 18: Variation of ΔIIP3 with Interferer and Signal Strength for a fixed (3%) EVM margin.

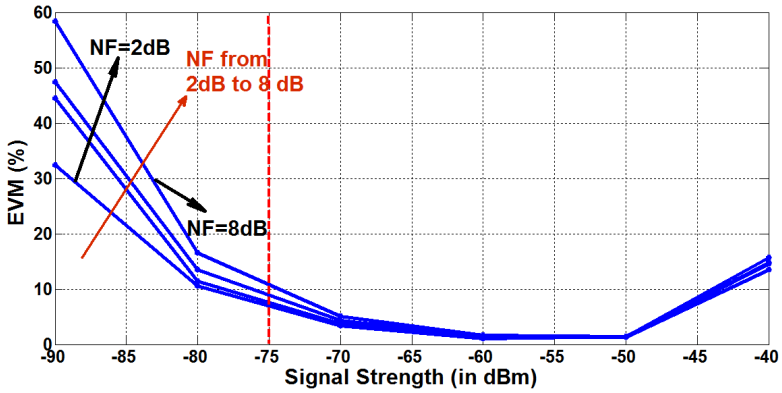

Figure 19: Variation of ΔNF with EVM margin and Signal Strength .

the controller needs to update the state variables only once per EVM calculation and hence should consume negligible power as compared to the front-end.

2.6 Simulation Results

In order to demonstrate the operation of the Fuzzy Controller based system adaptation for low-power 2 simple experiments were devised. We set up a RF receiver chain model with an orthogonally tunable LNA as the tunable element. An OFDM QPSK signal at 2.4 GHz passes though channel (with variable attenuation, variable strength interferer addition and constant thermal noise floor) before reaching the receiver. We

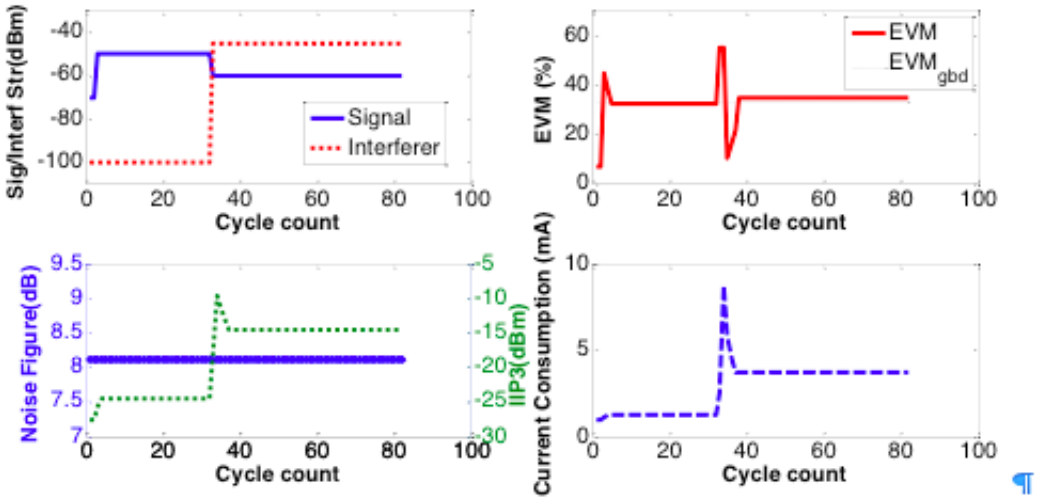

Figure 20: Transient Simulation for Experiment 1 showing Signal and Interferer Power, EVM and LNA IIP3, NF and Power Consumption .

vary the channel conditions to observe the performance and power consumption of the RF-chain-Fuzzy feedback control combination.

Experiment 1: We vary the signal strength and interferer strength of the received signal to show how the system/LNA adapts to the changing conditions. The experiment is demonstrated in Figure 20. Initially the signal becomes strong enough to hit non-linearity and hence EVM overshoots the threshold (by a small amount). In order to correct this, the Fuzzy controller increases the IIP3. It should be noted that in each decision cycle of the controller (denoted in Figure 20 as cycle count), the rate of rise of IIP3 is dependent on the deviation of the EVM from EVM_{gbd}. Therefore IIP3 changes slowly when EVM is close to EVM_{gbd} equilibrium position and fast when the system EVM is too low or too high. Once the EVM reaches EVM_{gbd}, the IIP3 is maintained constant. At cycle count 32, the signal strength decreases but interferer strength increases to a large value. The controller again adapts to this situation by adjusting the IIP3 to a high enough level. It must be noted that all through this experiment the NF remains at the highest possible value due to reasons discussed in Section 2.2.2.3. The LNA current consumption shows 4× variations (1 mA to 4

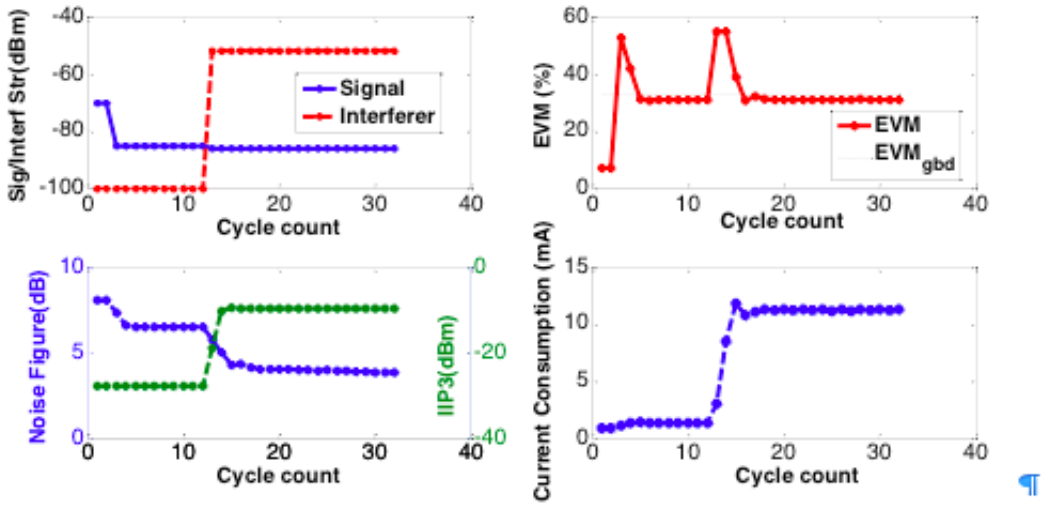

Figure 21: Transient Simulation showing Signal and Interferer Power, EVM, LNA NF and IIP3 and LNA Current for Experiment 2 .

mA) in this experiment but remains low as compared to the maximum current consumption ($\approx 11mA$) because NF constraints are relaxed and the circuit is not fully stretched to its maximum capabilities.

Experiment 2: In this experiment the signal strength is made much smaller so that the NF becomes critical. Initially there is no interferer and the NF of the LNA reduces in order to maintain an acceptable BER. Next a high power interferer is introduced and the Fuzzy controller detects the overshoot in EVM and adjusts both the IIP3 and the NF simultaneously so that EVM can be pulled down below EVM_{gbd}. As is evident the highest power consumption occurs when the signal is weak (requiring low NF) and the Interferer is strong (requiring high IIP3) simultaneously.

In such a circumstance both the specifications of the LNA are stretched to their maximum to ensure acceptable BER performance. However this is just a corner case and would occur rarely. Thus most of the time the circuit can operate in a low power mode. As seen from Figure 21 the savings in current can be as large as 10mA as the highest current is $\approx 11mA$ and the lowest current being $\approx 1mA$. Assuming the LNA consumes nearly 25% of the total current in a receiver chain we can achieve a

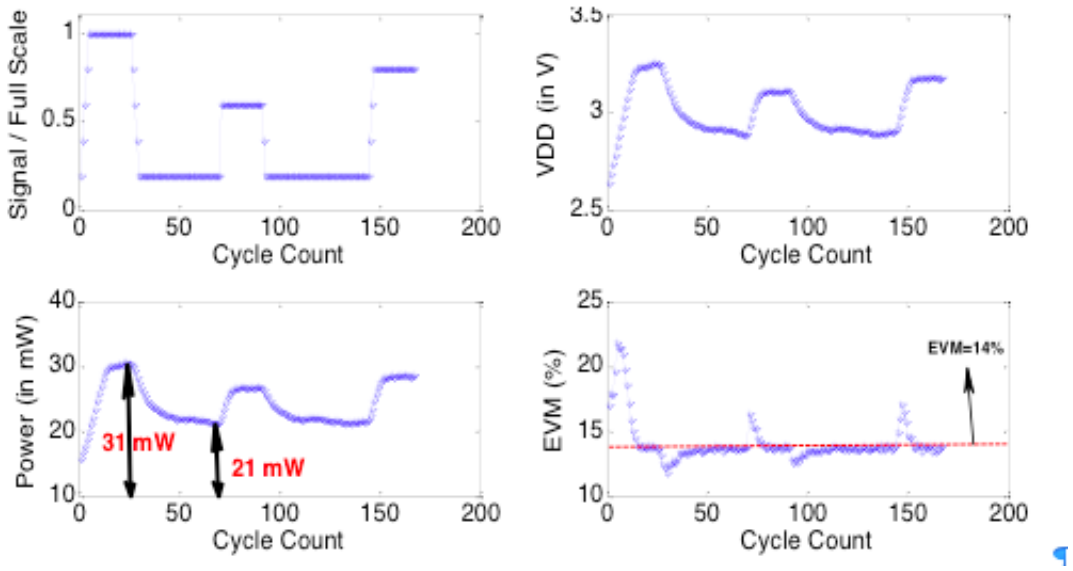

Figure 22: Relative signal strength, V_{DD} control, LNA Power consumption and EVM in the hardware setup .

maximum power savings of nearly 23% for the receiver.

2.7 Hardware Implementation

An experiment is performed in hardware to show the feasibility of the proposed concept. A 802.11 RF front end (PA / LNA) from Texas Instruments is used in the experiment where supply voltage is varied from 2.6 to 3.9 volts in steps of 0.1 volts and the signal strength is varied from (0.2∗fullscale) to the fullscale swing.

A mixer AD5382 is used for downconverting the 2.4GHz RF signal. With change in the supply voltage, linearity of the front end also changes which affect the EVM for a given signal strength. On the other hand, as the signal strength increases, the front-end goes into nonlinear region and EVM starts increasing. We set a desired EVM threshold of 14%(pertaining to a BER of 5×10^{-4} for 16-QAM) and formulate a Fuzzy control law which tunes the VDD control knob to modulate linearity of the device as a function of the EVM margin and input signal strength(known). The system is excited with signal of temporally varying strength and the EVM is measured in the baseband. Figure 22 shows the results of the experiment. We observe that the Fuzzy

control law allows for a smooth EVM response (without oscillations). Due to the supply voltage modulation the maximum power savings that is obtained is 33%(10 mW out of a total of 31mW). Thus these results corroborate the software simulation of proposed system.

2.8 Analytical deduction of tuning knob values

The Fuzzy logic based front-end adaptation control is a departure from the traditional LUT based control architecture. It can also be shown that an alternative approach with analytical solutions of optimum tuning knob settings in terms of channel impairments may be possible. In this section we try to formulate the problem to enable prediction of optimum tuning knob combinations(or LNA, Mixer performance specifications) as a function of the channel parameters like effective SNR, signal strength and interferer strength. The received signal consists of the OFDM channel of interest and two other OFDM channels which act as interferers. The intermodulation component from the interfering channels can reduce the effective SNR of the channel of interest.Similarly the SNR is also determined by the strength of the channel of interest. The three channels are centered at f_0, f_1 and f_2 as shown in Figure 23. Also as shown in the figure each channel has k OFDM sub-carriers. Now let us consider a typical front-end consisting of an LNA and mixer. Now the different strengths of the signal and interferer require that we break up our adaptation strategy into the following four cases:

1. Signal strength is low and Interferer strength is low
2. Signal strength is sufficient and interferer strength is high
3. Signal strength is low and Interferer strength is high

For case 3 we will have to operate at the highest effective NF and linearity(IIP3) and would lead to the highest power consumption. In this work we will formulate

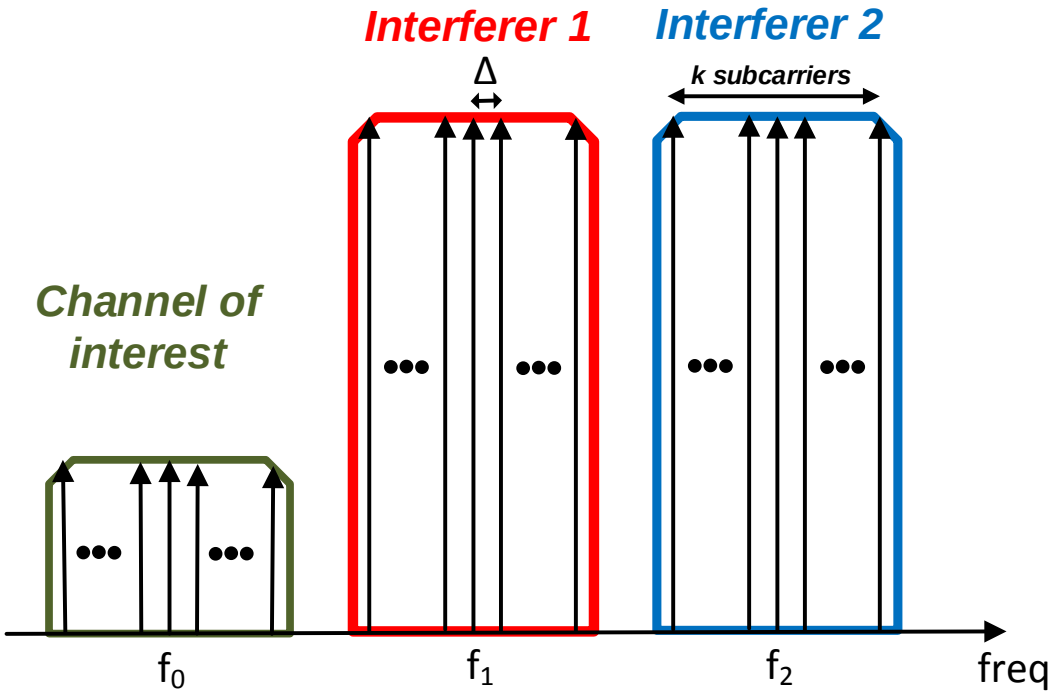

Figure 23: OFDM signal and interferer

strategies for the cases 1 and 2 such that the receiver operates at the margin of acceptable operation.

2.8.1 Low signal strength and low interferer strength

In this case the SNR is dominated by the signal strength to noise floor ratio. The linearity of the system can be set to the lowest possible value and the NF of the system must be carefully chosen according to the following relationship:

$$NF_{max} = SNR_{in} - SNR_{min} \tag{18}$$

Here SNR_{min} is the minimum required SNR to support an particular modulation technique. For our case we choose QPSK modulation for all subcarriers for both channel and interferer. The SNR_{min} for QPSK is 6 dB.

2.8.2 Adequate signal strength and high interferer strength

In this case the noise floor is set by the intermodulation components and hence the NF can be set to a relatively high value while the linearity needs to be carefully adjusted so that the system operates at the margin of acceptable operation. Assuming the signal and interferer to be tones it can be shown that:

$$\frac{IIP3_{min}}{S_0} = \left(\frac{SNR_{min}}{SIR^3}\right)^{\frac{1}{4}} \tag{19}$$

Here $IIP3_{min}$ is the minimum value of the IIP3 required, S_0 is the signal strength and SIR is the signal to interferer ratio. This in the log scale these quantities can be expressed as:

$$Margin = IIP3_{min} - S_0 = \frac{1}{2}\left[SNR_{min} - 3 \times SIR\right] \tag{20}$$

However equation 20 holds only for single tone based analysis. In practice the channels consist of multiple OFDM subcarriers. Let us consider the center tone in the OFDM signal channel at f_0. Let us assume that the m_{th} subcarrier from the first interferer (at f_1) and the n_{th} subcarrier from the second interferer (at f_2) cause an intermodulation product which interfers with this center tone at f_0. Thus:

$$f_1 + m \times \Delta - [(f_2 + n \times \Delta) - (f_1 + m \times \Delta)] = f_0 \tag{21}$$

This equation can be simplified to:

$$\Delta \times (2m - n) = f_0 - [2f_1 - f_2] \tag{22}$$

For the intermodulation components to fall in the signal channel the following condition must hold:

$$f_0 = [2f_1 - f_2] \tag{23}$$

Thus combining equations 22 and 23 we get:

$$2m = n \tag{24}$$

Now in our system let the number of subcarriers be k=128. Thus it can be shown that there are 64 solutions to the equation 24. Thus a factor of $10 * log_{10}(k/2)$ must be added to equation 20 to make it hold for OFDM signals.

$$Margin = IIP3_{min} - S_0 = \frac{1}{2}\left[SNR_{min} - 3 \times SIR\right] + 10log_{10}\left(\frac{k}{2}\right) \tag{25}$$

2.8.3 IIP3 calculation

For the receiver front-end in our simulation we consider the LNA shown in 24. In this LNA NF and OIP3 are orthogonally tunable. In the given LNA we can assume that both stages contribute to the NF while the linearity, which is a large signal quantity, is primarily a function of the second stage.

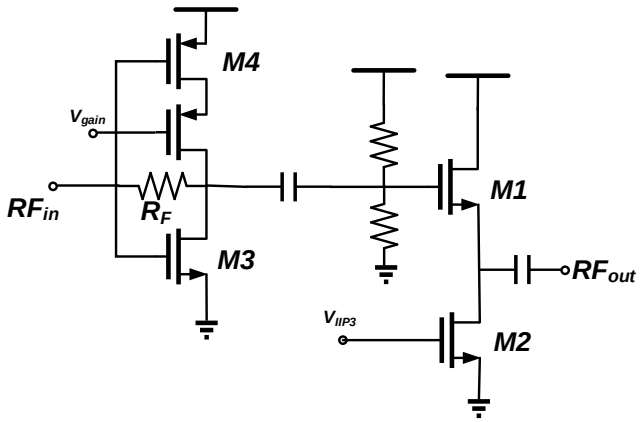

Figure 24: Orthogonally tunable LNA

It can be shown that:

$$A_{IIP3} = \sqrt{\frac{4}{3}|\frac{\alpha_1}{\alpha_3}|} \tag{26}$$

where,

$$\alpha_1 = \frac{\partial V_{out}}{\partial V_{in}} = 1 + \frac{1}{r_{o2}} \times \frac{1}{k'_n(V_{in} - V_{out} - V_T)} \tag{27}$$

$$\alpha_3 = \frac{1}{6}\frac{\partial^3 V_{in}}{\partial V_{out}^3} = \frac{-2K'^2_n r_o^2}{(1 + g_{m1}r_o)^5} \tag{28}$$

Here $K'_n = \frac{1}{2}\mu_n C_{ox}(\frac{W}{L})_1$ and $r_{o1} = r_{o1}//r_{o2}$. Thus equation 26 can be simplified to:

$$A_{IIP3} = \sqrt{\frac{4}{3}\frac{g_{m1}(1+g_{m1}r_o)^4}{2K'^2_n r_o}} \tag{29}$$

2.8.4 NF calculation

For the LNA in figure 24 it can be shown that the noise figure can be calculated as follows:

$$NF = 1+\frac{\gamma}{R_s(g_{m3}+g_{m4})}\left[1+\frac{1}{g_{m1}(g_{m3}+g_{m4})R_F^2}+\frac{g_{m2}/g_{m1}^2}{(g_{m3}+g_{m4})R_F^2}\right]+\frac{1}{(g_{m3}+g_{m4})^2 R_s R_F} \tag{30}$$

2.9 Simulation results

Exhaustive simulations were carried out on a receiver front-end with the LNA shown in Figure 24. The results generated from the simulations were then used to characterize the minimum required linearity and noise figure for different channel conditions and compared with the values predicted from theory (equations 18,20 and 25). The chosen modulation technique is QPSK requiring a minimum SNR of 6 dB. The system was first simulated for a low interferer and low signal strength and the NF of the system was optimized for different signal strengths. The optimum NF for different signal strengths is shown in Figure 25. As is clearly seen the optimum NF is nearly identical to the value predicted from analytical expressions.

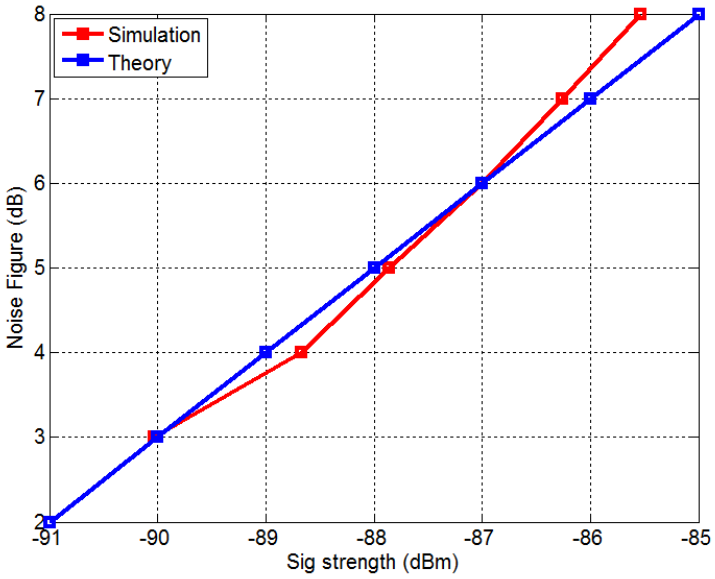

Figure 25: NF as a function of signal strength for low interferer strength

Similarly, the system is also simulated for the case of adequate signal and high interferer as shown in Figure 26. The system linearity is optimized for supporting QPSK modulation and the difference between IIP3 and signal strength is plotted versus the SIR for different signal strengths. The 'Predicted' curve corresponds to the equation 20 for single tone signals. The curve when adjusted for OFDM signals yields the line 'Predicted (adjusted)' which gives the result for OFDM channels. As seen clearly the simulation curves match the predicted result in the range in which IIP3 can be changed. Thus the analysis provided in previous section yields close match with simulated result.

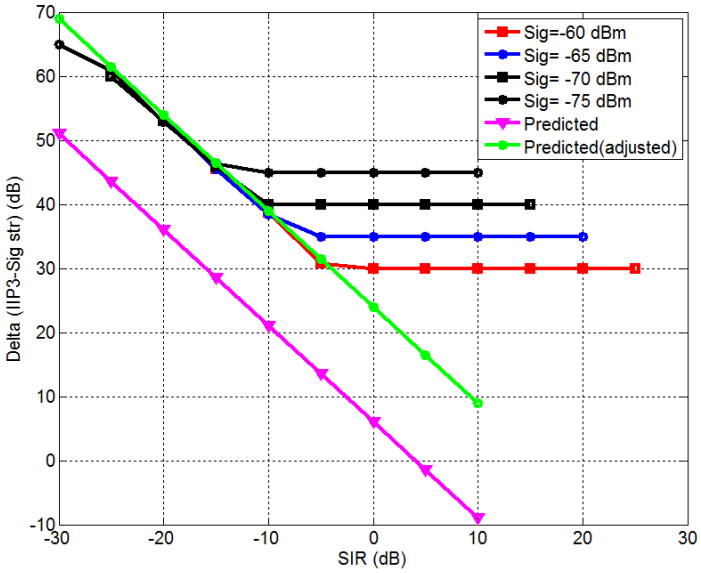

Figure 26: ($IIP3_{min}$-Signal strength) as a function of SIR for different signal strengths

2.10 Proposed methodology

Since the required linearity and NF can be predicted as a function of signal and interferer strength the analytical approach can be used to formulate a feedback control with the following steps:

1. Determine the signal, interferer and noise floor from sensors.
2. Calculate SNR, SIR.
3. Calculate NF_{max} and $IIP3_{min}$ required using equations 18 and 25.
4. Find current and bias settings to achieve desired NF_{max} and $IIP3_{min}$ using equations 29 and 30.
5. Set the appropriate values of voltages and currents.
6. Go back to Step 1.

The above discussion is summarized in the form of a flowchart shown in Figure 27

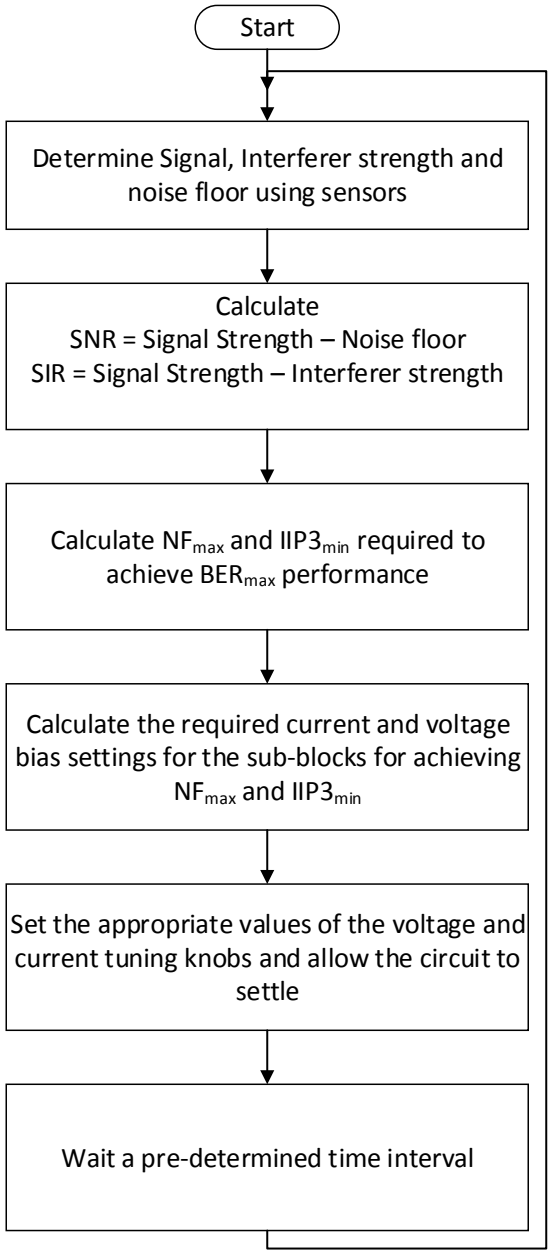

Figure 27: Algorithm for proposed analytical expression based adaptation

2.11 Summary

In this work a methodology for low-power adaptation of the RF front-end with on-the-fly reconfiguration using Fuzzy Controller has been presented. We use the test vehicle of an orthogonally tunable LNA to demonstrate the concept of locus-less receiver adaptation over changing channel conditions. One can implement tuning knobs in different front-end blocks, each of which tunes a circuit performance parameter orthogonally to the other parameters. Thus the concept itself is more generic than the implementation and can be expanded to incorporate multiple blocks in the system. The proposed intelligent control algorithm is a significant improvement over Bang-bang control in terms of steady state response. Further, an analytical expression based approach to the deduction of the optimum reconfiguration settings based on channel impairments is presented. Both of these methodologies provide essential tools for the design and deployment of control strategies for adaptive RF front-ends.

CHAPTER 3

REAL-TIME USE-AWARE ADAPTIVE RF TRANSCEIVER SYSTEMS FOR ENERGY EFFICIENCY UNDER BER CONSTRAINTS

3.1 Motivation

Prior work in the domain of adaptive low-power systems has focused on achieving the lowest power consumption possible for the highest throughput possible in a given channel condition. In traditional systems this is achieved by reducing throughput (by changing coding rate, modulation, MIMO modes) as the channel degrades while the power consumption remains constant. Adaptive systems have the capability to also modulate the power consumption of the front-end simultaneously with the throughput. In this work[71, 72] we show that for a given channel condition *the amount of power that can be saved is dependent on the data throughput requirements of the end-user application*. Certain end-user applications have constraints of operating at the maximum data rate possible and require the highest throughput possible (we call this Data Priority (DP) mode). In this mode energy-per-bit is not guaranteed to be the lowest possible. However in other applications data rate can be compromised to achieve optimal energy-per-bit (Energy Priority (EP) mode). Thus multiple low power modes could exist, each optimized for a different application (data rate vs energy-per-bit). The above discussion is summarized in Figure 28.

As compared to prior work the key contributions of this work can be summarized as follows:

1. This work shows, for the first time, that real-time channel adaptive RF transceivers

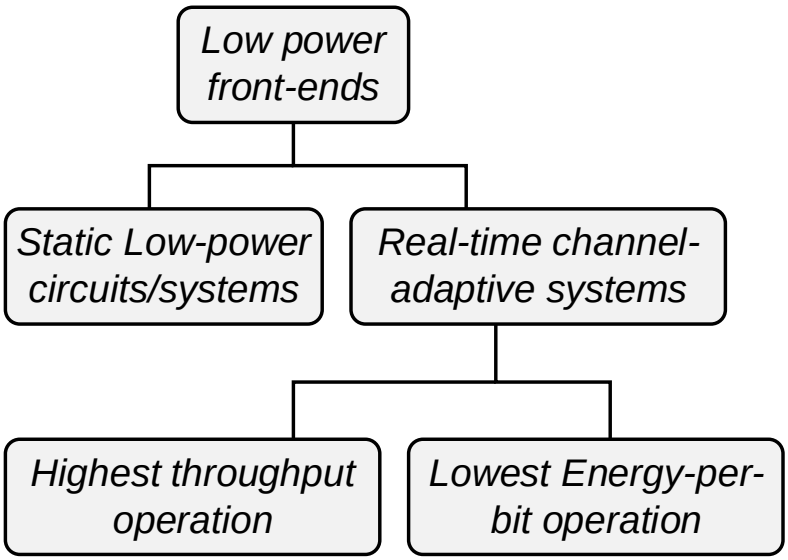

Figure 28: Classification of low-power techniques for radio front-ends.

can work in multiple low power modes depending upon the throughput requirements of the system to either optimize power consumption or the energy-per-bit in the system. The work demonstrates this for both transmitter and receiver in both simulation and hardware experiments.

2. Moreover, prior work has demonstrated channel-adaptation for single-input-single-output (SISO) systems. However unlike SISO systems, the presence of multiple-modes of operation in multiple-input-multiple-output (MIMO) RF systems results in different non-monotonically varying performance margins across different points of operation of a MIMO transceiver system. While the proposed concepts hold equally for a SISO systems, in this work we demonstrate use-aware adaptation for the test case of an environment-adaptive 2×2 MIMO transceiver as it seamlessly switches between multiple operational modes and modulation techniques depending on channel conditions to enable low power operation.

3. Prior work has not considered channel coding when demonstrating adaptive

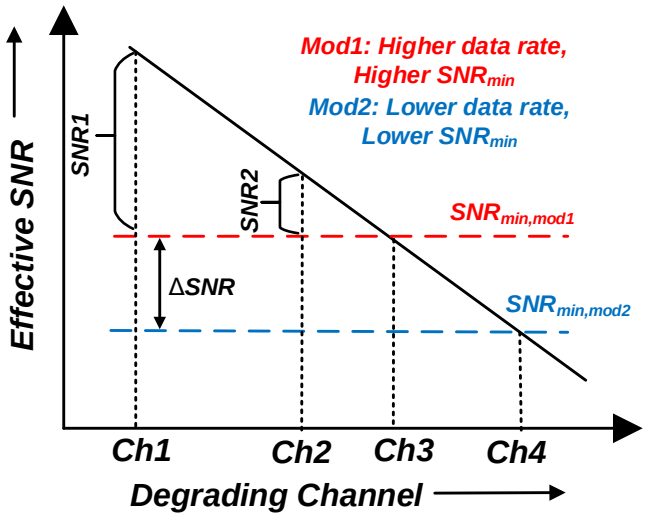

Figure 29: Effective SNR versus channel conditions with SNR margins.

systems. This work implements adaptation while switching between coding rates, modulation and different MIMO modes to show the benefits and trade-offs in power savings, energy-per-bit and throughput for different low-power adaptation modes.

3.2 Problem Formulation

To explain the need for use aware adaptation let us consider the operation of a adaptive RF front-end operating over a range of channel conditions. Here the word "channel" signifies the sum total of electromagnetic effects affecting the communication signal between the process of transmission of signal at the transmitter antenna(s) to the reception of the signal at the receiver antenna(s). Every particular channel condition results in an effective signal to noise ratio (SNR) due to combined signal degradation in channel and front-end combination. Thus when the channel is good available SNR is much more than the minimum required SNR (SNR_{min}). In such a case the front-end could be degraded to reduce power consumption while operating at the required maximum BER (BER_{max}) or EVM threshold (EVM_{th}). It must be

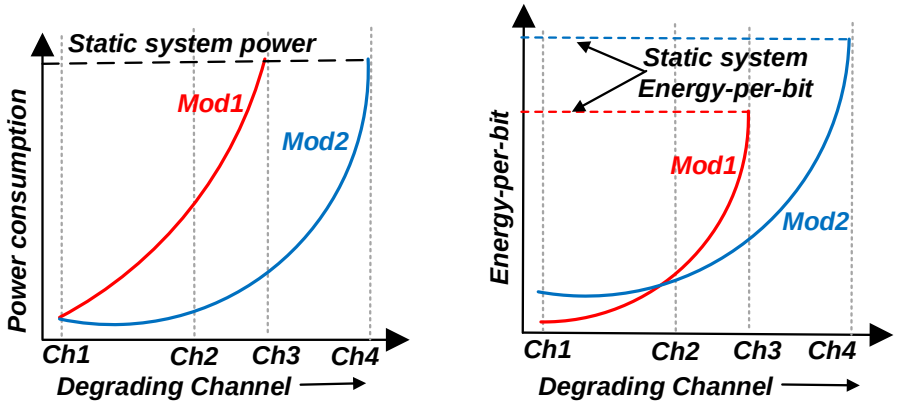

Figure 30: Power consumption and energy-per-bit with different channel condition.

noted that the relationship of the power savings to the SNR slack ($SNR - SNR_{min}$) is highly non-linear. Also, let us assume that the receiver be capable of operating in two different data rates Mod1 (high throughput) and Mod2 (low throughput). The two data rates have different minimum SNR requirements, $\text{SNR}_{min,Mod1}$ and $\text{SNR}_{min,Mod2}$ respectively. A higher data rate requires a higher fidelity signal and hence $SNR_{min,Mod1} > SNR_{min,Mod2}$. This situation is illustrated in Figure 29. Now let us consider the different illustrative channel conditions Ch1-Ch4 shown in Figure 29.

As shown in the figure for a good channel (Ch1) there is a lot of SNR margin (SNR1 for Mod1 and SNR1 + ΔSNR for Mod2) and hence the front-end can be degraded to a low performance-low power mode. The front-end can continue to operate in Mod1 (higher data rate) upto Ch3 (where SNR=$\text{SNR}_{min,Mod1}$) . However as channel degrades to Ch2 the SNR margin for Mod1 has decreased to SNR2 (low) while the margin for Mod2 (SNR2 + ΔSNR) is still relatively high. Thus, at this channel condition, with Mod1 operation the front-end cannot be degraded much, resulting in very high power consumption (shown in Figure 30). However for Mod2 operation significant SNR margin still exists and the power consumption can be made significantly lower through front-end degradation.

Now let us consider the metric energy-per-bit for the front-end. Energy-per-bit is defined as:

$$Energy - per - bit = \frac{Power\ consumption}{Throughput}$$

Energy-per-bit is an effective measure of how much energy the front-end spends to transmit or receive a fixed amount of data. The lower the energy-per-bit the longer the battery life of a device. For traditional systems (power consumption remaining constant), a low energy-per-bit necessitates a high throughput. Thus the best strategy is to operate at the highest data rate possible. However, this strategy is not necessarily optimal for modern adaptive systems which have adaptive power consumption. This is because energy-per-bit is no longer a sole function of the throughput. Assuming a SISO front-end in this case:

$$Power\ consumption = f(SNR, SNR_{min}) \tag{31}$$

where,

$$SNR_{min} = g(Modulation) \tag{32}$$

$$SNR_{min} = k(Channel,\ frontend\ configuration) \tag{33}$$

Again,

$$Throughput = T(Modulation) \tag{34}$$

Here f, g, k and T are functions which depend on the channel, front-end and protocol level parameters. A device may have relatively low energy-per-bit while operating at a low throughput (if power consumption is low). For our example, as shown in Figure 30 the crossover point for energy-per-bit occurs at or before Ch2. Thus although operating in Mod1 at Ch2 would ensure a higher throughput, switching to Mod2 at or before Mod1 would lead to a lower energy-per-bit.

Thus the above example illustrates that depending on the constraints on data throughput, the low-power operation can optimized in multiple ways. We formalize two different low-power modes as the following:

1. Data Priority (DP) mode: In certain applications the data rate is of prime importance. For example in a video or voice call the degradation in data rate may cause a drop in call. Hence in this mode the mandate is to:

- a. Ensure that the system operates always at the highest possible data rate for the given channel condition.
- b. Excess SNR is traded off for lower power consumption in the front-end while ensuring condition (a) is satisfied.

This mode would lead to the highest possible throughput. However the energy per bit of the data may not be optimal across all possible channel conditions.

2. Energy Priority (EP) mode:

In contrast with DP mode, there are certain applications where data rate is not of prime importance. These applications include background downloads of updates on mobile devices and synchronization of data across cloud platform devices. In these applications since the restriction on data rate is relaxed the same can be optimized to obtain lowest energy per bit of the RF front-end. This ensures that the battery lifetime is extended for the longest possible time. This is called the Energy priority mode. Figure 31 shows the operational boundaries for the two different modes for the example discussed earlier.

3.3 MIMO modes and performance margins

One of the primary reasons for the commercial success of MIMO systems is that they provide the flexibility to operate in both Spatial Multiplexing (SM) [16] and Spatial Diversity (SD) [17] Mode. In SM Mode, MIMO systems transmit two parallel data

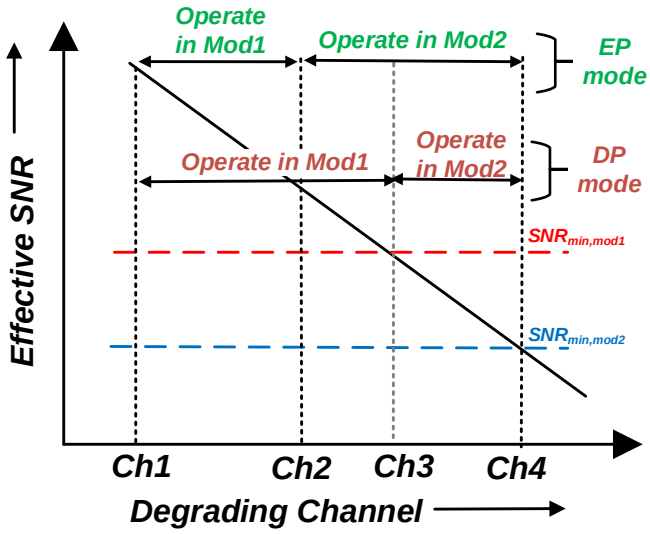

Figure 31: MIMO Data Rates and Switching Order .

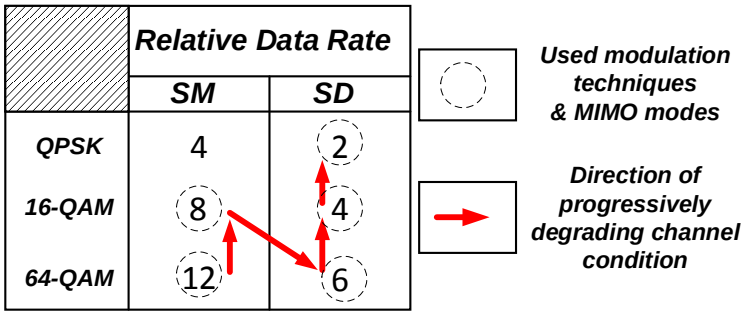

Figure 32: Switching points for different modes.

streams over the two spatially separated antennas thereby doubling the data rate over the same frequency bandwidth. When the wireless channel degrades, SM operation fails to meet system level performance specifications (BER_{max}) for values of the SNR metric below a predetermined level. Consequently, the MIMO system switches to SD mode of operation which can support lower SNR values while operating at an effective data rate of a SISO system. During the operation of the transceiver in each of these modes the higher protocol layers adaptively change the modulation technique (and channel coding rate) depending on the channel SNR so as to always transmit at the maximum data rate possible. This is shown in Figure 32.

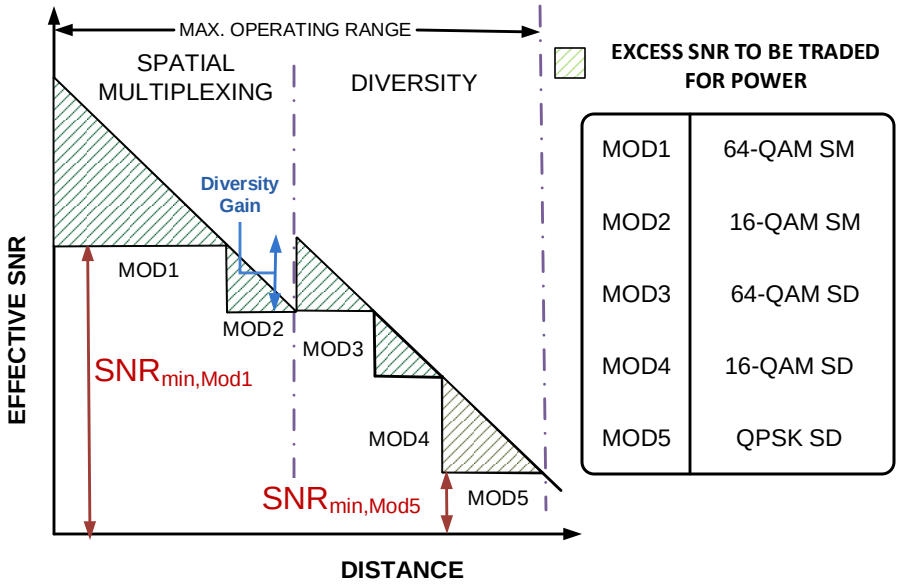

Figure 33: MIMO Operation and Performance Margins.

Figure 33 shows the effective SNR versus distance plot, annotated with SNR margin required for each mode and modulation technique used. As evident the SNR reduces with degrading channel conditions (for e.g. due to distance). For the best received SNR the system operates at the highest data rate possible and remains in this mode till the signal strength is just sufficient to support the the minimum required SNR to maintain an acceptable BER (SNR_{min}) for this mode of operation. Thereafter it switches to a mode having a lower data rate and hence a lower SNR_{min}. While switching between modes the system follows the order shown in Figure 32. However, as shown in Figure 33, even after adaptive modulation a significant signal margin (hatched region) is available which is not exploited by modern front-ends to reduce power consumption. It can be seen in Figure 33 that at the point of switching from SM to SD mode or from one modulation technique to the other, the effective SNR margin ($SNR - SNR_{min}$) is increased by the diversity gain due to the fact that signals are combined in SD mode or due to reduction in SNR_{min}. This provides further headroom for trading-off power versus performance in the MIMO architecture. By

carefully tracking the channel conditions we propose to achieve "Zero-SNR-margin" operation at ultra-low power levels. In this work we demonstrate that such adaptive low-power operation can be achieved in two separate modes as discussed in Section 3.2, with each of these modes catering to a different throughput requirement.

3.4 Adaptation methodology

3.4.1 Adaptation Metric

In order to trade-off power for performance it is necessary to determine the threshold of acceptable operation (or maximum acceptable BER) during the real-time operation of the device. However a large number symbols is required to calculate BER accurately and hence is not amenable for real-time feedback system. EVM requires significantly less time to determine from received symbols and is thus more suitable as a real-time metric for system-level performance. Thus, EVM which has a strong correlation with BER, is used as a metric. EVM is defined as:

$$EVM = \sqrt{\frac{1}{N}\frac{\sum_{i=1}^{N}||y_i - x_i||^2}{||x_{max}||^2}} \tag{35}$$

Here y_i and x_i are received and transmitted complex data in $(I + jQ)$ form, x_{max} is the transmitted outermost constellation point and N is the total number of symbols received. The relation between EVM and BER (P_b) for an M-QAM system with only AWGN noise is as follows [73]:

$$P_b = \frac{2\left(1-\frac{1}{L}\right)}{log_2 L} Q\left[\sqrt{\left(\frac{3log_2 L}{L^2-1}\right)\frac{2E_s}{N_0 log_2 M}}\right] \tag{36}$$

$$P_b \approx \frac{2\left(1-\frac{1}{L}\right)}{log_2 L} Q\left[\sqrt{\left(\frac{3log_2 L}{L^2-1}\right)\frac{2}{EVM_{RMS}^2 log_2 M}}\right] \tag{37}$$

where, $L = M^{(\frac{1}{2})}$ is the number of levels in each dimension of the M-ary modulation system, $\frac{N_0}{2}$ = noise spectral density, E_s=signal energy per symbol=$E_b log_2 M$ and $Q[.]$ is the Gaussian co-error function as defined in [74]. Since, $Q[]$ is an monotonically

decreasing function of its argument, BER increases with increase in EVM. Note that, EVM successfully captures all non-idealities in the channel and transceiver. It has been shown in [35, 71, 36] that a limit on the BER for a modulation rate translates to a threshold on the corresponding EVM. Prior work in [36] shows that for an acceptable maximum BER threshold of 10^{-4} the EVM thresholds for 64-QAM, 16-QAM and QPSK are 5%, 14% and 33% respectively.

3.4.2 Optimum tuning knob selection

In order to always operate at this EVM threshold, the specifications of the front-end must be adaptively varied with time. To achieve this, the RF front-end modules like LNA, Mixer, ADC and PA are designed to have tunable specifications such as Gain, IIP3, ADC resolution and P1dB. In the proposed methodology, the entire gamut of channel conditions is partitioned into a finite number (say m) of representative channels. In the design and characterization phase of the system a combination of tuning knob settings is found for each of the m channels such that, the Error Vector Magnitude (EVM) is maintained at threshold (EVM_{th}) of acceptable operation while the power is minimized. These combinations are stored in the form of a mn table (where n is the number of tuning knobs). The table is then stored on-chip. During real time operation the EVM of the system is constantly monitored and a control algorithm running on the baseband processor continuously attempts to maintain the EVM at EVM_{th} by changing the tuning knob settings using the stored LUT (Figure 34). For minimum power operation, the EVM of received constellations is monitored in real-time and performance such as gain, noise figure and linearity of the MIMO receiver is dynamically traded off for power consumption using a feedback control loop such that EVM is maintained close to (but below) EVM_{th}. Since this optimization is a one-time exercise performed during the design phase the complexity or time involved for this procedure is not a major concern.

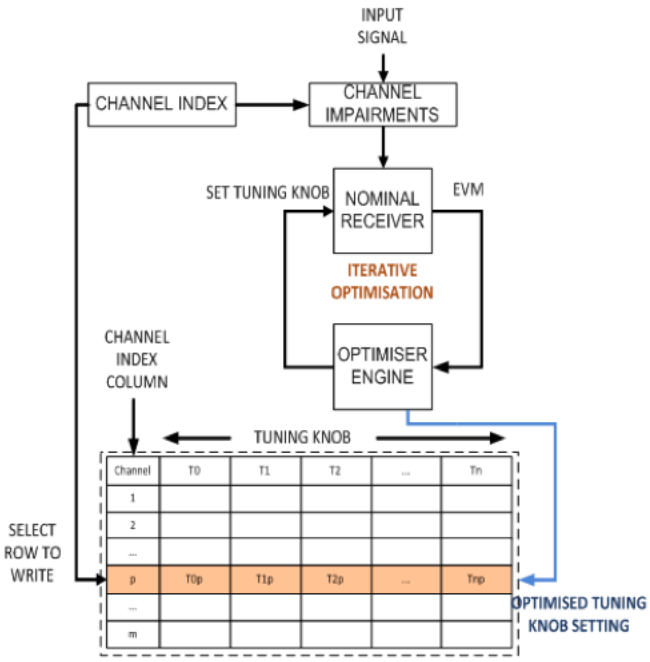

Figure 34: Offline characterization phase optimization .

The problem of finding a tuning knob combination for a given channel condition for near-zero EVM margin operation is a constrained global optimization problem. One approach to solve such an optimization problem is to use a multi-start constrained optimization [16]. In this approach multiple points (say k) in the n-dimensional search space are generated which comply with the constraints of the problem (EVM <EVM_{th} for this case). Each of these points is then used as a starting point by a local optimizer to converge to a local basin of attraction. Thus at the end of the process a list of minima is obtained, each minima corresponding to a different starting point. If sufficient number of starting points is selected then it can be stated with a high confidence that the minimum of the local minima so obtained is the global minima. This work utilizes this approach to solve for the minimum power point. For a system with tuning knobs $T = [T_1, T_2, ..., T_N]$, power consumption PDC, EVM and given channel condition Ch, our goal is to:

$$Minimize\ PDC = f(T)\ \ s.t.\ EVM(= g(T, Ch)) < EVM_{th}$$

Here we assume that the each tuning knob T_p (p=1 to N) has multiple states separated by an increments of Δ_p. Let the final optimized tuning knob combination be called T_{opt} and the optimized power consumption as $P_{DC,opt}$. Also, we shall refer to the value of the p-th tuning knob after the q-th iteration as $T_{p,q}$. Let there be nstart number of starting points. The pseudocode for the above optimization for the channel condition Ch is as follows:

$for\ (g = 1\ to\ nstart)$

$choose\ T_0 = [T_{1,0}, ..., T_{N,0}]$

$iter = 1$

$while\ (|EVM - EVM_{th}| > \epsilon\ and\ iter < maxIter)$

$Calculate\ grad(j) = \partial P_{DC}/\partial T_{j,iter-1}$

$Choose\ 'm'\ s.t.\ abs(grad(m)) = max\{|grad(j)|, j = 1toN\}$

$T_{m,iter} = T_{m,iter-1} + \Delta_j \times sign\{-\partial P_{DC}/\partial T_{m,iter-1}\}$

$T_{j,iter} = T_{j,iter-1}\ forj \neq m$

$T_{iter} = [T_{1,iter}, ..., T_{N,iter}]$

$EVM = g(T_{iter}, Ch)$

$P_{DC} = f(T_{iter})$

$iter = iter + 1$

$end\ while$

$T_{save}(g) = T_{iter},\ P_{save}(g) = P_{DC}$

$end\ for$

$P_{DC,opt} = min\{P_{save}(1), ..., P_{save}(nstart)\}$

$T_{opt} = T_{save}(k),\ s.t.\ P_{DC,opt} = P_{save}(k)$

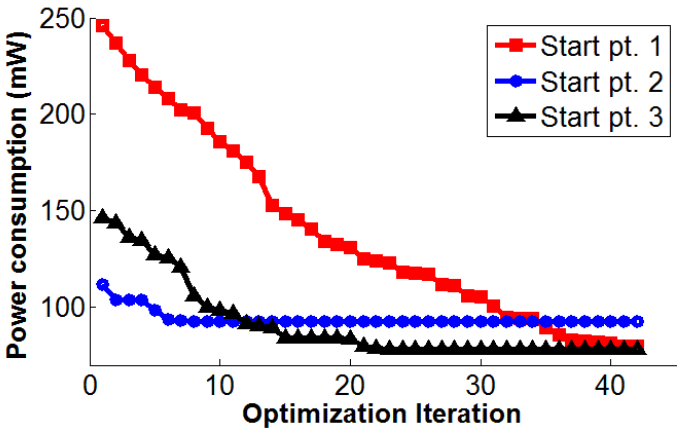

Figure 35: Convergence of multistart optimization.

The optimization is carried out in the off-line characterization phase of the device. Since it is not done in real-time, the time to convergence is not a critical criterion to evaluate the effectiveness of the algorithm. Moreover the algorithm must work with discretely spaced values of the tuning knob variables (since in practice only discrete states of the bias, supply and other tuning knob values is implementable). Considering these requirements a gradient search algorithm is chosen as the local optimizer for the algorithm. The multi-start technique serves to increase the confidence of finding the global optimum to a large extent. The starting points are chosen at random (while satisfying the EVM constraint). The nominal operating knob combination (corresponding to the highest power consumption) is always included as a starting point. The convergence of power for a particular channel condition with three starting points for the system described in Section 3.5.1 is shown in Figure 35.

3.5 Transceiver Adaptation

3.5.1 Receiver adaptation

3.5.1.1 System Description

The system considered here is a 2×2 WiMAX MIMO OFDM transceiver operating at 2.4 GHz. In this system, the modulation schemes used are 64-QAM, 16-QAM and

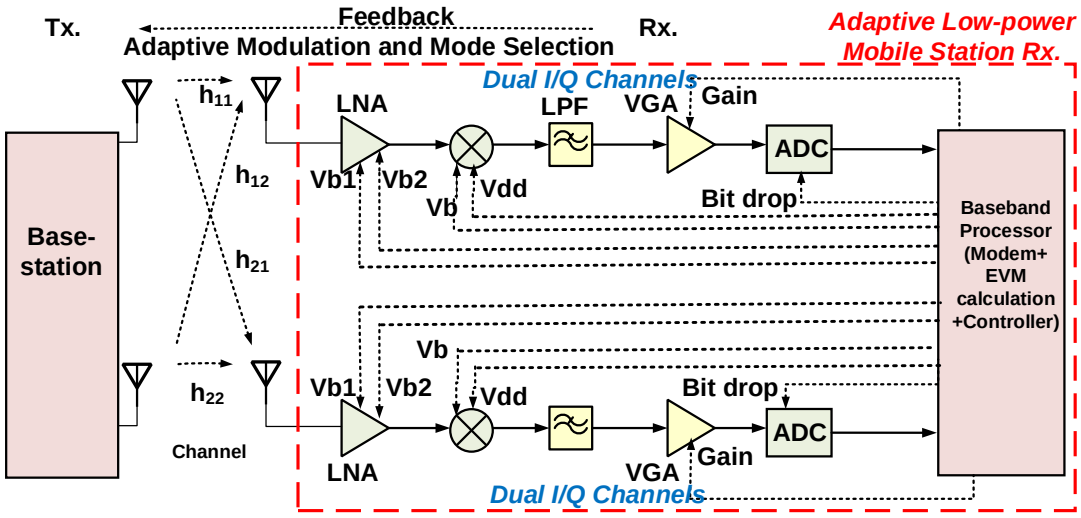

Figure 36: Adaptive MIMO receiver RF front-end.

QPSK. The transmitter is modeled as transmitting with a fixed power level throughout the course of operation. As shown in Figure 36 there is a feedback information path from the receiver to the transmitter which enables adaptive modulation and adaptive MIMO modes.

3.5.1.2 Tunable circuit design and system model

The receiver incorporates 2 chains, each with an LNA, Mixer and ADC. The output of ADC feeds to the baseband unit. For simulating the system the tunable circuit elements (except the ADC) are designed and simulated at the SPICE level, their behavioral models are extracted and subsequently used in MATLAB to perform complete system simulation.

- **LNA:** The LNA has been designed to have the Gain-NF and the linearity to be orthogonally tunable to each other [35]. This LNA is used as a tunable front-end block in the receiver chain. Figure 37 shows the design and layout and Figure 38 shows the current consumption across tuning knobs for the LNA. The LNA has 2 tuning knobs V_{Gain} and V_{IIP3} which are used to change the gain-NF and linearity of the LNA almost independent to one another. This also results in

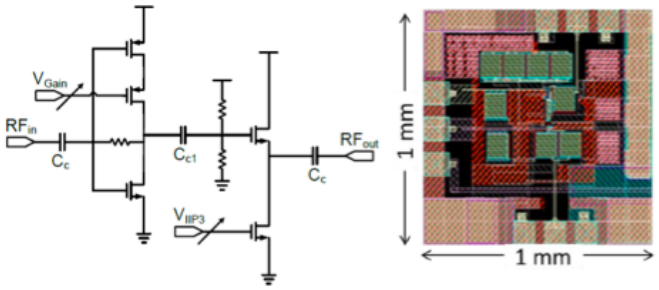

Figure 37: Schematic and layout of orthogonally tunable LNA .

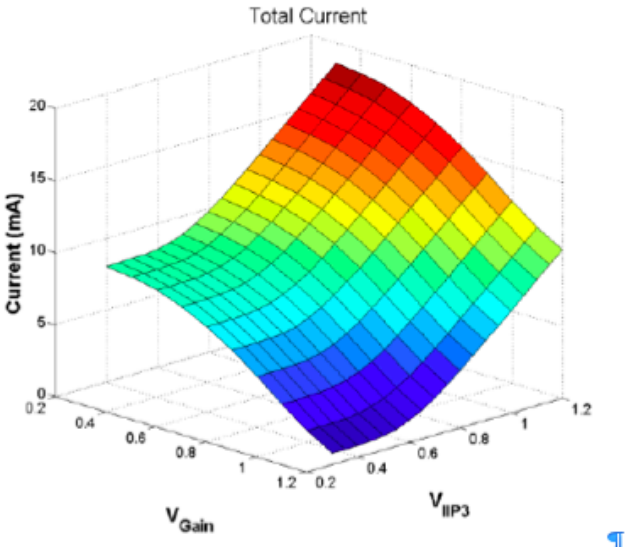

Figure 38: Current consumption across tuning knob combinations.

significant variation in current across the tuning knob space, from a maximum of 18.5 mA (lowest NF, highest linearity) to a minimum of 0.76 mA (highest NF, lowest linearity).

- **Mixer:** A tunable Gilbert-cell mixer with 2 tuning knobs (V_T and V_{dd}) is used (Figure 39). The two bias voltages can be used to trade-off Gain-NF versus Power. It has a maximum gain of 11.84 dB and an IIP3 of 21 dBm. The maximum power consumption is 33.75 mW.

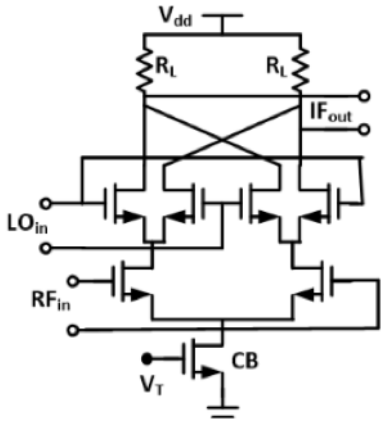

Figure 39: Tunable mixer schematic with V_T and V_{dd} as tuning knobs .

- **ADC:** An 10-bit ADC is implemented with a capability to reduce power by reducing resolution through bit-dropping. The power consumption is modelled to scale linearly with the number of bits dropped.

  The channel is modeled to have attenuation due to Path Loss (PL), noise floor and multipath fading characteristics. The current channel model consists of the following components:

  - *Path loss (PL):* Relatively slow changing signal attenuation with distance of the mobile station (MS) from the base station (BS). If d is the distance between the BS and MS antennas then: $PL \propto d^{(-n)}$ where $n \approx 2.5 - 3$ depending on atmospheric conditions.
  - *Noise Floor:* The channel is modeled to have fixed additive white Gaussian noise (AWGN) floor.
  - *Non-Line of Sight (NLOS) multipath fading:* In an urban environment there is no direct line of sight path from the base-station to the mobile-station. In such an environment multiple reflected indirect signal paths are summed at the antenna to get the effective signal. This can be modelled as a signal whose amplitude has a Rayleigh distribution. Such a Rayleigh

faded attenuation is much more rapidly changing than path loss because small variations in position of the antenna causes changes in the phases of the summing signals.

A key assumption here is that fading does not change significantly over the duration of a packet. The system is designed to track the effective attenuation due to different channel impairments. Each of the h parameters (shown in Figure 36) follows a similarly distributed (but not temporally identical) fading channel. Modern radio front-ends already have sophisticated sensors/circuits and baseband algorithms built-in to evaluate the magnitude of channel impairments like effective path loss and interferer strength. Two such widely-used metric is Received Signal Strength Indicator (RSSI) and Received Channel Power Indicator (RCPI), which gives an estimate of the in-channel power received and hence the total attenuation from the channel. Given the strength of the transmitted signal (usually specified by standard and hence is known in advance), the path loss can be computed.

3.5.1.3 Receiver adaptation results

In order to demonstrate channel adaptive low-power operation we must identify the EVM margins that inherently exist in the MIMO RF front-end. Figure 40 shows the working of a static MIMO RF system across varying channel conditions. For a given MIMO mode (say SM 16-QAM) as PL increases, the SNR degrades resulting in a reduced EVM margin. This continues until the EVM is equal to EVM_{th} for that MIMO mode. If the PL increases any further, the system must switch to a lower data rate (SD 64-QAM in this case) to operate within the maximum BER constraint. Let us denote the PL at which a system switches from i-th mode to the (i+1)-th mode to be PL_i. The maximum EVM margin for a particular mode occurs at the switching point between the previous (higher data rate mode) and the particular

mode considered. This is because switching from a higher data rate to a lower data rate opens up new SNR headroom through:

- reduction in SNRmin requirement across modulation rates and hence an increase in EVM threshold (EVM_{th})
- an increase in effective SNR (when switching from multiplexing to diversity).

Thus the maximum power savings can be achieved at this point of transition PL_i. Figure 40 shows the variation of EVM as Path Loss increases from 90dB to 150dB. The graph also shows the EVM_{th} for different modulation techniques. The difference between the EVM at any PL and the EVM_{th} for the modulation technique used at that PL gives the EVM margin for that PL. As shown in Figure 40 , the system switches between different modes and modulation techniques in the sequence illustrated in Figure 32. The EVM margin at a particular PL is a key indicator of how much power can be saved at that particular PL. We next analyze and present the results for the two modes of low-power operation.

i) Data Priority (DP) Low-Power Mode: In this mode the system operates at the highest data rate possible at any particular channel condition. Hence the EVM margins illustrated in Figure 40 are traded-off for power using a multi-dimensional constrained optimization algorithm discussed in Section 3.4B. Figure 41 shows the optimized power consumption versus the PL for the MIMO RF front-end. It can be seen from Figure 41 that the maximum power consumption takes place at those values of PL where EVM is nearly equal to EVM_{th}. That is maximum power consumption occurs when the channel is just good enough to sustain a certain communication mode and thus the block level specifications of the receiver components cannot be degraded any further. The channel-adaptive receiver leads to 3× power savings over a static-receiver.

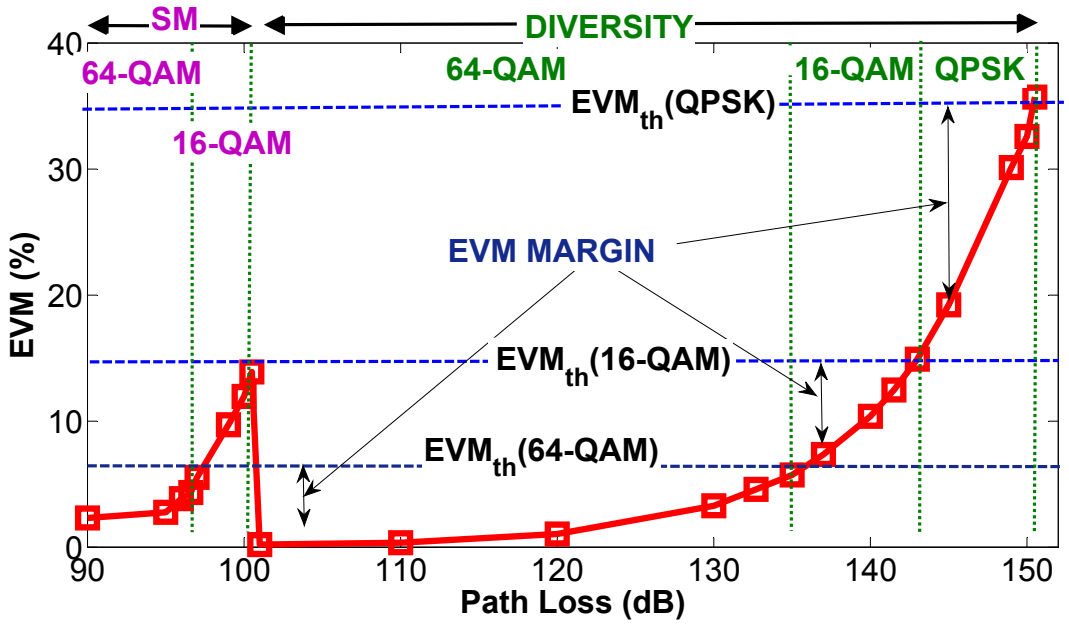

Figure 40: EVM values for a nominal receiver over different Path Loss .

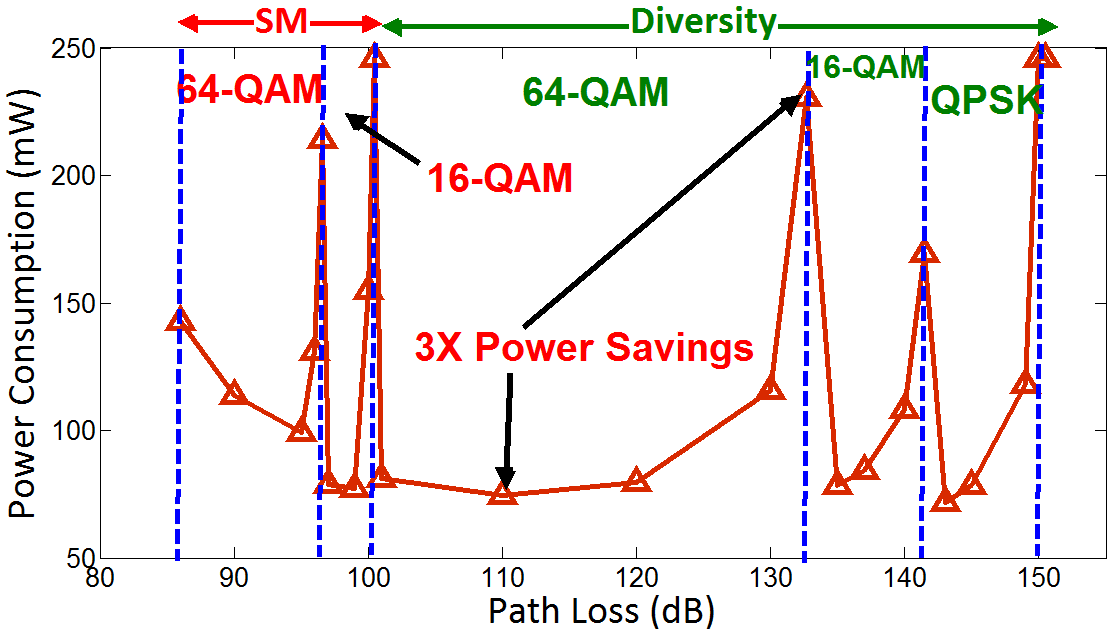

Figure 41: MIMO Receiver Power consumption in DP mode .

ii) Energy Priority (EP) Low-Power Mode: In Energy Priority mode the restriction to operate at the highest data rate is relaxed. The energy-per-bit in a MIMO system is proportional to a metric M defined as follows:

$$M = \frac{Power}{Bits\ per\ Symbol * Multiplexing\ factor} \tag{38}$$

Here bits per symbol is $log_2(x_i)$ where x_i = 64, 16 or 4 depending on whether the modulation used is 64-QAM,16-QAM or OPSK. In this work, in order to achieve lowest Energy per bit the metric M has been be minimized in the EP mode.

Let P_{kj} be the optimized power consumption for the k-th communication mode for the j-th channel condition. Then for the j-th channel the mode of operation should be such that the optimum proxy metric M is achieved, i.e.

$$M_{opt,j} = min(\{P_{kj}/(b_k * m_k)\}) \tag{39}$$

Here b_k is the bits per subcarrier in an OFDM system and m_k is the multiplexing factor (1 for SD and 2 for SM). However P_{kj} is a very complicated non-linear function of channel conditions and the power versus tuning knob profile of the individual blocks in the receiver. Moreover power consumption and bit rate do not scale linearly. Thus the approach adopted for the optimization is to plot the metric M for all communication modes over the entire gamut of channel conditions. This is shown in Figure 42. The power consumption is optimized for the MIMO front-end for all modes of operation over the set of discrete PL conditions spanning the entire gamut of channels. Thereafter the corresponding values of M are plotted. The value of M for a operational mode (say SD 64-QAM, i.e. point "A" in Figure 42) peaks sharply near the boundary of its operation (PL=135 dB) i.e. where EVM =EVM_{th}. Near these points the M values for this mode of operation are higher than the next lower mode (i.e. SD 16-QAM). Thus although it is possible to transmit at the higher data

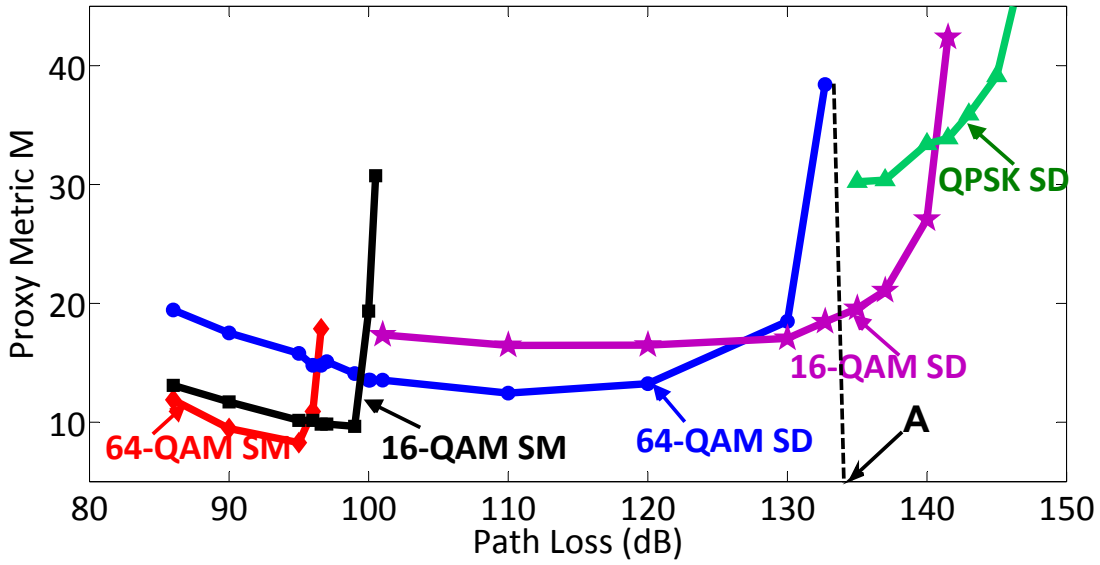

Figure 42: Proxy metric (M) over channel conditions for different MIMO mode .

rate near this boundary, in order to have the lowest energy per bit it is required to switch to a lower data rate. In summary, EP mode is achieved by following the curve having the trajectory of lowest M value at any point of time (in Figure 42) at any particular path loss.

Figure 43 shows the plot of M versus the quantized channel index for both EP and DP modes of operation. Each of the discrete PL points, for which the front-end is optimized, is a channel condition and can be denoted by a channel index. The highest channel index corresponds to the maximum PL and hence the worst case channel. Similarly, the lowest Channel index corresponds to the lowest PL and hence the best case channel. EP mode can save upto 2× energy per bit over the DP mode. The penalty is paid in terms of data throughput. The relative throughput of both modes versus the channel index is shown in Figure 44. It is seen that for certain channels EP mode can be 1.5×slower than the DP mode.

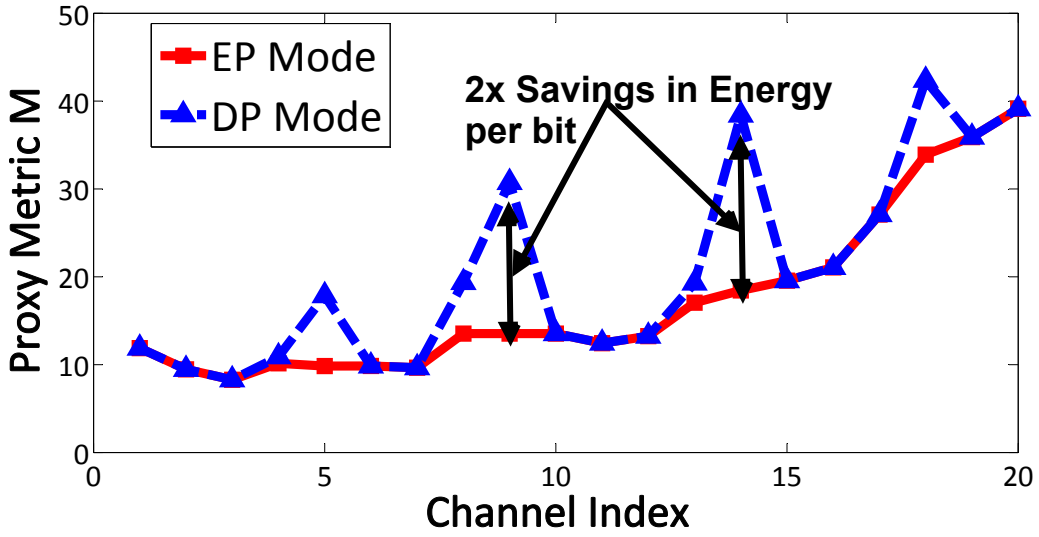

Figure 43: Relative Energy per bit comparison between EP and DP mode.

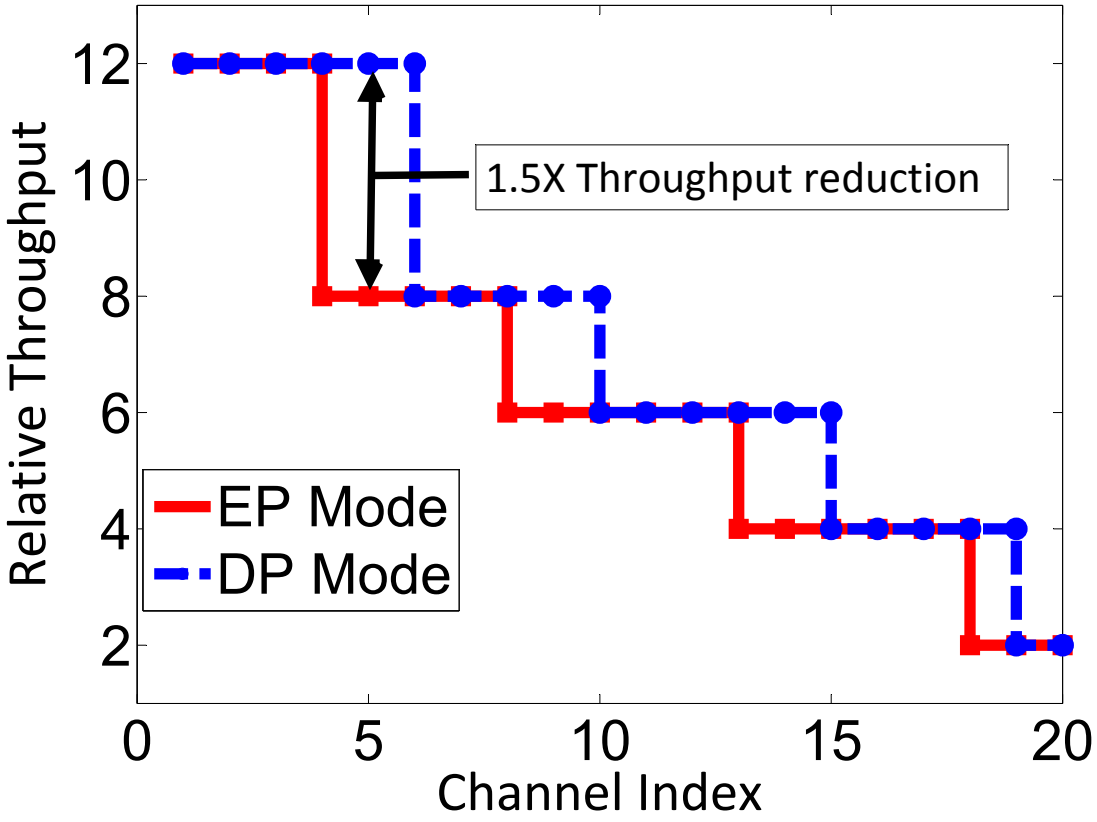

Figure 44: Relative throughput comparison between EP and DP mode.

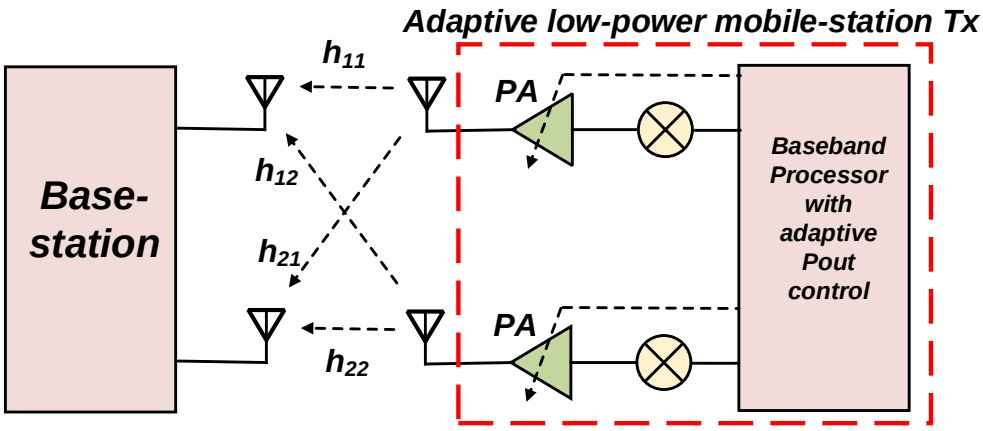

Figure 45: Adaptive low-power MIMO transmitter.

3.5.2 Transmitter adaptation

3.5.2.1 System Description

Figure 45 shows the schematic for a MIMO transmitter front-end with tunable power amplifiers. The power amplifier (PA) is one of the most power-hungry blocks in the system. Requirement for large output power and high linearity in the PA means that the power consumption is very high. However the highest power consumption of the PA often corresponds to the highest output power and highest linearity (we take P1dB as metric of linearity) of the PA. This peak performance is only required for the worst case channel. For other channels (when the effective SNR is more than the minimum required SNR) the output power can be reduced. This in turn reduces the linearity requirement of the PA. Thus if the PA can be reconfigured to operate at a lower linearity (shown in Figure 46) along with output power back-off, significant savings in d.c. power consumption can be achieved.

3.5.2.2 Tunable PA design and system model

An adaptive PA (2.4GHz, 16 dB gain) has been designed in TSMC 0.25μ CMOS process for single-stage class A operation (Figure 47). The operating point trajectory for changing gate and drain bias voltages is shown in Figure 48. Lower values of

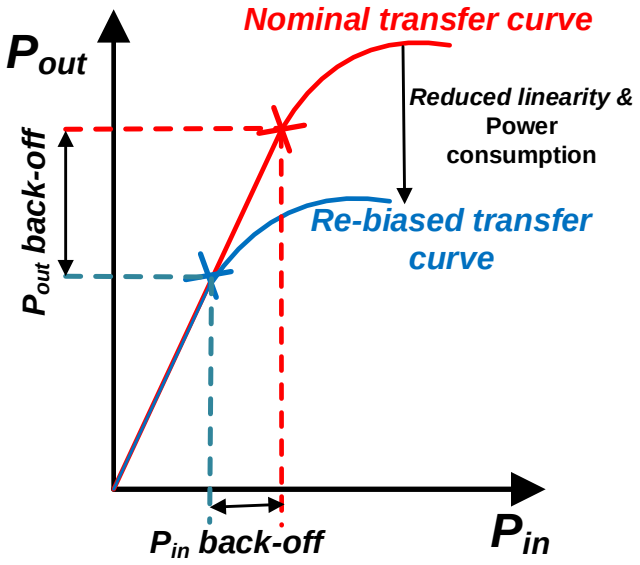

Figure 46: Power back-off and re-biasing in PA.

biasing points reduce the signal swing, in turn reducing P1dB. But this reduction in P1dB allows reduced DC power consumption in the PA. Hence, depending on the channel conditions when high P1dB is not required, the PA can be operated at lower power consumption levels without compromising linearity.

The variation in PA power consumption with changing linearity P1dB is shown in Figure 49. The channel model used in these simulations is the same as for the receiver adaptation case discussed in Section 3.5.1. The behavioral model of the

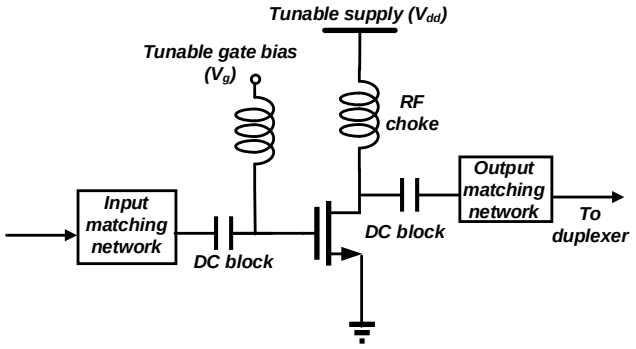

Figure 47: Adaptive class A PA circuit.

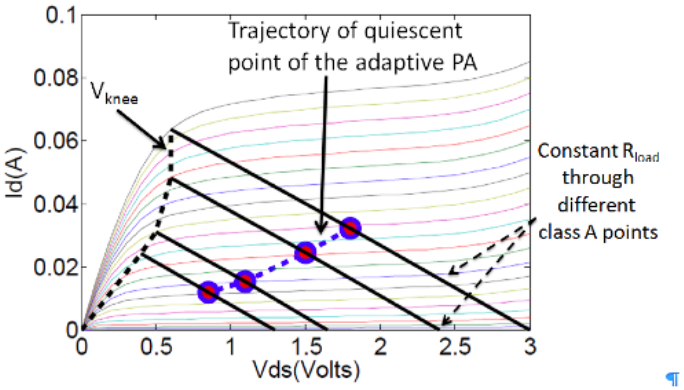

Figure 48: PA operating point trajectory.

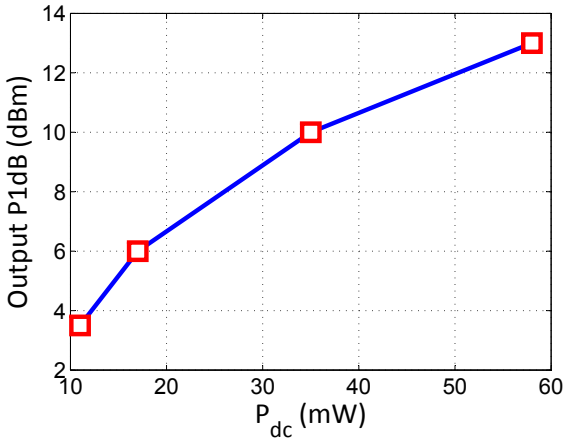

Figure 49: Power consumption versus Linearity of the PA

PA is extracted from circuit simulations and used in MATLAB for complete system simulations.

3.5.2.3 Transmitter adaptation results

The transmitter system is optimized for both highest throughput low-power operation (DP mode) and lowest energy-per-bit-mode (EP mode). As shown in Figure 50 across degrading channel conditions the relative energy-per-bit (quantified by the quantity M described in equation 38) in DP mode can be upto 4× larger than in EP mode. The savings in energy-per-bit comes at the cost of reduced throughput of up to 2× as shown in Figure 51. Thus, depending on the throughput requirements of

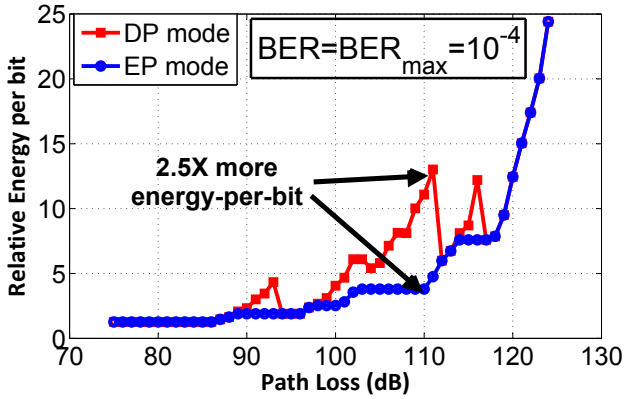

Figure 50: Relative energy-per-bit (M) across different channel conditions for adaptive transmitter for EP and DP modes.

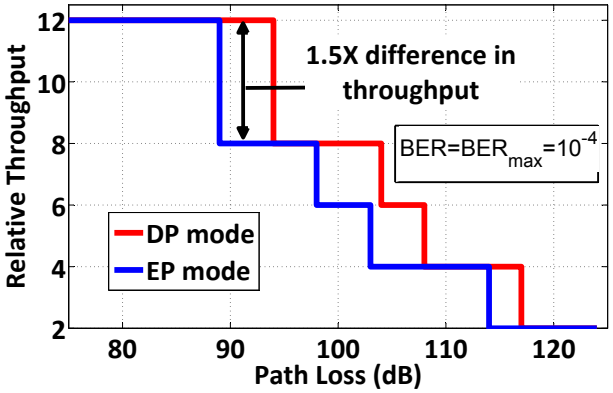

Figure 51: Relative throughput across different channel conditions for adaptive transmitter for EP and DP modes.

the application accessing the RF transmitter front-end different low-power strategies could be adopted to prioritize either throughput or energy-per-bit.

3.5.3 Effect of Coding Rate

So far, in this work it has been assumed that the front-end adapts its power consumption, while switching between MIMO modes and modulation techniques. Thus variation in throughput is due to change in MIMO modes and modulation techniques

only. However in addition to the above, modern communication systems employ coding techniques [75] to lower the SNR_{min} for a given BER and modulation technique. Through coding redundant bits are added to the transmitted data stream so that these could be used for error correction at the receiver. Thus for certain channel conditions for which the BER (without coding) was above the maximum acceptable value (BER_{max}), could have BER at or below the BER_{max} with coding. This is equivalent to a gain in SNR due to coding. However since additional bits need to be transmitted in excess of the information bits, coding leads to a degradation of the throughput of a system. In this section we demonstrate that the proposed DP and EP modes of adaptation can lead to significant savings even when coding is considered in addition to the MIMO modes and modulation techniques. We demonstrate this with the help of a MIMO transmitter, but the results hold for SISO and MIMO transmitter and receiver systems.

In order to determine the effect of coding rate on the BER of a system, the BER of an OFDM system in AWGN channel is studied for QPSK for different coding rates. The coding has been implemented with the help of a convolutional encoder with a constraint length of 7 to get a code rate of $3/4, 2/3$ and $1/2$. Code rate is defined as follows:

$$Code\ rate = \frac{Information\ bits\ transmitted}{Total\ bits\ transmitted} \tag{40}$$

Therefore to transmit every 10 information bits, 20 bits are to be transmitted to achieve a coding rate of 1/2. This leads to significant SNR gain over the uncoded data stream. The rates 2/3 and 3/4 are achieved by "punctured coding" which involves dropping a fraction of the extra bits added by the encoder, thereby boosting the effective throughput at the cost of a reduced SNR gain. a software-controlled adaptive coding and decoding system can be implemented as shown in Figure 52 Initially a convolutional encoder encodes the raw data to a rate 1/2 code. Thereafter

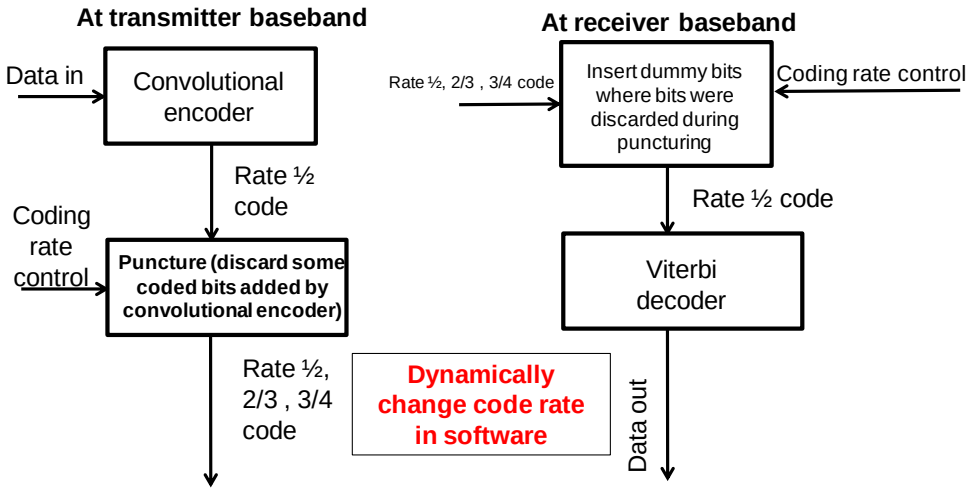

Figure 52: Implementation of software controlled dynamic coding rate selection

depending upon the desired coding rate some bits appended by the convolutional encoder is dropped. At the receiver end the baseband processor inserts dummy bits in place of the bits dropped to get a 1/2 rate code. Thereafter a viterbi decoder decodes this 1/2 rate code to extract the original raw data transmitted. The BER vs. SNR plot for QPSK modulation techniques is shown in Figure 53. For QPSK, at a BER of 10^{-4} a code rate of 1/2 gives 6 dB coding gain over the uncoded stream. Rate 2/3 and 3/4 have higher effective throughput than rate 1/2 code but provide less SNR gain. Similar results can be observed for 16-QAM and 64-QAM.

Due to the SNR gains of different coding rates, the EVM_{th} for these coding rates also increase from the uncoded EVM_{th} . Figure 54 shows the simulation results for EVM_{th} for different modulation and coding rates for a BER of 10^{-4}. These EVM_{th} are used in system level simulations to demonstrate the efficacy of the DP and EP modes for a RF transmitter in a MIMO system (described in Section 3.5.2) in presence of coding gain. For the simulated system, Table 2 shows the possible choices of the MIMO mode, modulation technique and coding rate which are available to higher protocol layers and the baseband processor.

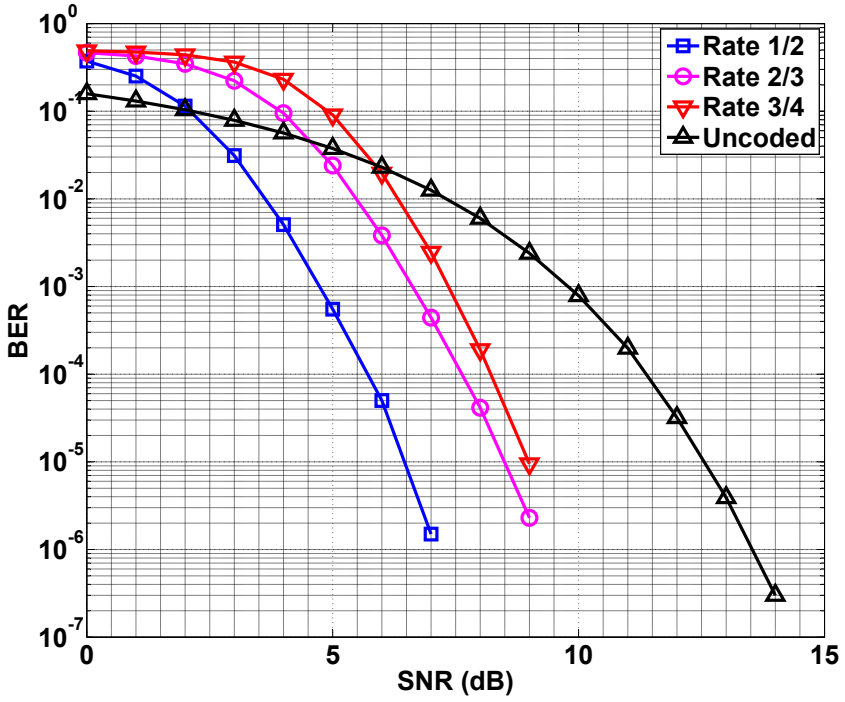

Figure 53: BER with SNR for different coding rates for QPSK.

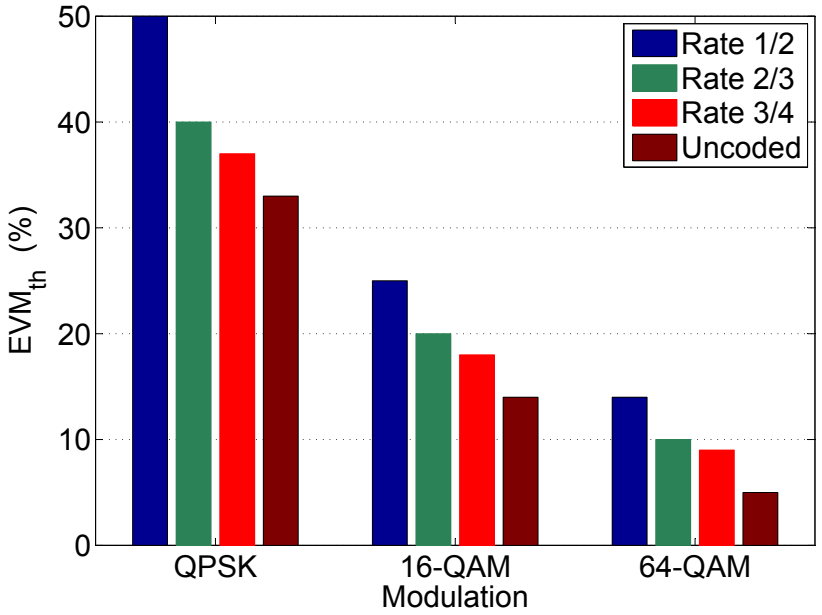

Figure 54: EVM_{th} for different coding rates and modulation techniques.

Table 2: Possible choices of mode, modulation and code-rate

MIMO mode	Modulation	Coding rate
SM	64-QAM	3/4
SD	16-QAM	2/3
	QPSK	1/2

Each combination of MIMO mode, modulation and coding rate has its own EVM_{th} and throughput. The relative throughput for all combinations has been tabulated in Table 3 arranged in decreasing magnitude. During optimization phase, for a channel condition the mode giving the highest possible throughput (DP mode) or lowest energy-per-bit (EP mode) is chosen. The resultant relative energy-per-bit is shown in Figure 55. The result has been compared to traditional front-ends which have a constant power consumption but variable throughput (channel dependent MIMO mode, Modulation and coding rate). It can be seen that DP mode performs worse than EP mode in terms of energy-per-bit. However DP mode has lower energy-per bit than traditional system for most channel conditions. The throughput of the system is plotted in Figure 56. Traditional systems would have the same throughput as the SP mode, however EP mode has significantly lower throughput for many channel conditions.

3.6 Hardware Validation

3.6.1 Receiver adaptation

In order to prove the feasibility of the proposed concept a hardware demonstration consisting of a 2×2 MIMO system operating in spatial multiplexing and diversity modes at 2 GHz is setup. In the setup, a tunable RF MIMO front-end is setup as shown in Figure 57. Each front-end chain consists of an up-conversion

Table 3: Relative Throughput For Different Mode, Modulation And Code Rate

MIMO mode	Modulation	Coding rate	Relative Throughput
SM	64-QAM	3/4	9
SM	64-QAM	2/3	8
SM	64-QAM	1/2	6
SM	16-QAM	3/4	6
SM	16-QAM	2/3	5.33
SD	64-QAM	3/4	4.5
SM	16-QAM	1/2	4
SD	64-QAM	2/3	4
SD	64-QAM	1/2	3
SD	16-QAM	3/4	3
SM	QPSK	2/3	2.67
SD	16-QAM	2/3	2.67
SM	QPSK	1/2	2
SM	QPSK	3/4	1.5
SD	QPSK	3/4	1.5
SD	QPSK	2/3	1.33
SD	16-QAM	1/2	1
SD	QPSK	1/2	1

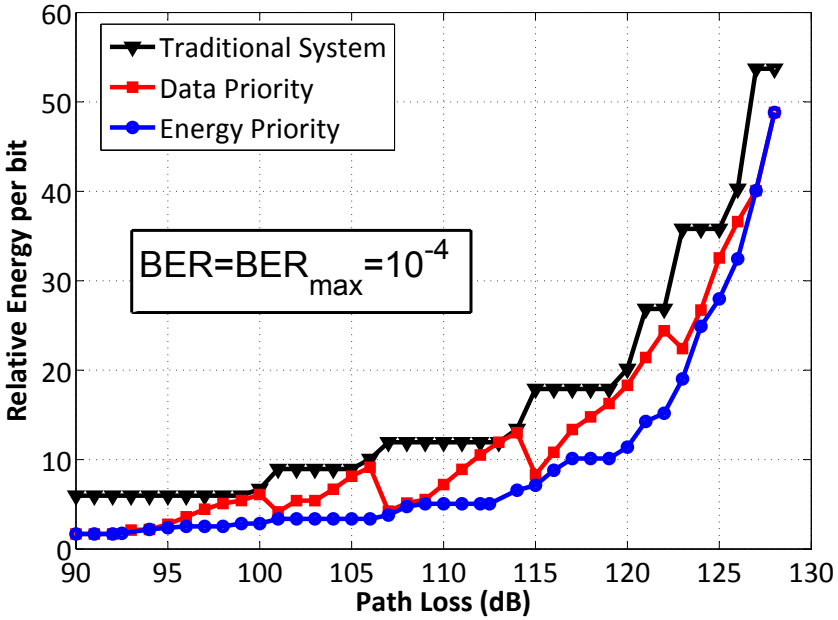

Figure 55: Relative energy-per-bit comparison with coding.

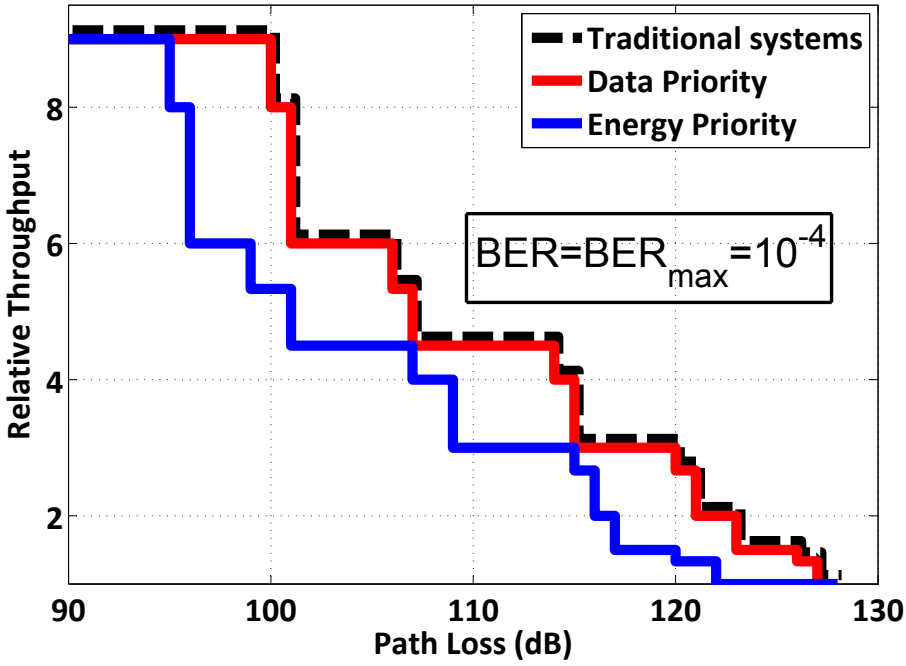

Figure 56: Relative throughput comparison with coding.

mixer ($MAX2039$) (part of the transmitter) and the RF receiver front end with LNA (RF2370) and down-conversion mixer ($ADL5801$). Each of the LNA and the down-conversion mixer has tunable bias and supply knobs (a total of 4 knobs per RF chain) to trade-off performance versus power. An OFDM modulated random data stream is generated in MATLAB and sent across the RF chain through a DAC (NI $PXI-5412$). The output of the RF chain is acquired by an ADC card (NI $PXI-5105$). A 2×2 channel is implemented in software after the signal is acquired by the digitizer. Fifteen different channel conditions are created through attenuation and noise addition. Channels are ordered from best to worst, with channel 1 being the best and channel 15 the worst.

In the setup the performance of the system in terms of power consumption and EVM is recorded across all possible combinations of the 4 tuning knobs for 15 different channel conditions (enumerated by channel index). This is done for both spatial

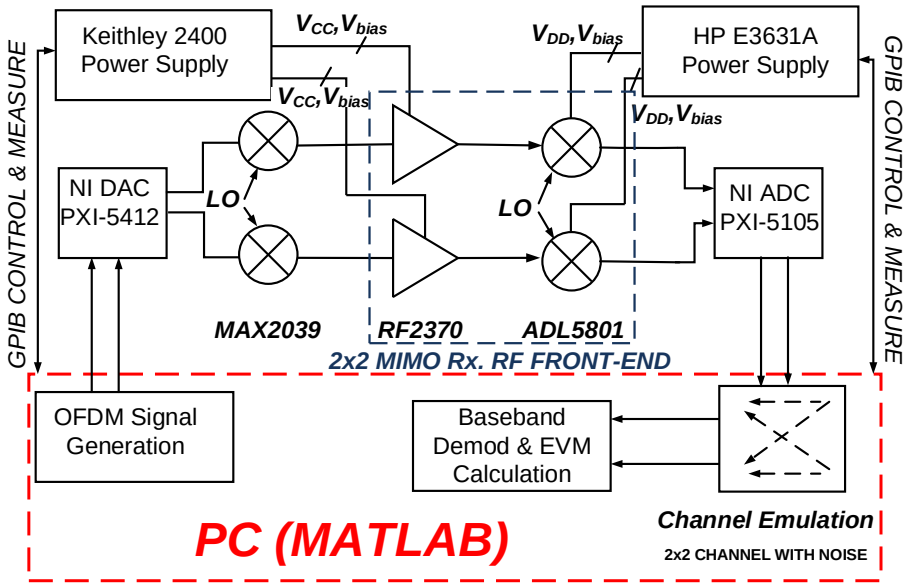

Figure 57: Hardware setup to demonstrate receiver adaptation.

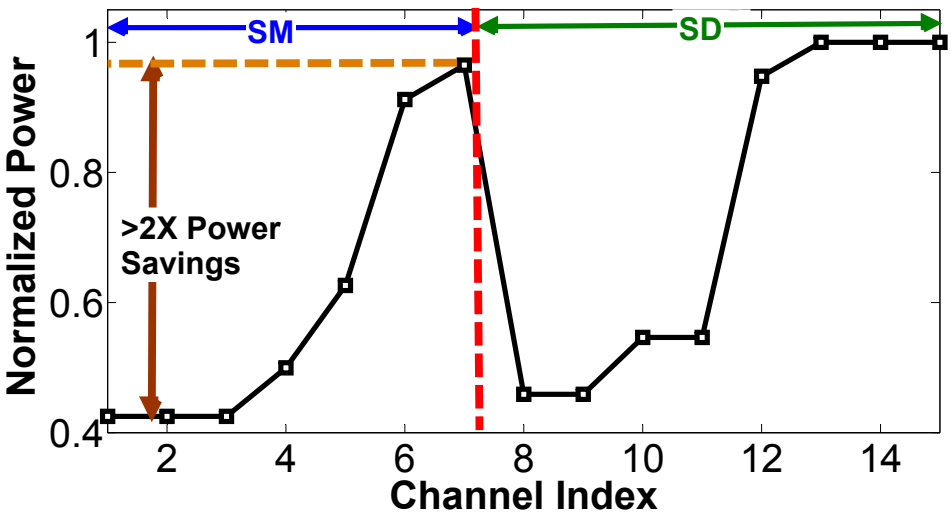

Figure 58: DP mode demonstrated in hardware setup.

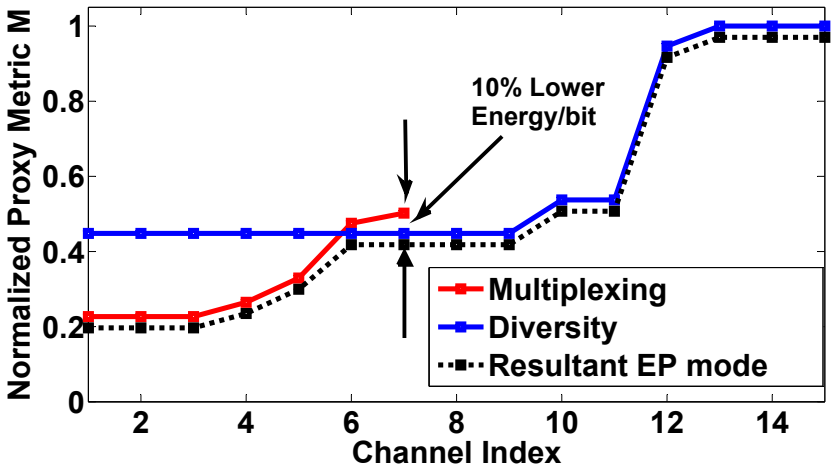

Figure 59: EP mode demonstrated in hardware setup.

diversity and spatial multiplexing mode for QPSK modulation. Subsequently, assuming an EVM threshold of 33%, the tuning knob combination with lowest power consumption is selected for each channel. The relative power consumption in an adaptive RF front-end across 15 channels is shown in Figure 58. From this graph it can be seen that substantial savings (up to 2×) in power by real-time tracking of the channel conditions can be obtained. The operation in EP mode is shown in Figure 59. EP mode demonstrates additional energy per bit savings (upto 10%) over DP mode operation. This hardware setup thus demonstrates the efficacy of the proposed low-power technique for MIMO RF front-end.

3.6.2 Transmitter adaptation

Although, in this work the concept of use-aware front-end adaptation has been demonstrated in simulation for a MIMO transceivers, it holds true for SISO transceivers as well. To demonstrate transmitter adaptation we use a SISO front-end as shown in Figure 60. The key tunable element in the front-end is the tunable PA (MAX2242) whose linearity can be traded off with power consumption by changing the V_{BIAS} setting. As V_{BIAS} is changed from 1V to 2V the linearity of the PA reduces and so does

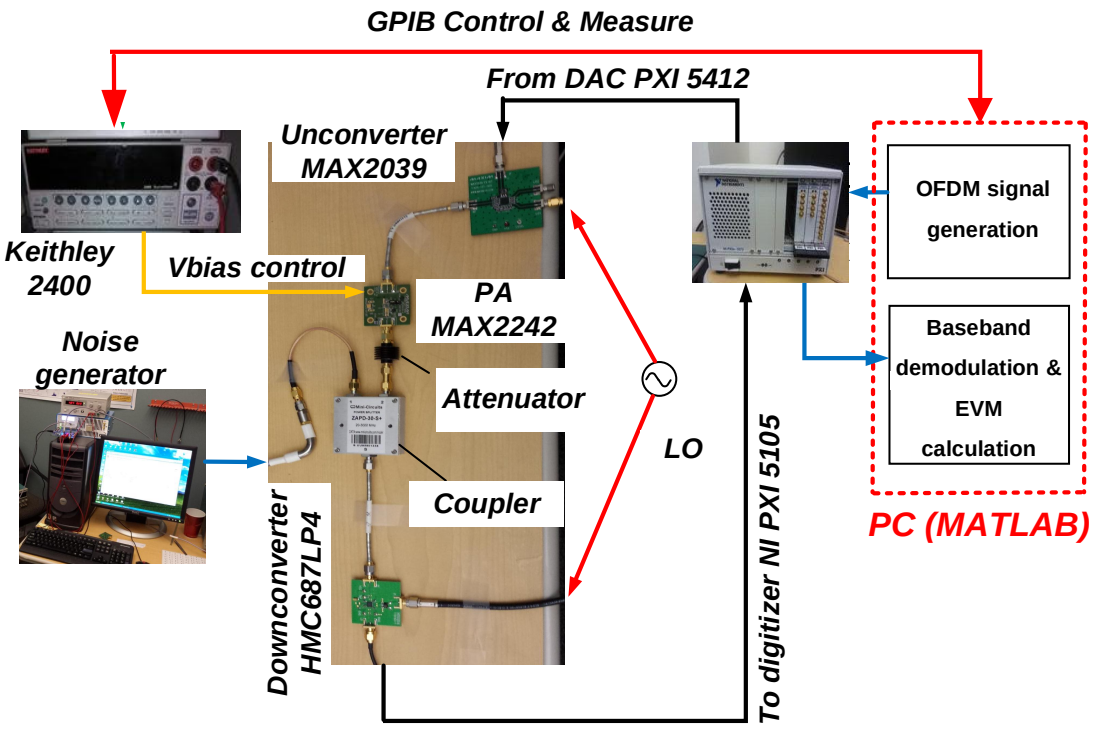

Figure 60: Transmitter adaptation hardware setup.

the current consumption. The relationship of VBIAS with linearity back-off and current consumption is shown in Fig 61. The OFDM base-band signal generated by the PC and PXI 5412 DAC is upconverted to a center frequency of 2 GHz by MAX2039 upconversion mixer. The channel is emulated through attenuation and noise addition. Different channel conditions are created by addition of different amount of noise is generated through the setup shown in Figure 60. The received signal is downconverted by HMC687LP4 downconversion mixer and captured by PXI5105 digitizer. Both the DAC and the digitizer are mounted on the same chasis and operate at 60 MSPS. The system is setup to operate with QPSK modulation for two different code-rates: 1 and 1/2. From prior simulation data it is determined that for a BER of $10-6$ the EVM_{th} for the 2 code-rates are 19.5% and 42.5% respectively. The details of the setup are summarized in table 45.

The band-limited channel noise is synthesized through the algorithm suggested in

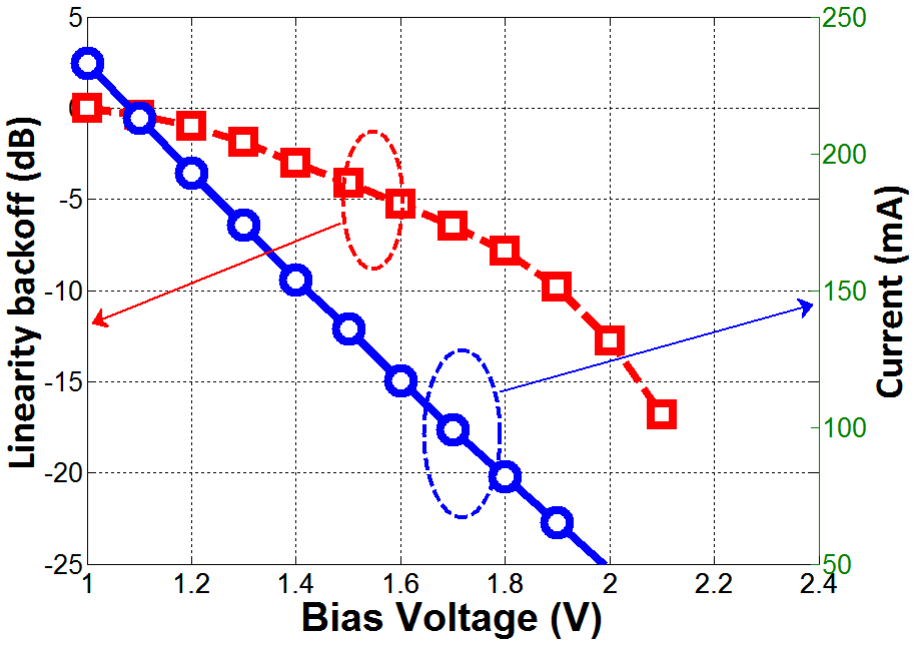

Figure 61: Transmitter characteristics .

Table 4: Adaptive Transmitter Hardware Setup

Transmitter	Baseband signal generation	PC (MATLAB)
	DAC	PXI 5412 (60 MSPS)
	Upconversion (@ 2 GHz)	MAX2039
	Tunable PA	MAX2242
Channel	Attenuation	20 dB (Fixed)
	Noise generation @ 2 GHz	Noise generator setup
Receiver	Downconversion (@2 GHz)	HMC687LP4
	Digitizer	PXI5105 (60 MSPS)

[76] with a single DAC matrix model. By setting discretely sampled digital data of the desired type of channel noise as the target waveform, the algorithm is capable of digitally controlling the noise characteristic of the synthesized waveform even in the high-order Nyquist zones. This is achieved by optimizing the input data sequence to the DAC in such a way that the distortion, noise floor and unwanted spectral spurs within the given bandwidth of a certain image tone at DAC's output is minimized. This targeted image spectrum is then used as the primary output of the band-limited noise generator. Other possible methods for test generation and test response acquisition have been discussed in [77, 78, 79]

The noise generation setup injects variable amounts of noise into the system to create three different channel conditions which are labelled as "good" (Channel 1), "bad" (Channel 2) and "worst" (Channel 3). Both the output power and linearity of the PA can be changed simultaneously depending upon channel conditions. The power consumption or Energy-per-bit of the PA can be optimized depending on the channel condition and the type of operational mode (DP or EP) selected. Figure 62 and 63 shows the power consumption and relative energy-per-bit of the adaptive PA at different channel conditions for the 2 different code rates.

The PA cannot operate at channel 3 with a code-rate of 1 because the EVM $>\text{EVM}_{th}$ for even the highest power consumption. As can be seen the power consumption increases with worsening channel conditions. At channel 2 the power consumption is 3.3× higher for a code-rate of 1 as compared to a code-rate of 1/2. However the throughput is only 2× higher (for code-rate=1). This results in a 40% less relative energy-per-bit when operating in code-rate 1/2 (as compared to 1). Thus depending on the mode of operation selected (EP or DP) at channel 2 the code-rate selected would be different. This would lead to a benefit in throughput (2×, if operating in DP mode) or energy-per-bit (40%, if operating in EP mode). Table 5 summarizes the above discussion.

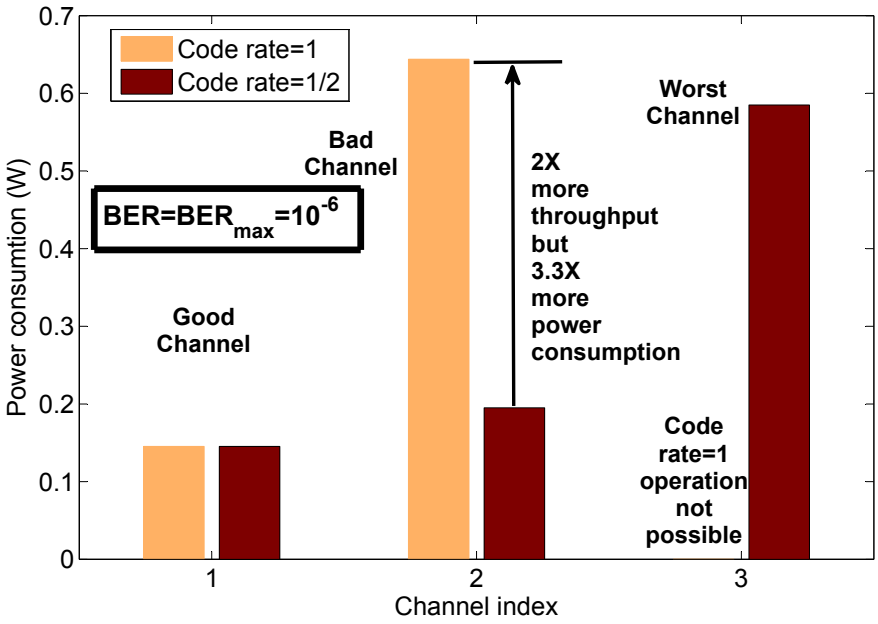

Figure 62: PA power consumption across different channels and code rates .

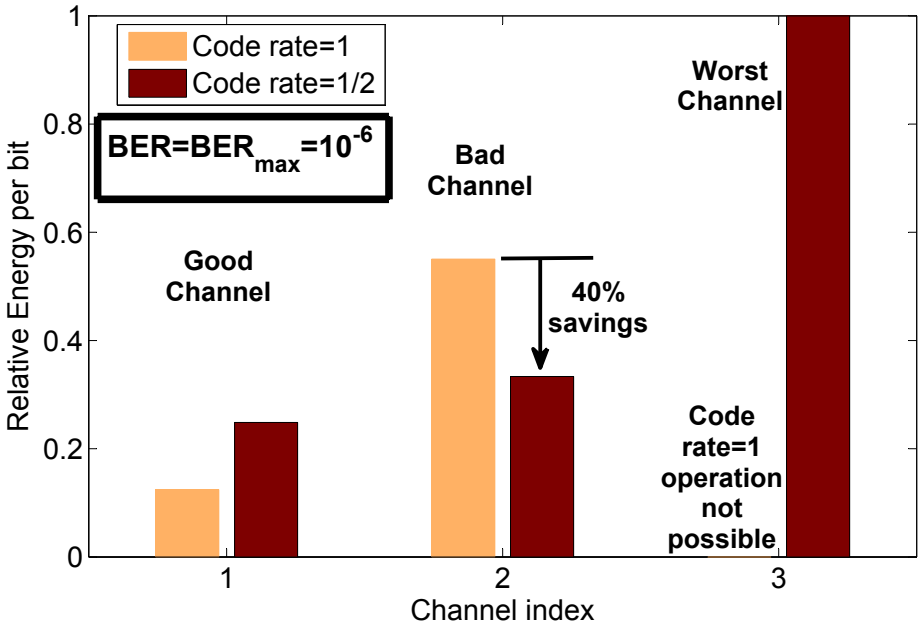

Figure 63: PA relative energy-per-bit across different channels and code rates.

Table 5: Code-Rate Used For Different Channel Condition And Modes

Channel	Good(1)	Bad(2)	Worst(3)
DP	1	1 ($2\times$ *throughput compared to EP*)	1/2
EP	1	1/2 (40% *less energy − per − bit compared to DP*)	1/2

3.7 Summary

This work establishes that low-power channel adaptive front-ends may be designed to operate in multiple modes to either guarantee highest throughput operation or to ensure lowest energy-per-bit operation. The concept is illustrated using a low-power MIMO transceiver, with adaptive RF front-end, switching between multiple modulation techniques, MIMO modes and channel code-rates. The same principles also hold for SISO systems. The proposed theory is then demonstrated in hardware systems for both receiver and transmitter. Depending upon the throughput requirements of the application using the front-end one of the proposed modes could be used for communication. The results presented in this work assume a particular channel model. Optimization of baseband processors for more complicated channel models have been demonstrated in prior literature [80]. A higher dimensional or more complicated model of the channel space would change the variation of EVM across the tuning knob space for different channel parameters. This would lead to different values of optimal tuning knob combinations across channel space. However the underlying concept of use-aware adaptation proposed in the current work would still drive the optimization process and the different trade-offs for the DP and EP modes of operation. A study of the two proposed adaptation modes for different types of channel models (for e.g. correlation effects, Doppler effects, presence of interferers)

could be an interesting subject of future research. Thus this work presents a key advancement in the domain of adaptive front-end design which is critical for low-power communication system development.

CHAPTER 4

ADAPTIVE RF FRONT-END DESIGN VIA SELF-DISCOVERY: USING REAL-TIME DATA TO OPTIMIZE ADAPTATION CONTROL

It has been established in prior research that significant power can be saved by *dynamically* trading off the performance of individual RF modules for power consumption across changing channel conditions. It has also been shown that the control law that reconfigures the RF front end must take into account the process corners from which the RF devices are selected in order to trade off performance for power in an *optimal* manner (minimum energy/bit at prescribed data throughput). Design of such an optimal control law is virtually intractable due to the complexity of simulating the RF front end across all *possible* channel *and* device process conditions. Hence, existing control algorithms are based on a coarse sampling of the channel $\times$ process space, suffer from modelling inaccuracies and are inherently sub-optimal from a performance vs. power perspective. In contrast, in this work, we propose a RF front end control methodology that is *optimized during real-time operation*, does not require up-front simulation across all channel $\times$ process conditions and is not susceptible to simulation inaccuracies. This results in far more robust/optimal control as opposed to current practice. A simulated annealing (SA) based framework for process optimization is proposed along with the use of built-in sensors for monitoring of performance and power. Simulation results and hardware data are presented to show the feasibility of the proposed approach.

4.1 Problem Formulation

A key difficulty in formulating the control law above is that of determining how multiple RF module "control" parameters (e.g. bias currents/voltages) must be modulated across different channel conditions to save power without compromising bit error rate. Assuming N control parameters $[p_1, p_2, .., p_N]$ in a feedforward control system, N functions are determined $p_1 = f_1(CQ),\ p_2 = f_2(CQ), ..., p_N = f_N(CQ)$ to compute the values of the parameters $[p_1, p_2, .., p_N]$ from the current estimated value of wireless channel quality CQ with the objective of minimizing system level power consumption across all channel conditions CQ. Determination of the functions $f_1(),\ f_2(),\ ...,\ f_N()$, is currently performed via simulation of the nominal RF system across diverse channel conditions and by a nonlinear optimization algorithm for minimizing RF system level power consumption [1, 35]. This is possible only via use of (approximate) behavioral level RF models along with statistical channel models and is inherently very compute-intensive. A Fuzzy Logic based approach to solve the same problem has been proposed in [81]. The modelling accuracy and computational complexity problem is made worse by the observation in [64] that in addition to the channel quality CQ, the functions $f_1(),\ f_2(),\ ..,\ f_N()$ must also include as input, the process conditions corresponding to each RF device. In fact, it is shown that if the control law for a nominal device is applied to a process-perturbed device, as much as 50% excess power may be consumed by the latter for specific channel conditions (50% excess power over a control law for the process perturbed device that also takes process conditions into account).

Assume that we are concerned with M RF modules (LNAs, mixers, PA) and that we associate M process conditions $[PC_1, PC_2, ..., PC_M]$, with each of these M RF modules. To accommodate process conditions along with channel quality CQ, the control law formulation can be restated as determining the functions $f_1(), f_2(), .., f_N()$ such that $p_i = f_i(CQ, PC_1, PC_2, .., PC_M),\ i = 1, 2, ...N$ in such a way that system

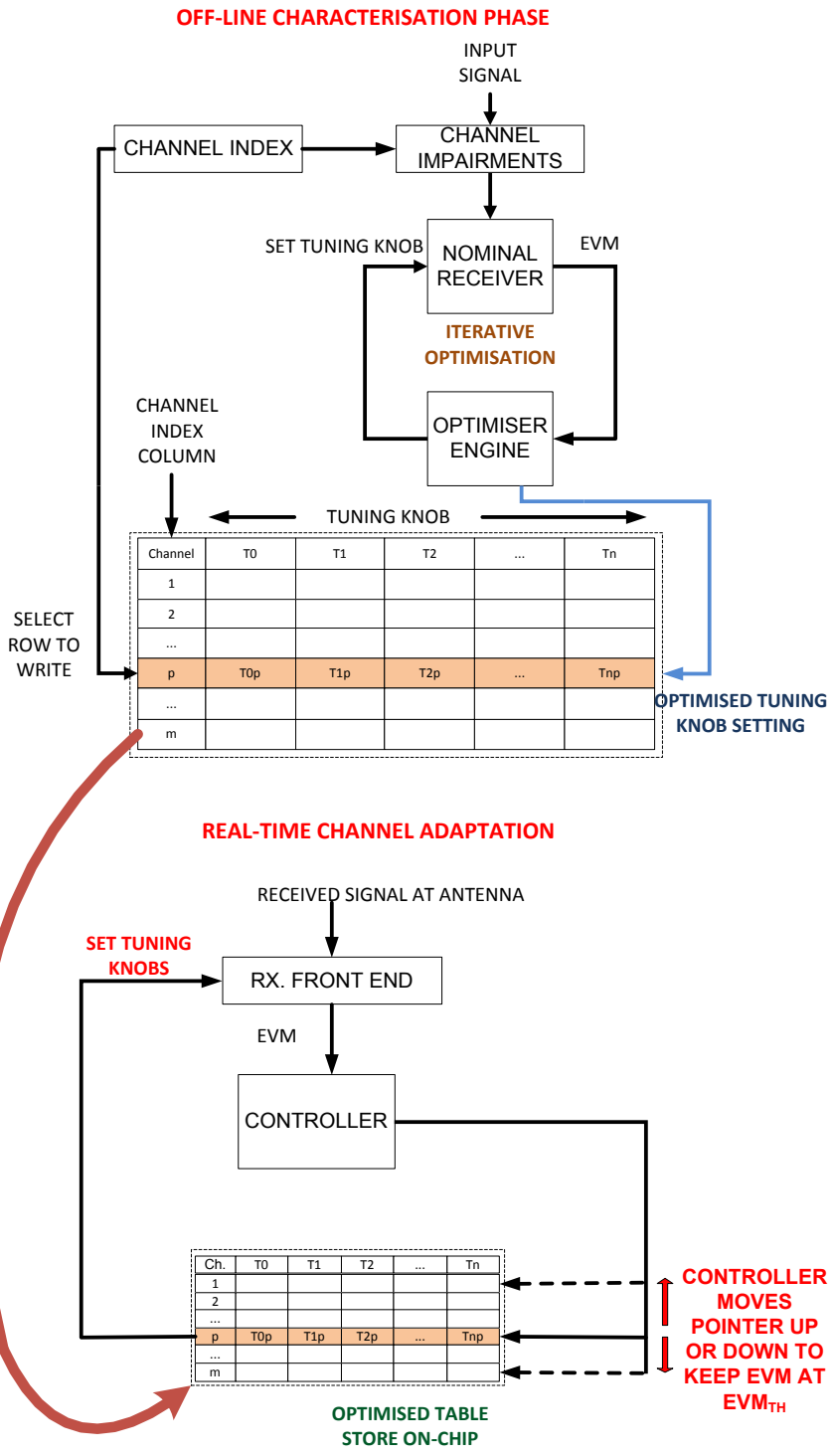

Figure 64: Low-Power Channel-adaptive RF Receiver proposed in [1]

level power consumption is minimized across *all channel and process conditions*. This results in an *explosion of simulation and optimization complexity* across all channel

and process conditions and clearly requires that in addition to channel quality CQ, the process condition (or specifications of individual RF module that are related to the process conditions/aggregate threshold voltage) must also be known for all the RF modules concerned. The latter requirement is not easy to satisfy due to the difficulty of measuring the performances of embedded RF devices and requires the use of sophisticated BIST techniques [38] with performance/area overhead.

The existing low-power channel adaptive RF system[1] is shown in Figure 64. Here, the entire gamut of channel conditions is partitioned into a finite number (say m) of representative channels. In the characterization phase of the system a combination of tuning knob settings is found for each of the m channels such that, the Error Vector Magnitude (EVM) is maintained at threshold (EVM_{th}) of acceptable operation while the power is minimized. These combinations are stored in the form of a m×n table (where n is the number of tuning knobs) as shown in Figure 64. The channels are ordered such that the first row represents the best channel (and hence minimum power consumption) and the last row represents the worst case channel (maximum power consumption). This optimization can be done with a constrained optimization algorithm [1]. The table is then stored on-chip. During real- time operation the EVM of the system is constantly monitored and a control algorithm running on the baseband processor continuously attempts to maintain the EVM at EVM_{th} by changing the tuning knob settings. If the EVM increases the feedback loop attempts to bring it below EVM_{th} by moving the pointer to the following row of the table (having higher power consumption). Similarly it moves the pointer back when the EVM is below EVM_{th}, saving power.

As explained earlier a critical drawback of this method is that it does not consider process variations. In order for this scheme to be process tolerant, the table must be modified for every device on which it is stored. [64] proposes that this problem may be tackled by constructing a number of such tables for different processes (based on

simulations) and storing only one of these tables on-chip by process detection at time of testing. However this results in very coarse approximations and hence sub-optimal results.

One way to resolve this problem is to allow the system itself to "discover" the optimum nature of the functions $f_1(), f_2(), .., f_N()$ *so that simulation and power optimization across all channel and process conditions are not required.* We call this "*Self-discovery*" and in the proposed methodology the system automatically customizes these functions for each process perturbed front-end based on real-time EVM (from baseband processor) and power (from current sensor) measurements. The system uses nominal settings obtained in off-line simulations as a starting point to converge to the optimized channel-adaptation control for each individual front-end.

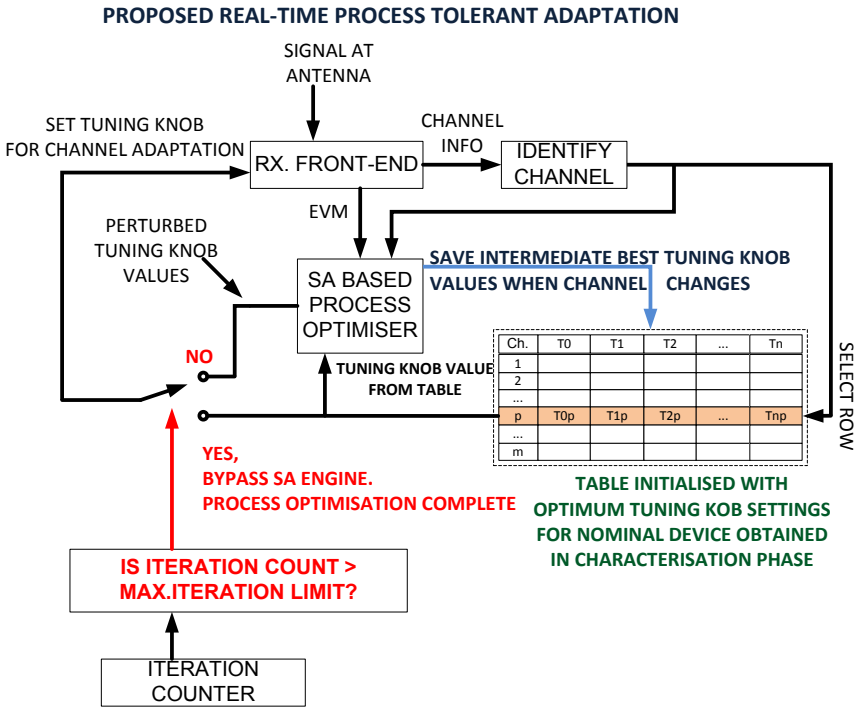

Figure 65: Proposed methodology

4.2 Methodology

The proposed methodology for RF system control is illustrated in Figure 65. In this scheme, the system tries to "*discover*" the optimal channel-dependent low-power configuration in presence of process variations while simultaneously adapting to channel conditions. It uses the stored table for nominal device as the starting point of process optimization. During real time operation the system detects the channel conditions using sophisticated sensors and switches to the tuning knob settings stored on the appropriate table row. The real-time process adaptation engine perturbs the tuning knob settings around the stored value in the table, to find other settings in the N-dimensional knob space which might give a better performance for the particular device. This exploration continues till the channel conditions change. At that point, it updates the particular row of the table with the best combination it has found

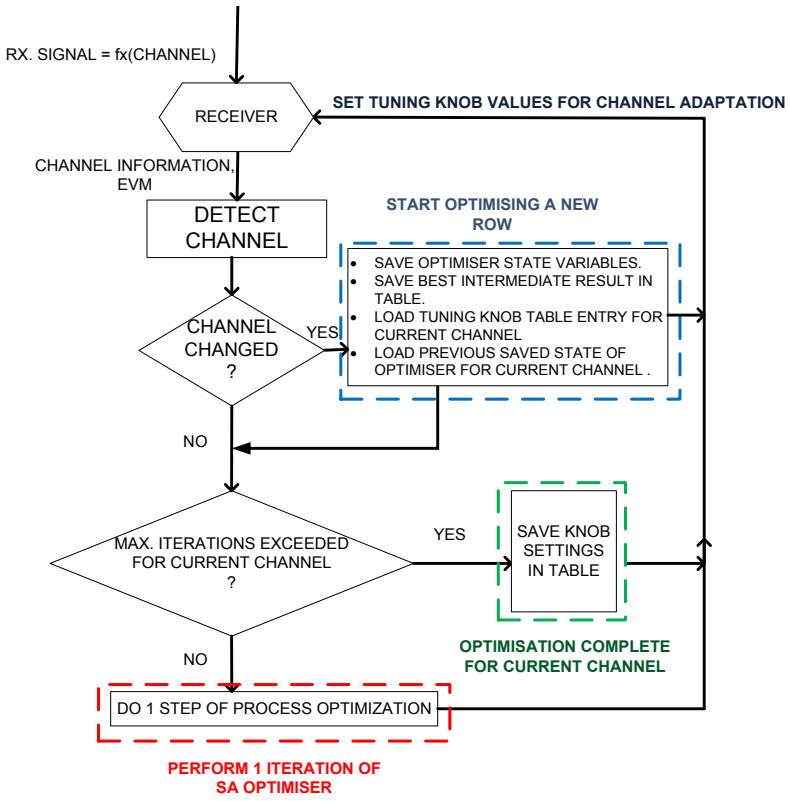

Figure 66: Flowchart illustrating optimization algorithm

over the search time. Thereafter it resets the optimizer's internal state values to start working on the table-row corresponding to the changed channel conditions. This "*load-search-save*" process carries on till a sufficiently large predefined number of iterations are exceeded. Thereafter the process optimization is deemed to be complete and the optimizer may be bypassed. Henceforth, the device continues to adapt to channel conditions with process optimized tuning knob combinations loaded directly from the table (Figure 65). The above discussion is summarized in the form of a flowchart in Figure 66.

The underlying algorithm used for such an optimization is Simulated Annealing (SA) (discussed in Section III) which is a stochastic optimization technique. Since the channel keeps on changing for a mobile device the optimization for a particular row of the table cannot be completed in one uninterrupted sequence of operations. Thus the entire table optimization is actually an aggregate of a number of optimizations, one for each row of the table, each of which is temporally distributed according to the sequence of channel condition occurrences.

4.2.1 Stochastic Optimisation:Simulated Annealing(SA)

In a real world scenario the tuning knobs can only be changed in fine discrete steps starting from a stored initial condition. Moreover the relationship between the EVM and tuning knob parameters and process is computationally intractable; the algorithm needs to be implemented on the system without significant overhead and the optimization should converge quickly. For these reasons, we use SA optimization technique [82, 83]. A SA process starts with a system in a known tuning knob configuration (s_0) at known "energy" (or cost function, say F) and an initial "temperature" (T_0). The energy of the system is dependent on the current configuration(s) of the system. The system is perturbed slightly to a new state (s_{new}) to get a new energy (F_{new}). The amount of perturbation is directly proportional to the temperature T

(which decreases continuously). If F_{new} is less than F we take s_{new} to be the new configuration. However, if F_{new} is greater than F then we can accept the new state s_{new} with a certain probability, which decreases with decreasing temperature. This algorithm when run for sufficient time converges to an optimal configuration giving minima for the energy function F.

4.2.2 Heuristics used in Simulated Annealing

In this section the heuristics used in the various functions used in the simulated annealing algorithm are described.

4.2.2.1 Temperature

In SA the slower the rate of cooling of T the more time it takes for the solution to converge. However it also means the search space is more thoroughly explored forming a fundamental trade-off. In the proposed system the temperature T at any iteration is given as:

$$T \leftarrow T_{prev} * 0.95 \tag{41}$$

4.2.2.2 Neighbour selection

The 'neighbour' function takes the current tuning knob combination and perturbs it by a random amount depending on the temperature of the system to produce the next state of the system. The amount of perturbation is directly proportional to the instantaneous temperature(T) of the system.

4.2.2.3 Energy function F

The aim of the algorithm is to find the optimum configuration for a system given a particular channel condition so that it may maintain the system at a maximum allowable EVM(EVM_{th}) with minimum power consumption.The initial estimate of the optimal knob configuration(s_0) for the system is obtained through offline characterisation for nominal device. The initial EVM for a particular channel (and hence a

particular row in the table) is given by:

$$EVM_0 = f(s_0, process) \tag{42}$$

The initial EVM(EVM_0) solely determines the nature of Energy function to be used in the subsequent optimization process.If the device performs worse than nominal then $EVM_0 > EVM_{th}$, we want to reduce EVM to close to EVM_{th} ,choosing our Energy function to be:

$$F = abs(EVM_{th} - EVM) \tag{43}$$

If the device performs better than nominal we have $EVM_0 < EVM_{th}$ and we can trade-off some additional power for performance. Hence we choose the power consumption value obtained as in Section IIIC:

$$F = Power \tag{44}$$

4.3 System Description

4.3.1 Receiver Architecture

The receiver chain with the feedback loop for the control circuitry is shown in Figure 67. The feedback loop consists of the forward receiver chain, the channel EVM calculation and the control logic which tunes the LNA gain and $IIP3$, ADC over sampling ratio(OSR) and the FFT word size to operate at the threshold of acceptable BER(EVM). Some of the most important building blocks are described below:

- **LNA:**The system has a tunable LNA with a bias knobs V_{cs} $(0.5V - 0.8V)$ and tunable supply V_{dd} $(1V - 1.8V)$ which can be use to modulate its performance. It has a nominal Gain, IIP3, NF and Power of $17.9dB, -12dBm, 3.3dB$ and $32.7mW$ respectively. The tuning knobs were selected to achieve maximum tunability for the circuit.

- **Mixer and Filter:** We use a mixer with [69] operating at 2.4 GHz with $1.1dB$ power gain, $19.7dBm$ $IIP3$ and $13.6dB$ NF.

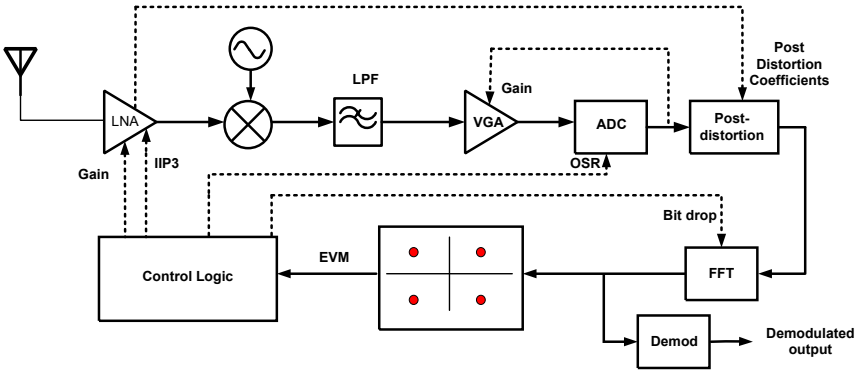

Figure 67: Receiver Chain

- **Sigma-Delta ADC:** The output of the VGA is sampled and quantized by a continuous time sigma-delta converter. For an n^{th} order continuous time delta-sigma modulator with a quantization step of $\triangle$ the in-band quantization noise is given by:

$$n_0 = \frac{e_{rms} * \pi^n}{\left[\sqrt{2n+1}.OSR^{\frac{(2n+1)}{2}}\right]} \tag{45}$$

$$where \quad e_{rms} = \frac{\triangle}{\sqrt{12}} \tag{46}$$

For our work we use a second order delta-sigma modulator ($n = 2$) with a $3-$bit quantizer. Thus by varying the sampling rate we vary OSR ($= 2, 4, 8$) and hence the quantization noise added n_0. The power consumed by a Continuous-time Sigma Delta ADC can be decomposed into 3 parts, i.e. power consumed by the analog circuitry (P_{ana} consumed by OTAs), power consumed by the digital circuitry (P_{dig} consumed by ADC and DACs) and the power consumed by the decimation filter following the modulator (P_{filter}). We assume P_{dig} and P_{filter} scale linearly with OSR.

- **FFT Processor:**The post-distorted output is passed through a FFT processor with an adaptive word size. The word size can be traded off with power [84]. The power values given in [85] are for 64 point FFT. For our case we have a 128 subcarrier signal. Hence we scale the power numbers to fit our case.

Thus effectively in our system we have 4 tuning knobs V_{cs} and V_{dd} (LNA), OSR (ADC) and bit drop (FFT Processor). All the models in this study are simulated in MATLAB.

4.3.2 Channel Model and Channel Quality Estimation

In order to adapt to channel conditions the receiver must first estimate the quality of signal it receives. In our system the channel is characterised by several effects like attenuation, fading , interferer addition and noise addition. For the sake of brevity the detailed modelling of channel effects is not discussed in this work.

Modern radio front-ends already have sophisticated sensors and baseband algorithms built in which sense the channel quality. One such widely-used metric is Received Signal Strength Indicator (RSSI), which gives an estimate of the in-channel power received. [68] discusses a method of detecting the power of in-band interferers.This is done by sensing the total in-band power by using a power detector between the mixer and the channel-select filter. The RSSI can then be subtracted from the in-band power to get the in-band interferer power. [69] discusses the design of a wide-band jammer detector which can be used to sense the total power received at the receiver. Thus combining both the outputs of interferer power detectors one can

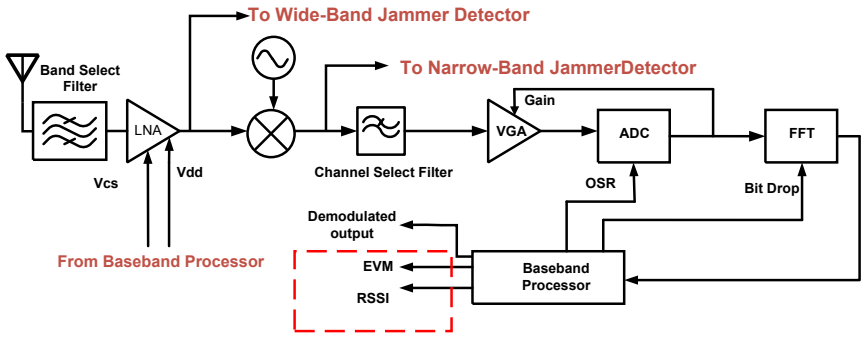

Figure 68: Detailed schematic of the proposed RF chain and baseband circuit showing signal and interferer estimation points.

get the idea about the total interferer power at the input of the LNA. Combining information from both RSSI and interferer strength estimation the system can estimate the appropriate configuration in the loci which it needs to adopt.

4.3.3 Current Consumption Estimation

At every iteration of the optimization, it is required to monitor on-chip power consumption at different knob values as tuning knob vs. power relation changes from device to device with process variation. The RF front end is powered by a dedicated voltage regulator where the error amplifier senses the difference between the reference voltage and the supply voltage.In [86] the output voltage of the error amplifier changes as the supply current changes so that it can maintain the supply voltage to the fixed level. By monitoring this error voltage at different tuning knob settings, current flow and hence power consumption can be computed.

4.3.4 Resource overhead

The main tasks involved in the algorithm are Neighbor selection (random number generation), Temperature calculation (iterative multiplication) and Energy function calculation (very simple function of the EVM and Power sensors). Thus SA algorithm can be implemented as a software routine on the digital processor which can easily handle such a task. If required the random number generation hardware could also be implemented as an ultra-low power, low-area block as in [87]. In terms of additional memory the algorithm requires the storage of Iteration counter, Temperature and Energy functions for successive iteration for every channel($3 * m$ additional bytes of memory for every m channels). If we assume that each OFDM symbol is $4\mu s$ long and it takes approximately 10000 symbols for EVM calculation, then we only need to run one iteration every $40ms$ ($\sim 25Hz$). Moreover this process-adaptation mechanism can be switched off once a predetermined number of iterations are complete.

4.4 Results

In this work a set of 8 channels ranging from bad to good (channel 1 is worst and channel 8 is best) is constructed and the proposed idea is demonstrated on these set of channels. For a BER of 5×10^{-4} the EVM threshold for QPSK modulation is 35%[1]. We keep a guardband of 2% to get an $\text{EVM}_{th} = 33\%$.

4.4.1 Nominal Table

During design and characterization phase of the transceiver system a nominal table is constructed. Since this is a one-time procedure the time taken to optimize is not of major concern. In our case we use a simulated annealing technique to obtain the initial table. The methodology is similar to the "EVM_0<EVM_{th} case" described in section II. In SA a slower cooling schedule tends to give a more accurate optimized value. Thus a much slower cooling schedule (as compared to the real-time optimization) is used. Here in every iteration:

$$T \leftarrow T_{prev} * 0.98 \tag{47}$$

The optimized channel dependent power consumption for the nominal case and EVM and Power convergence with iteration for a particular channel is shown in Figure 69.

4.4.2 Real-time evolution of the table

In order to demonstrate the real-time temporally distributed stochastic process adaptation procedure we assume that the receiver encounters the channels with a certain probability distribution. In this work all channels are assumed to occur with equal probability. However the adaptation works for all types of probability distribution of occurrence of channels. Using Monte-Carlo simulations a number of process variant instances of the LNA are generated. Starting from the nominal settings, the system is

simulated with randomly occurring equiprobable channel conditions to observe how the table is modified with time. We demonstrate the adaptation using 2 instances of the LNA at two extreme ends of process variation.

(1) Instance 1 results in the system performing better than the nominal and $EVM_0 < EVM_{th}$ across the 8 channels with the settings of the nominal table. Hence there is scope to trade off additional power versus performance(use cost function in equation (44)). The simulated annealing algorithm adapts the table in real time with successive perturbations. This is shown in the Channel versus EVM and Power curves in Figure 70. Here for N iterations the receiver is expected to encounter each of the 8 channels for $N/8$ iterations(given uniform likelihood of occurrence). *Thus we see that in the case of Instance 1 we can achieve significant savings in power* ($\approx 33\%$).

(2) Instance 2 results in the system performing worse than the nominal. Hence $EVM_0 > EVM_{th}$ for all the 8 channel conditions when operating with nominal knob

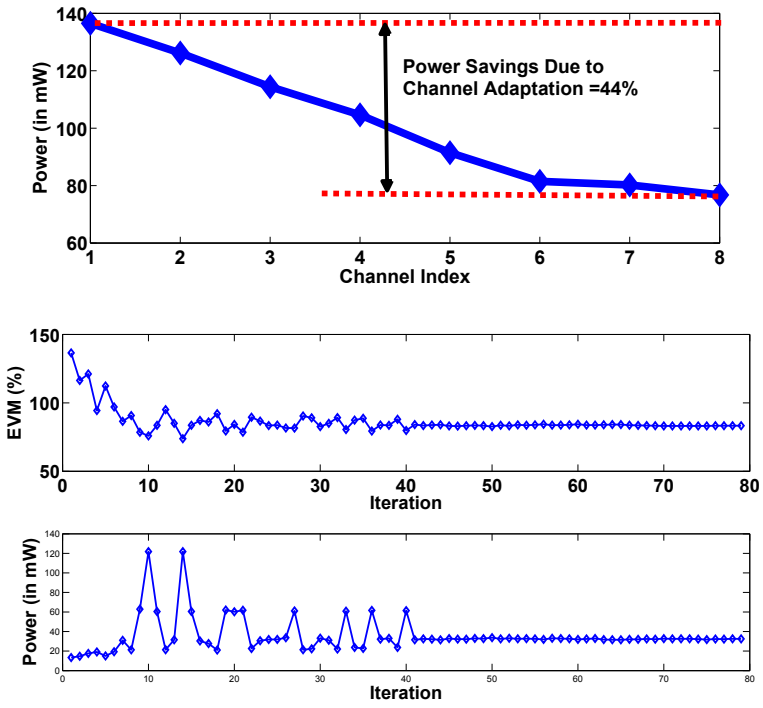

Figure 69: Optimized Power Consumption for nominal device across channels and EVM and Power convergence for a particular channel

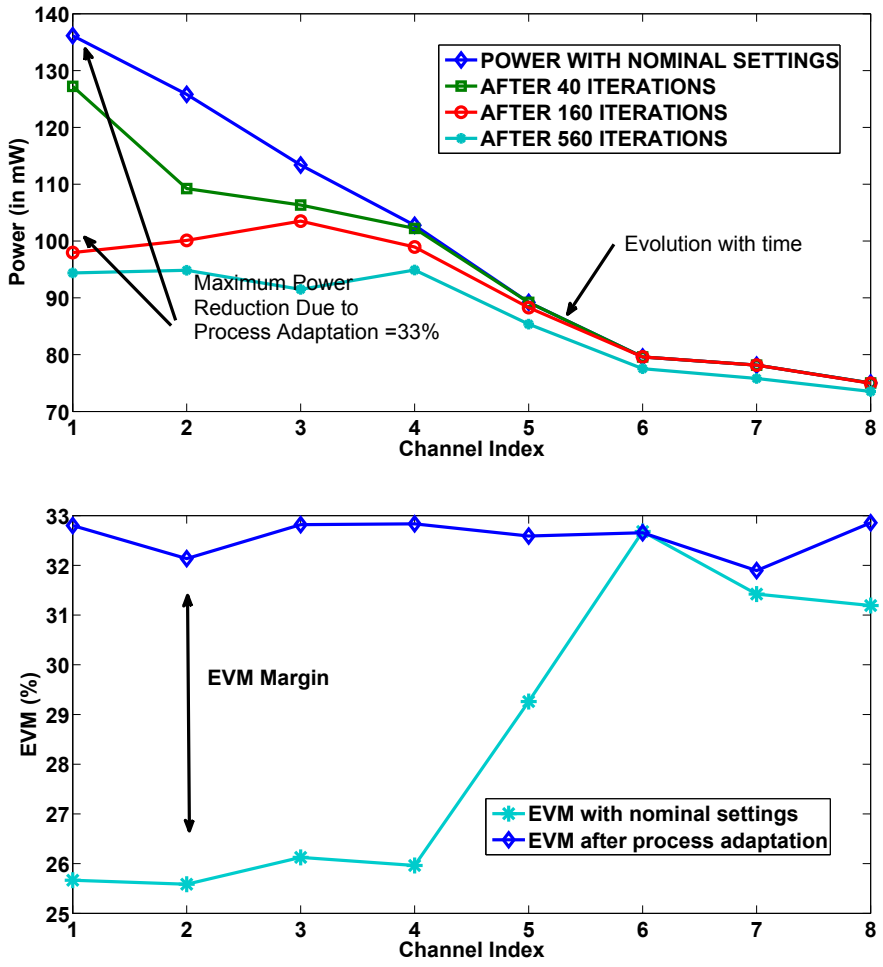

Figure 70: Evolution of Power and EVM of System 1 with time

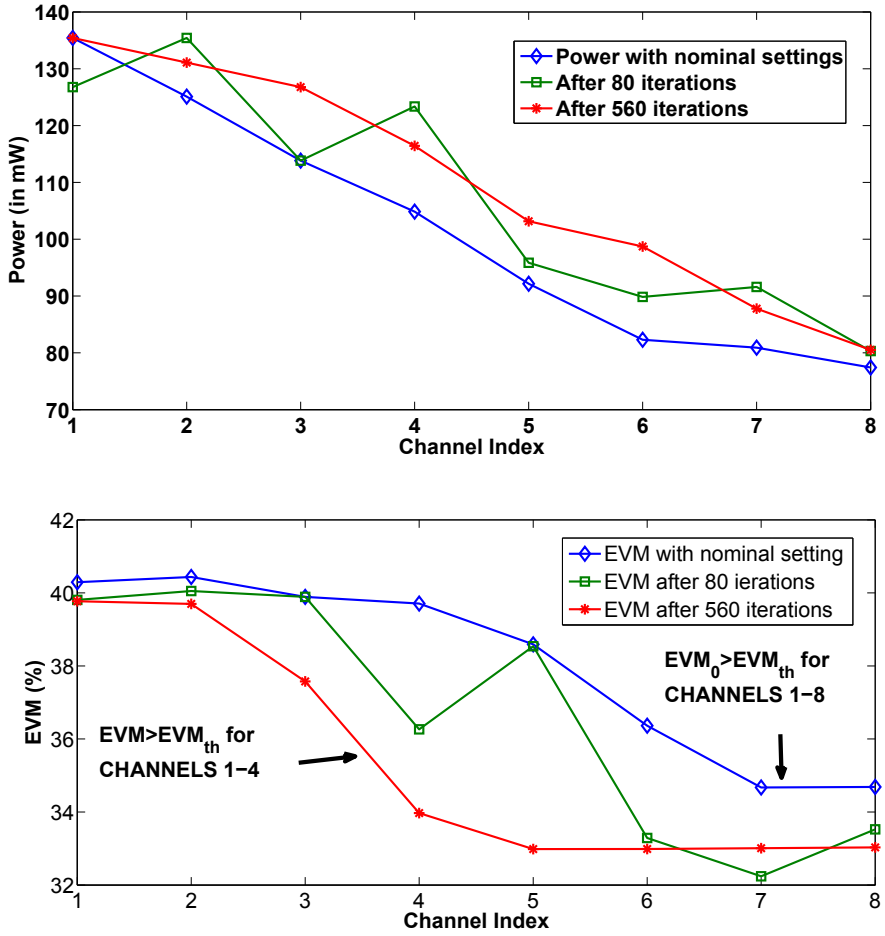

Figure 71: Evolution of Power and EVM of System 2 with time

settings. Thus the process adaptation algorithm(using cost function described in equation (43)) tries to bring the EVM close to EVM_{th}, thus leading to an increase in power consumption across different channels. This is shown in Figure 71. *In this case the performance of the LNA is so degraded, that the receiver might not work for some channels even after process adaptation. In this case we observe that initially the device does not perform within the* 33% *EVM bound for any channel whereas after process adaptation it operates correctly for* 4 *channels(index* 5 *to* 8*) and is inoperable in the remaining* 4*. Thus it operates in a reduced capability as compared to total failure without process adaptation.*

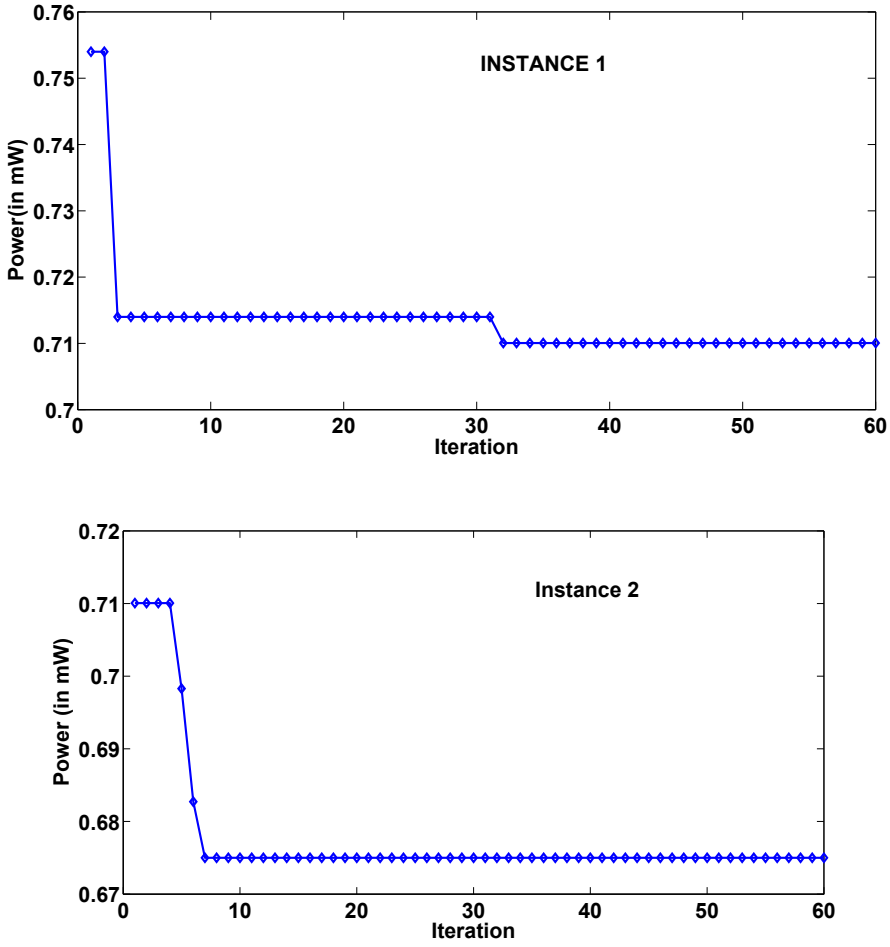

Figure 72: SA based optimization demonstrated on hardware.

In this setup it was observed that for each channel setting the algorithm converged to a steady state within 70 iterations. Hence the maximum number of iterations required would be $560(= 70 * 8)$ for a set of equally likely channels. However in this case study the instances with the most widely varying performances have been chosen. It may be noted that the perturbation process may lead to reduced throughput during the duration of process optimization. However since this process would last for first few seconds of the radio device lifetime, this is a minuscule loss considering the significant benefits achieved.

4.5 Hardware Validation

A SISO transceiver is constructed in hardware. The baseband processing of the system implemented in MATLAB. The system consists of an up-conversion mixer (RF 2638) followed by a highly linear amplifier ($MAX2247$). A down-conversion mixer (MAX 2039) was used. A NI-DAQ system is used for signal delivery and response acquisition. It consists of an arbitrary waveform generators (PXI 5112) and one digitizer (PXI 5412), which were used to perform the data conversion operations. To emulate process variation effects in the receiver chain, the amount of noise added to the input signal was varied and 2 process instances were created. $Instance$ 2 had better performance (due to lower noise addition) than $Instance$ 1. The supply of the amplifier was used as a tuning knob and varied between $2.5V$-$2.9V$. $Instance$ 1 is taken as the nominal device. QPSK OFDM stimulus was used to calculate EVM of the system. Setting an $\text{EVM}_{th} = 35\%$ the power of $Instance$ 1 is optimized using SA algorithm. This forms the nominal tuning knob setting. Then using the knob setting for $Instance$ 1 as an initial condition, the SA algorithm was applied on $Instance$ 2 to optimize for process. Nominal knob setting was $2.79V$ and $Power = 0.71mW$. The knob setting for $Instance$ 2 converged to $2.7V$ for a power of $0.675mW$. The best Power values found during SA run on $Instance$ 2 are demonstrated in Figure 72. As the optimization proceeds new low-power values are found and power decreases. Although in this case only one tuning knob is used, this method is generic and can be easily expanded to multiple knobs, giving significantly more savings.

4.6 Summary

This work presents a methodology which allows an RF front-end to dynamically trade-off module level performance with power even in the presence of significant process variations. As compared to previous approaches this requires no simulation/characterization for process or embedded BIST techniques. Two contrasting

cases are studied. *Instance* 1 shows considerable power savings (33%) over the non-process tolerant adaptation. *Instance* 2 demonstrates that in presence of process variability, this new scheme ensures that the device works for a much larger set of channel conditions than otherwise possible in [1]. Hardware results also demonstrate power savings in presence of process variability. Thus this work addresses the important area of low-power adaptive RF system design at very small design nodes where process variations become critical.

CHAPTER 5

SELF-LEARNING RF RECEIVER SYSTEMS: PROCESS AWARE REAL-TIME ADAPTATION TO CHANNEL CONDITIONS FOR LOW POWER OPERATION

Prior research has established that dynamically trading-off the performance of the radio-frequency (RF) front-end for reduced power consumption (Figure 73) across changing channel conditions, using a feedback control system that modulates circuit and algorithmic level "tuning knobs" in real-time based on received signal quality, leads to significant power savings. It is also known that the optimal power control strategy depends on the process conditions corresponding to the RF devices concerned. This leads to an explosion in the search space needed to find the best feedback control strategy, across all combinations of channel conditions and receiver process corners, making simulation driven optimal control law design impractical and computationally infeasible. Since this problem is largely intractable due to the above complexity of simulation, we propose a *self-learning* strategy for adaptive RF systems.

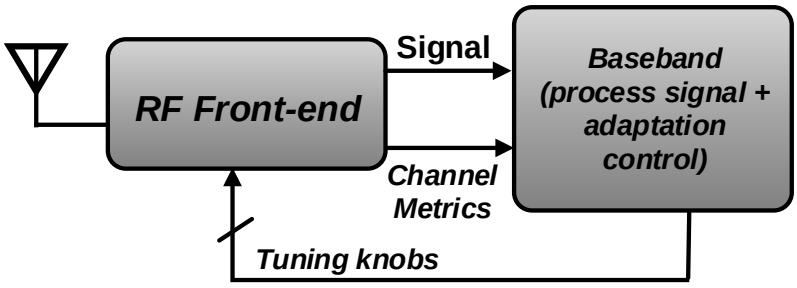

Figure 73: Adaptive receiver front-end architecture.

In this approach[88] a system is presented which harnesses the computational capabilities of general purpose microprocessors in today′s wireless devices to implement a neural network based learning methodology which formulates the optimum reconfiguration strategy across channel conditions during the operational life-time of the device. Single-input-single-output (SISO) and Multiple-input-multiple-output (MIMO) receiver front-ends are used as test vehicles to prove that with minimal additional infrastructure the RF systems could learn the optimum tuning knobs for minimum Quality-of-Service (QoS) operation over the entire gamut of channel conditions.

5.1 Motivation

In the technique proposed in [64], the combination of simulating all channel conditions across all process corners becomes infeasible as the dimension and desired granularity of the process space becomes moderate. Moreover process detection with fine granularity also becomes a critical to the low-power operation of the front-end. Process variations are due to manufacturing uncertainties in values of several independent parameters such as effective channel length (L_{eff}), the oxide thickness (t_{ox}), the dopant concentration (N_a), transistor width (w), interlayer dielectric thickness (t_{ILD}), interconnect height and width etc. Moreover process variation maybe both inter-die and intra-die [89]. Thus for each such process variant RF front-end a table of optimized tuning knob settings across all channel conditions needs to be calculated. This clearly becomes intractable with rising process space dimensionality and increasing granularity of channel characterization.

To get an estimate of the number of process instances required to span the process space with desired granularity let us take the following example: let the dimensionality of the process space be P for each RF chain of a MIMO front-end. In each dimension let there be L levels (or L bins) to quantize the amount of variation in that particular dimension. Hence for each RF chain the number of process instances to span the

entire process space should be:

$$X = L^P \tag{48}$$

Considering intra-chip variations for a front-end with M chains the total number of process instances assuming intrachip variation is:

$$N = L^{PM} \tag{49}$$

Assuming that the channel is m-dimensional with K_i ($i = 1$ to m) bins in each channel-dimension, to quantize the channel conditions then, the total number optimizations needed to be solved in an n-dimensional tuning knob space is given by:

$$Optimization\ count = L^{PM} \prod_{i=1}^{m} K_i \tag{50}$$

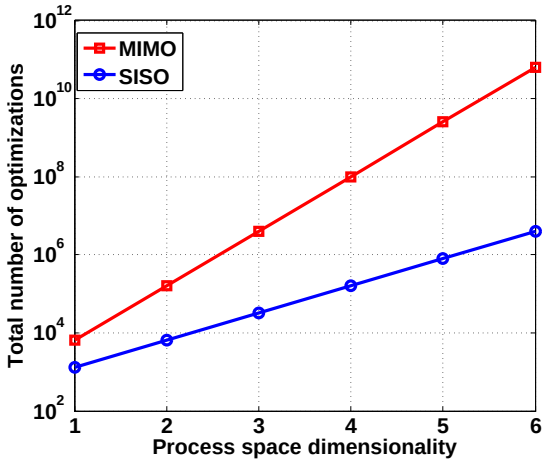

Figure 74: Rise in design characterization complexity with process variation dimensionality in simulation driven optimization

5.2 Learning based process resiliency

As shown in 74 with increasing dimensionality of the process space the number of pre-characterized tables (N) reaches impractical proportions (assuming $M = 2,\ L = 5$)

and the number of optimizations is even higher. To solve the above problems, we propose a self-learning approach in which the RF device "learns" how to best adapt to changing channel conditions under the process corner the device corresponds to (unknown at the start of the learning process) to save power. Self-learning based techniques have been used in model- update problems [28] but have not been used in the domain of adaptive front-end design. This technique has two benefits. Firstly, this eliminates any design phase optimization using channel models. Secondly, since the online real-time learning algorithm learns the characteristics of the particular device it is running on, it ensures the adaptation mechanism is optimum for the process conditions the RF device corresponds to. This is particularly important in MIMO systems where the large number of tunings knobs and process variables due to multiple RF chains makes design phase characterization nearly impossible. The proposed self-learning methodology uses built-in sensors and learning algorithms to incrementally build the real-time adaptation strategy for the entire gamut of channel conditions leading to significant power savings in the long run.

5.3 Problem Formulation

Let us consider a general RF receiver system 8 which has multiple operational configurations based on the values of n tuning knobs $(T_1, T_2, ..., T_n)$ (bias, supply etc.). Let the dimensionality of the process parameter (PC) space be p, where PC_i is the $i-th$ process parameter. Therefore:

$$T = \{T_1, T_2, T_3, ...T_n\} \tag{51}$$

$$PC = \{PC_1, PC_2, PC_3, ...PC_p\} \tag{52}$$

Let us assume that the receiver adaptation is driven by m channel parameters (e.g. signal strength, noise, interference):

$$F = \{F_1, F_2, F_3, ...F_m\} \tag{53}$$

The power consumption (P_{DC}) of the RF front-end is a function of the front-end configuration (T) and also the process conditions. Thus:

$$P_{DC} = f(T, PC) \tag{54}$$

Receiver adaptation is performed in a way such that the received symbol bit error rate (which is determined by the quality of the wireless channel as well as the fidelity of the RF receiver) is less than specified upper limit value. It has been shown in [4, 8, 9] that the error vector magnitude (EVM) of received symbols can be used as an alternate metric since it has a strong correlation with BER and takes significantly less time to determine with high accuracy. If we consider the RF front end as an extension of the wireless channel, we can write:

$$EVM = g(F, T, PC) \tag{55}$$

Here, the EVM is due to the combined effects of the wireless channel quality, determined by F as well as the fidelity of the tunable RF front end (determined jointly by the tuning knob settings T as well as the process parameters PC). We desire to find the set $T_{opt} = \{T_{1opt}, T_{2opt}, ..., T_{nopt}\}$ of optimal tuning knob values for any given set of channel conditions determined by F and process conditions determined by PC that minimizes power consumption while maintaining $EVM < EVM_{th}$ (large values of EVM are associated with higher BER values), where EVM_{th} is determined by the specified upper limit of allowed BER of the wireless receiver. Stated mathematically the problem is as follows: Find the mapping function $\mu()$,

$$T_{opt} = \mu(F, PC) \tag{56}$$

Such that receiver power consumption P_{DC} (function of T_{opt} and process parameters PC) is minimized and:

$$EVM = g(F, T_{opt}, PC) < EVM_{th} \tag{57}$$

Note that the function $\mu()$, varies from chip to chip due to the fact that each chip corresponds to a different set of process parameter values PC. To determine $\mu()$, it is necessary to know the functions $f()$ and $g()$ described above. As discussed earlier, finding $\mu()$ using simulation driven optimization across the space of parameters $F \times PC \times T$ is intractable. In the following section, we propose a novel real-time learning based approach in which the function $\mu()$ is learned on-the-fly on a per-chip basis, resulting in significantly improved power savings across a wide range of operating conditions.

5.4 Overview of the approach

Our goal is to derive the mapping function μ (Eq. 56) on-the-fly using a real-time learning algorithm. The system can acquire knowledge about the nature of the functions f and g (described earlier) through simple experiments (random perturbations of the tuning knobs T) during real-time operation. Initially, only partial and localized information (in the $F \times T$ space) regarding f and g is available. As time proceeds, the receiver encounters a greater variety of channel conditions and hence, builds a more complete picture of the functions f and g. The functions f and g are "discovered" by the learning algorithm incrementally over time over a subspace of $F \times T$ that is most relevant to the process corner corresponding to device under test. As increasing levels of knowledge about the functions f and g become available, the mapping function μ is updated to cover larger domains in the F space. After this process runs for a length of time across which the wireless device is expected to experience the majority of channel conditions it will see during normal day-to-day operation, the system

automatically develops a complete low-power adaptation strategy based on its own performance and on the channel occurrence statistics it is operating under. During this training period, the device operates as designed, delivering service to the end user with marginal high power consumption overhead, with the overhead reducing significantly as the learning process is completed. As a consequence of the learning strategy, if the user operates the receiver in close vicinity of a cellphone tower the majority of the time, the wireless system will consume less power than when the user is located in an urban "cluttered" environment inside buildings with significant path loss. Note that the system can also be "retrained" to adapt to different working environments as desired.

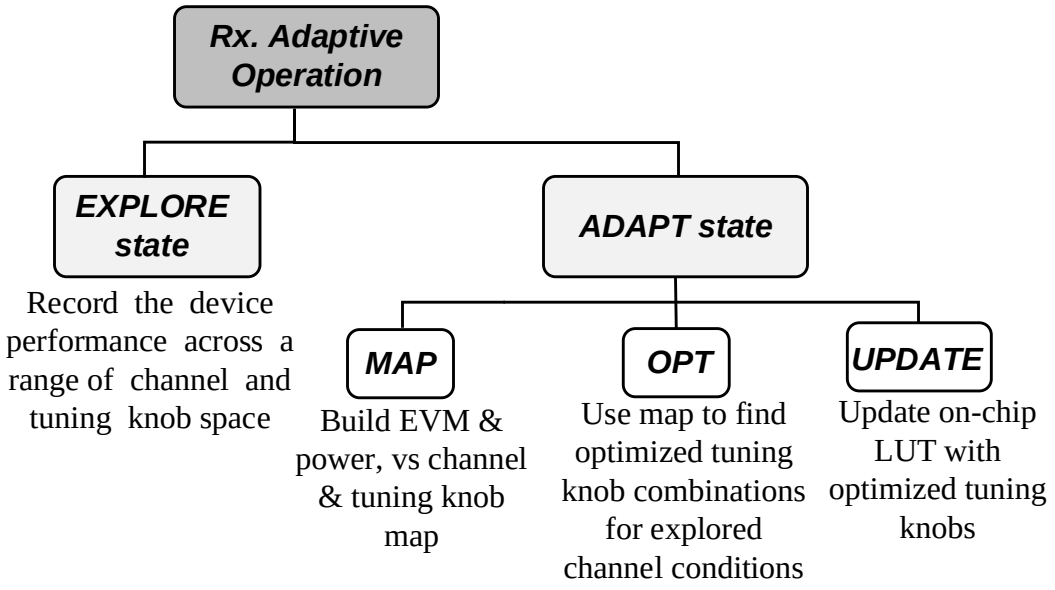

Figure 75: Operational states & phases of proposed learning based adaptation

The proposed self-adaptation methodology can be split into *two* states: EXPLORE and ADAPT (Figure 75). The EXPLORE state encompasses the time during which the device is not actively communicating data with the base-station and is not charging. During this state, the device intermittently requests for specific "exploration/training packets" (EXP packet, incorporated into communication protocol) to

be transmitted to itself from the wireless base-station. During these EXP packets the device randomly perturbs the tuning knobs (T_{rand}), computes the EVM, senses the channel and power consumption (P_{DC}) and stores these data in an on-chip buffer (Figure 76). Thus, such pre-designed exploration packets are used to record the device performance across a range of channel conditions and tuning knob combinations. ADAPT state is the period of time during which the device is charging and not being used. This gives the opportunity for more computation intensive tasks without significant effect on battery charge level. The information recorded in EXPLORE state is used in ADAPT state for finding the optimum knob setting for adapting to each channel condition.

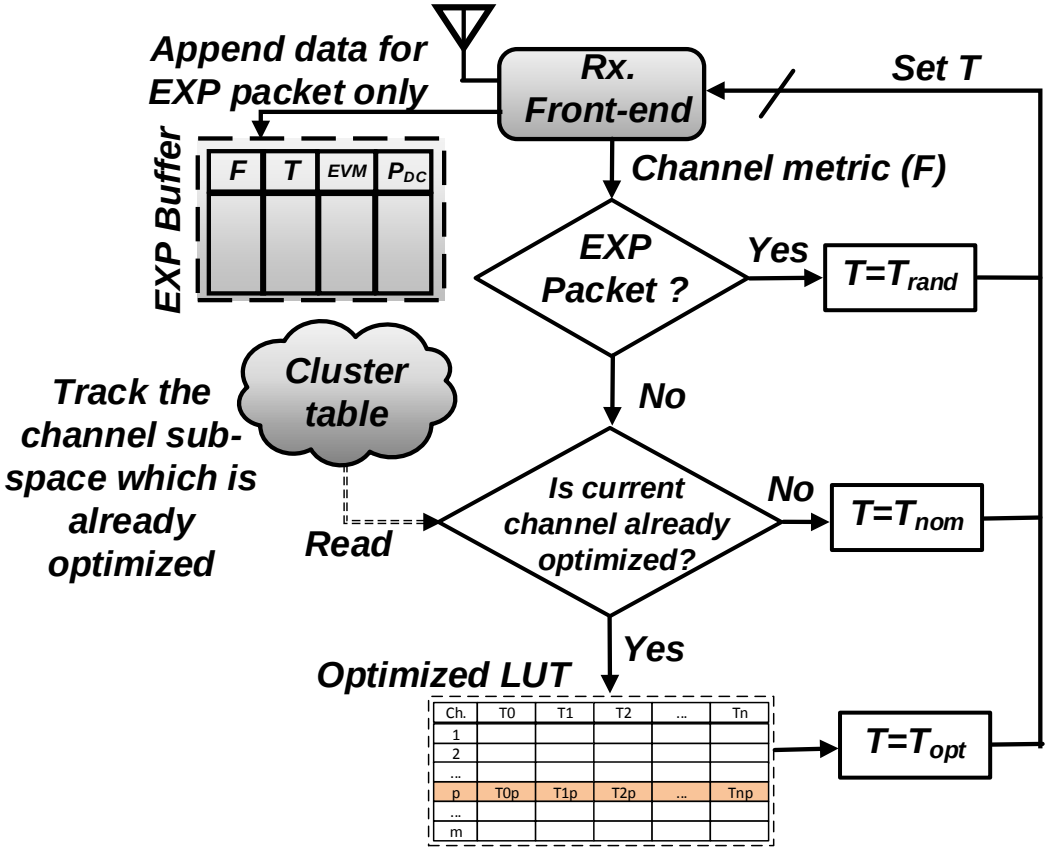

Figure 76: System operation in the EXPLORE state

In all other packets except the EXP packets, normal adaptive operation is maintained i.e. the tuning knobs are either set to the optimized tuning knob setting (T_{opt}) or the nominal knob setting (T_{nom}) depending on whether optimization for the current channel is complete or not. In order to determine if the optimization is complete for the current channel, the algorithm uses an on-chipcluster table which continuously tracks the sub-space (F_{sub}) of the channel (F) space for which optimization is complete.

Each time the system enters the ADAPT state, the system executes three consecutive operations (or phases) (Figure 77). All the operations in the ADAPT state are executed in software (on the general purpose processor) while the device is charging. Firstly, the information stored in EXP buffer is used in the MAP phase to incrementally build a model (in software) of the power consumption and EVM performance of the system across channel and tuning knob combinations. Also, the new data is used to calculate an updated cluster table to reflect the current F_{sub}. Thereafter, using this incrementally emerging model, the optimum tuning knob combinations (T_{opt}) are discovered in the OPT phase.

Care is taken to do this optimization only over the region of F space where sufficient experimentation has already been done in EXP phase (as indicated by the cluster table). Finally, the optimum knob combinations (T_{opt}) and the updated cluster table are used to update the channel vs T_{opt} LUT (μ) and cluster table stored on baseband processor in UPDATE phase. The individual phases are described in detail in Section 5.5

The EXPLORE and ADAPT states are executed iteratively until the optimum tuning knob combinations are discovered over the entire channel space (Figure 78).

Comparison with Simulated Annealing(SA) based approach

Prior work [90] proposes a random perturbation (through simulated annealing) based method to modify the stored optimum knob combinations for the nominal

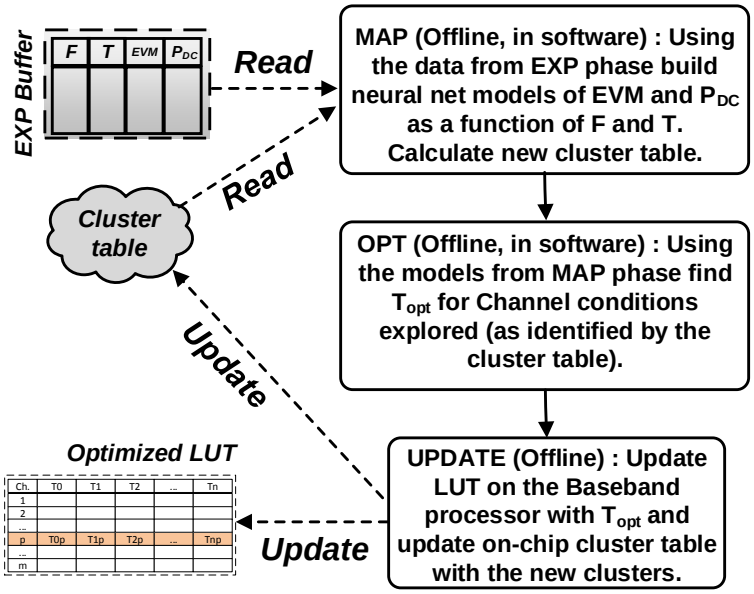

Figure 77: System operation in the ADAPT state.

process instance to tailor it for the device of interest. The technique proposed in [90] starts off with the nominal "locus" (or channel vs tuning knob table for nominal process) and gradually modifies it on- the-fly to reach the optimum locus for the process varied instance. In contrast to the technique proposed in this work, the prior technique starts off with a nominal locus and also does not employ a neural network based mapping technique. The prior technique has a number of drawbacks. Firstly, since the technique starts off with the LUT optimized for a nominal process, in case the performance of the device is worse than nominal device, it will be unable to perform within the QoS bounds for many channel conditions. This continues until the technique arrives at the optimal knob combinations for those channels. This complete loss of data connectivity for many channels may be unacceptable for the end-user and is not at all desirable in a front-end. Secondly, as discussed earlier, the data collected in EXPLORE state is used to find the optimum knob settings. It can be argued that this data can be used directly to find the optimum knob settings without resorting to any mapping/modeling techniques. This can be done by maintaining

running registers for different channel conditions which record the best tuning knob combination amongst the EXP data encountered thus far. However it can be shown that such an approach would require significantly larger time to optimize for the entire channel space. This is because, the EVM and P_{DC} surfaces in the $\{F, T\}$ space are generally well- behaved curves without abrupt variations. Such surfaces hence can be approximated by a neural net using a much sparser sample (compared to the entire set of points) in $\{F, T\}$ space).

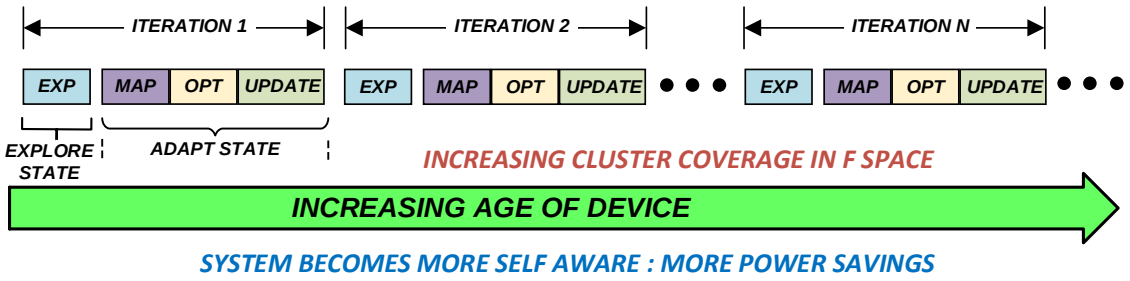

Figure 78: Iterative operation of the different phases.

Figure 79 shows how the optimized power consumption changes with increasing number of EXP packets encountered when no mapping technique is used for the setup discussed in Section 5.7. Each curve corresponds to a different channel condition and hence a different optimized power consumption ($P_{DC,OPTi}$, $i = 1$ to 4). It be seen that the number of EXP packets required for each channel condition for the optimized power consumption to reach its lowest value ranges from 100 to 2000. Assuming an average EXP packet requirement of 500 the total number of packets required for total optimization of the entire channel space (assuming channel is 2 dimensional with 16 quantization levels in each dimension) is 128,000. Using a neural net based mapping technique the same task can be achieved in 10,000 EXP packets (a 10× reduction in optimization time). Hence mapping with neural nets leads to a much faster optimization as compared to prior techniques.

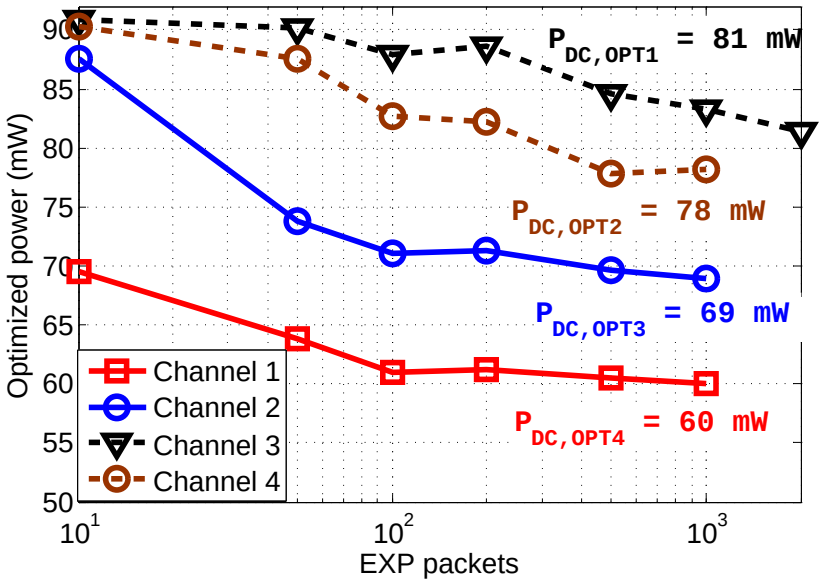

Figure 79: Optimized power as a function of the number of EXP packets encountered across different channel conditions.

5.5 Detailed discussion of adaptation states/phases

In this section we discuss the individual states/phases in greater detail:

5.5.1 Exploration State (EXPLORE)

The goal of this state is to acquire information regarding P_{DC} and EVM characteristics of the front-end across different channel conditions and reconfiguration modes. When the RF receiver is communicating with a transmitter (e.g. a base station) during real-time operation, the system perturbs the tuning knobs values (e.g. bias and supply voltages) during reception of predetermined "training packets" (EXP packets) to record the EVM and P_{DC}. These "training packets" are requested when the front-end is not being used by system applications for active data transfer. The tuning knobs are perturbed such that the entire range of permissible tuning knob values is explored over time. The recorded information can be stored in a buffer (file) on-chip in the form of a table as shown in Figure 77 and 80.

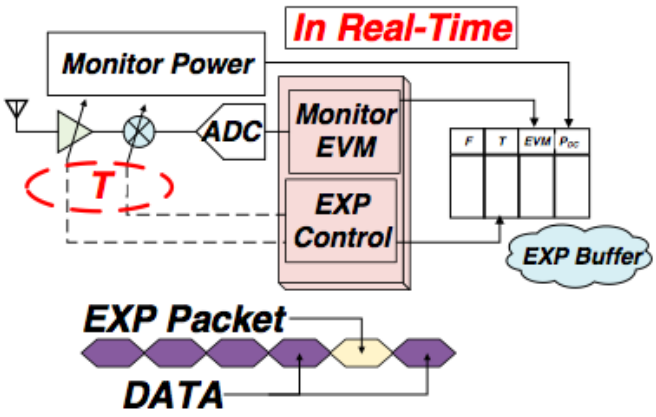

Figure 80: Ilustration of the EXPLORE state.

Here, the vector F (channel quality) is estimated by on-board sensors and built-in metrics (RSSI, RCPI interferer strength). The perturbation of the tuning knobs is performed by the baseband processor which also records the T vector in the EXP buffer shown. Since, the EXP packet is requested when no active data communication is going on no throughput penalty is paid for incorporation of these packets into the communication architecture. In most cases, the mobile devices are not used for voice or data communication for a large fraction of the total device "ON" time. Thus these time periods can be conveniently used for experimentation.

5.5.2 Map Phase (MAP)

The goal of the system in the MAP phase is to use the information gathered in the EXPLORE state to build a map of its power and EVM characteristics across different channel conditions and tuning knob values (entirely in software). These characteristics are related to the T and F vectors through the functions f and g defined earlier. However, it is difficult to find an analytical expression to model the equations f and g. Alternatively, the functions are constructed using two artificial neural nets (ANN) implemented in software as shown in Figure 81. These neural nets can be trained through supervised learning algorithms using the data stored in the

EXPLORE state.

It must be noted that the set of channel conditions experienced by the RF device grows with time. At any point of time, the maps will have the integrated information from all previous experiments, which may not have covered the entire $\{F, T\}$ space. Thus, it is important to also keep a track of the region in the $\{F, T\}$ space for which the ANNs have been adequately trained. This can be done by using an Evolving Clustering Method (ECM) [31] to build a table of clusters formed from the data gathered in the EXPLORE state. ECM requires some amount of computation and must be done in software (during offline state, not during real-time communication). The final cluster table is however stored on-chip. The ECM performance and its features have been discussed in Section 5.6.

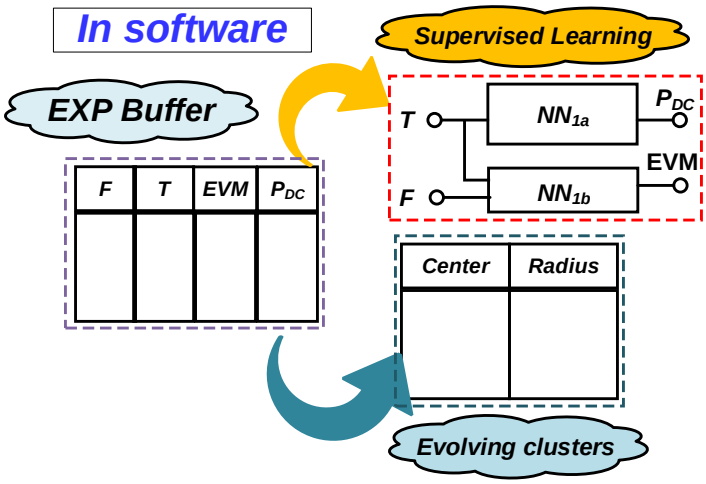

Figure 81: Illustration of the MAP phase.

Every mobile device today has a general-purpose processor for running applications and a baseband processor for communication tasks. The MAP phase (and the subsequent OPT and UPDATE phase) can be executed on a software running on the general purpose processor. They can be implemented to run only during the ADAPT state (i.e. when device is charging). It may be pointed that modern mobile devices

(phones, tablets etc.) goes through such an ADAPT state (when battery is charging and device is idle) for several hours every day. Once the data in the file is incorporated into the neural net through training, the on-chip file/buffer may be flushed (wiped clean) to prepare for the next EXPLORE state.

5.5.3 Optimization Phase (OPT):

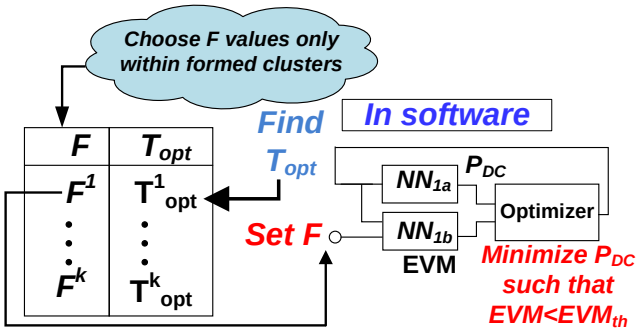

Figure 82: Illustration of the OPT phase.

In the OPT phase, the objective is to use the knowledge base developed in the MAP phase to generate the optimum configuration strategy. It must be noted that at any point of time, the neural net map is correctly trained only for a subspace F_{sub} of the entire channel space F. This subspace, F_{sub}, is the set of channel conditions for which the device has already encountered and performed a large number of tuning knob perturbations. The system can confidently predict the performance of the front-end for all tuning knob combinations in the subspace F_{sub}. Trying to predict a configuration strategy for a channel condition outside F_{sub} can lead to erroneous results. In OPT phase, a set of channel vectors F_1 to F_k are selected spanning F_{sub} (Figure 82). Thereafter, for each of these channel vectors, F_i, the optimum tuning knob combination is found such that P_{DC} is minimized and EVM ¡ EVM_{th}. This optimization is done with the help of the neural nets trained in the MAP phase using a constrained optimization algorithm (e.g. gradient search).

5.5.4 Update Phase (UPDATE):

The set of optimized tuning knobs (T^i_{opt}) generated in the OPT phase are used to update the reconfiguration strategy (μ) stored in a LUT associated with the baseband processor. The LUT is an m-dimensional table with each of the entries being an n-tuple of tuning knob combinations. After each UPDATE phase, the $n-$tuples in the m-dimensional space are updated with the optimum configurations corresponding to different channel conditions for low power operations. Additionally, in the UPDATE phase the updated cluster table is written to the on-chip cluster table. After each iteration of EXPLORE state and MAP, OPT and UPDATE phases, more entries in the LUT are updated with the optimum configuration setting. This allows the system to react to increasingly diverse channel conditions with optimum power consumption and performance.

5.6 Cluster formation

As explained in Section 5.5, in order to prevent erroneous prediction of EVM and P_{DC} from F and T we need to track the subspaces F_{sub} for which relevant data has been learned. One way to achieve this is by storing every point encountered in the F space during EXP phase. However this leads to a huge memory requirement and also is inefficiently slow in terms of processing. A more efficient way to achieve this is by clustering the observed F values and maintaining a table containing the list of clusters on-chip. A cluster is a multi- dimensional hyper-sphere which enables us to keep track of the subspace F_{sub} which has been adequately explored. The advantage of clustering, in this case, is that the system does not need to maintain a list of all the previous F values it has encountered. Instead, only a set of centers and radii of hyper- spheres needs to be stored. These spheres encompass all the points in the m-dimensional hyperspace corresponding to channel conditions encountered before.

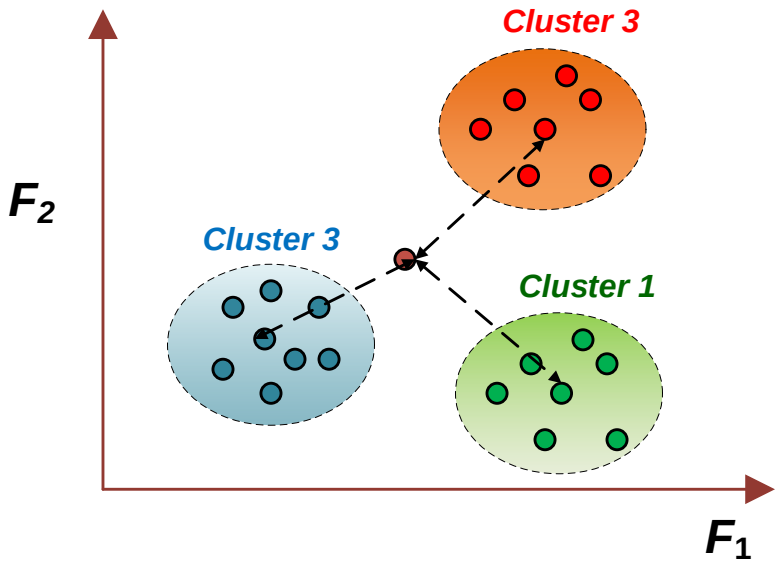

Figure 83: Clustering in F space.

K-means clustering [91] is the most popularly used clustering technique used. However, it requires the system to store all the data points and thus, is not suitable for iterative adaptive cluster generation. The Evolving clustering method (ECM) [92] alleviates the problems of K-means clustering because it does not require the storage of all the possible data points. This algorithm requires a pre-defined maximum cluster radius (r_{max}) and maintains a list of the existing cluster centers and radii. Given an m-dimensional data point, ECM calculates the distance of the point from the centers of the stored pre- existing clusters (Figure 83). Thereafter, it does one of the following:

(a) If the point is inside any existing cluster it does nothing.

(b) If the point is outside all existing clusters but within a pre- defined maximum radius of a cluster, the radius of the cluster is increased to include the particular point and the center is updated.

(c) If the point is outside all existing clusters and there are no clusters which can

grow (upto the pre-defined maximum radius) to include the data point, then a new cluster is created with zero radius and with the new point at its center.

The above discussion is summarized in the form of a flowchart as shown in Figure 84.

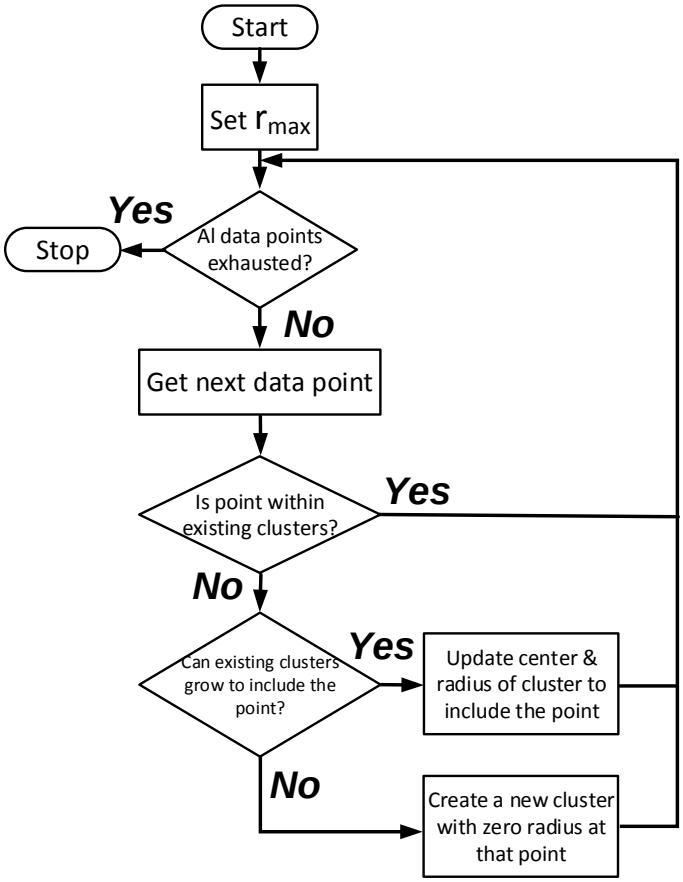

Figure 84: Cluster evolution flowchart.

In our system, we have modified this algorithm to additionally count the number of data points in a particular cluster. This is done to ensure that- given a value of F value lying within a cluster, the system has complete knowledge of the P_{DC} and EVM for all possible tuning knob combinations in T at that particular F. If T_{comb} is the total number of possible tuning knob n-tuples (each knob can have finite number of discrete settings) then an F value from a cluster can be used to predict P_{DC} and EVM only if the cluster has had $k \times T_{comb}$ (k is a pre-defined number greater

than 1) number of hits (since perturbations in T are random, just T_{comb} number of perturbation experiments may not suffice).

5.7 Overhead and protocol level implications

Channel impairment sensing: In the methodology presented in this work, sensing the channel quality is an important task that needs to be performed during the real-time operation of the device for the iterative learning to work accurately. As shown in [93] modern RF front-ends can adapt efficiently to effective signal strength (equivalently effective path loss given a constant transmit power) and interferer strength. The wireless channel is a multidimensional quantity with propagation loss, shadowing, multi-path fading and interferer strength as its components. The effect of the channel components (attenuation, shadowing and fading) is encapsulated in the form of a channel matrix H such that if X and Y be the transmitted and received signal then $Y = H.X + N + I$ where N and I are the noise and interference vectors respectively. Preamble and pilot tone based techniques can be used to estimate the channel matrix H in RF systems [94]. From an estimate of H ($\hat{H}$) one can solve for the estimated transmitted symbols $\hat{X}$. Moreover $\hat{H}$ can also be used to calculate the effective signal strength (or effective path loss (PL)). Modern radio front-ends already have sophisticated sensors/circuits [95] and baseband algorithms built-in to evaluate the magnitude of channel impairments like effective path loss and interferer strength. Two such widely-used metric is Received Signal Strength Indicator (RSSI) and Received Channel Power Indicator (RCPI), which gives an estimate of the in-channel power received and hence the total attenuation from the channel. The key difference between the two is that while RSSI calculates signal strength over the preamble (and hence uses $\hat{H}$), RCPI calculates signal strength over the entire frame and is thus more accurate. [68] discusses a method of detecting the power of in-band interferers. This is done by sensing the total in-band power by using a power detector between the

mixer and the channel-select filter. [69] discusses the design of a wide-band jammer detector which can be used to sense the total power received at the receiver. Thus combining both the outputs of interferer power detectors one can get the idea about the total interferer power at the input of the LNA.

To summarize, a combination of both RSSI/RCPI and interferer strength estimation enables the system to estimate the quality of the channel. Since modern front-ends already implement such sensors and metrics, the proposed methodology will not consume additional power or silicon area over existing infrastructure.

Memory requirement: The proposed methodology requires on-chip memory to store the EXP buffer (Figure 76) and the table of nominal knob settings. As explained earlier, that the vector F is *two* dimensional and let us assume that each quantity is quantified by a byte of data. Let us also assume that there be a total of *ten* tuning knobs (say) in the RF front-end. Also let us assume that the buffer can store the results of 500 EXP packet experimentation data (buffer is wiped clean after each UPDATE phase). Then the memory requirement for the buffer is approximately of the order of 5 kilobytes. Similarly for the optimum configuration table if the number of levels in each dimension of F be 20 with 10 tuning knobs then the total memory requirement is 4 kilobytes ($20 \times 20 \times 10 = 4000$ bytes). For the on-chip cluster table assuming the maximum number of clusters to be 100, the total memory required is 400 bytes (storing center, radius and count). Thus, the combined on-chip memory requirement is less than 10 kilobytes.

Neural network implementation: The neural network required for learning the power and performance of the front-end can be implemented as a software application on the general purpose processor in the mobile device. Modern mobile devices have extremely capable processors which can easily handle the neural network implementation. Since this is a software application which runs when the system is charging and not being used it contributes very little to the overall system overhead, both in

terms of throughput and power consumption. Moreover even this small overhead reduces to zero once the training is complete.

The neural network is implemented as a multi-layer feed-forward (MLF) neural network [96]. The network consists of neurons which are ordered into layers. The first layer and the last layer are known as the input and output layers respectively. Between these layers, there are additional layers known as hidden layers. Figure 85 shows the structure of a MLF neural network with *two* hidden layers. In this illustration there are n inputs with $d1$ and $d2$ being the number of neurons in the *two* hidden layers. The $i-$th neuron in one layer is connected to the $j-th$ neuron in the next layer by the weight $w(i,j)$. Here the vector M_k is the input to the $k-th$ layer. As shown in the figure, the inputs of a layer k $(k = 1, 2, 3)$ are weighted and combined using the weight matrix w_k (a 2-dimensional matrix containing the elements $w(i,j)$) and bias values (b_k) are added to it. The sum is then passed through a transfer function f_k to obtain the input of the next layer (M_{k+1}). Thus from the above description:

$$M_{k+1} = f_k\ (M_k.w_k + b_k)\ , k = 1, 2, 3 \tag{58}$$

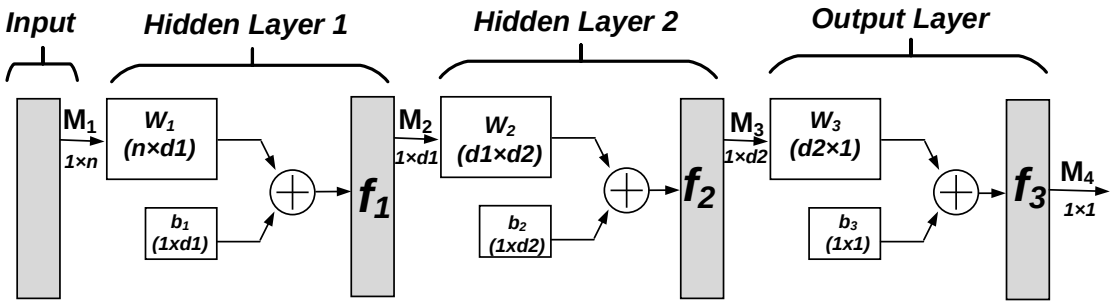

Figure 85: MLF neural network with 2 hidden layers.

The overhead and speed of prediction using the neural network is discussed in section [5.8].

Throughput overhead: As discussed in Section 5.5, during the EXPLORE state

system is not actively communicating data. Since the system is idle (more likely) then there is no effect of the incorporation of EXP packets on throughput.

Power overhead: For the ADAPT state, the battery is charging and hence there is no significant effect on the battery charge. For the EXPLORE state a small power overhead will be present due to the extra EXP packets the front-end has to process over and above the data packets. However this can be made a small number (implementation specific). For our implementation we assume a 10% overhead in power consumption during EXPLORE state. However once the optimization is complete this overhead reduces to zero since no more EXP packets are required.

EVM calculation: To calculate EVM with high confidence the calculation must be performed over a sufficient number of OFDM symbols. An EVM calculation over a small number of OFDM symbols has a large uncertainty as shown in Figure 86. Let, Δ is the guardband to deal with the uncertainty in EVM calculation. Then:

$$EVM_{th,actual} = EVM_{th} - \Delta \tag{59}$$

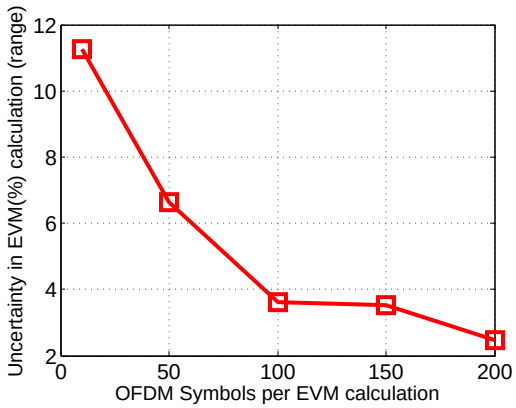

Figure 86: Variation of uncertainty in EVM with the number of OFDM symbols used for EVM= 33%.

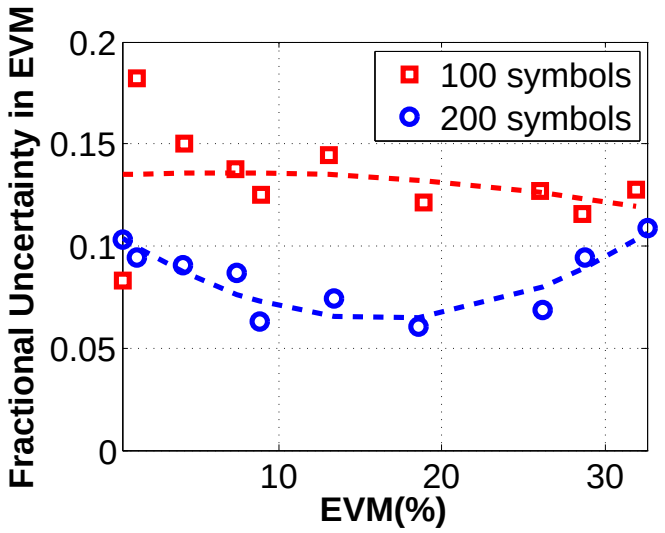

Figure 87: Fractional uncertainty in EVM across a range of EVM values.

So the system must be designed to have a larger guardband around the threshold for a smaller number of OFDM symbols per EVM calculation. Therefore, this would mean lesser power savings as the $EVM_{th,actual}$ is lower than EVM_{th}. The uncertainty in EVM as a fraction of the actual EVM remains relatively constant across the entire range of EVM as shown in Figure 87 . For our system we assume a guardband of 2% on the EVM_{th} of 35% (QPSK modulation with BER of 10^{-4}).

5.8 Simulation setup and results

5.8.1 MIMO Front-end

a) RF front-end: In order to demonstrate the efficacy of the proposed methodology, we use a 2.4 GHz MIMO OFDM front-end (Figure 88) as a test vehicle. Each chain contains a tunable LNA with a bias voltage and supply which can be used as tuning knobs. Figure 89 shows the schematic and gain of the 2 LNAs in the 2 RF chains across a range of V_{bias} (V_{b_cs}) for $V_{dd} = 1.8V$. A Gilbert cell mixer provides tunability through adaptive bias settings. Through Monte Carlo simulations process variant instances of LNA and mixer are generated for each of the two chains. The circuits

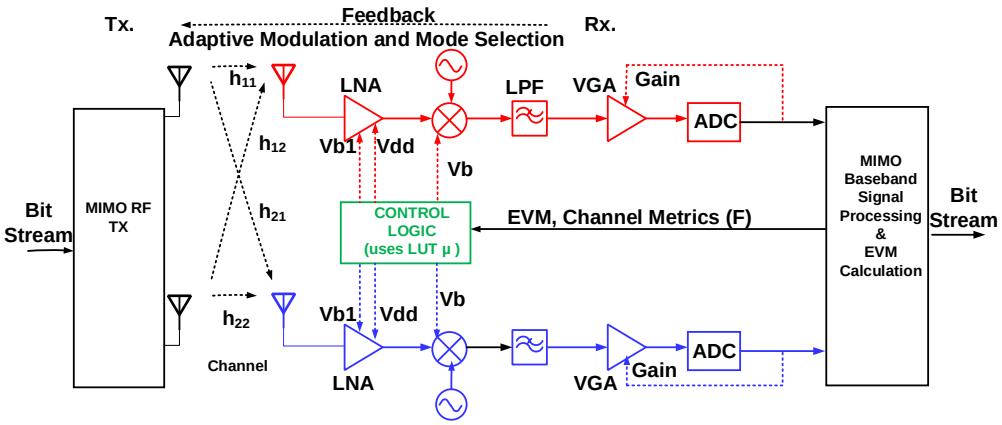

Figure 88: Process dependent adaptation of MIMO front-end.

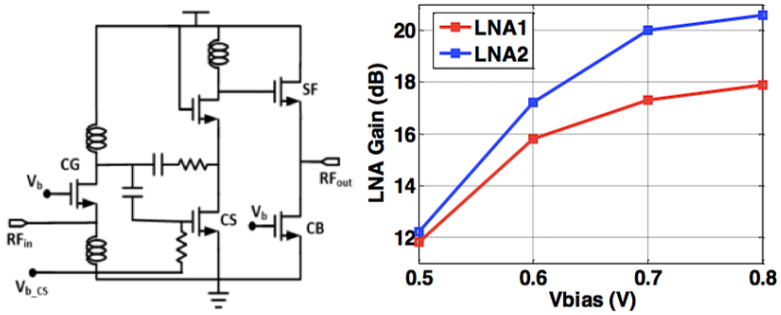

Figure 89: LNA Schematic and LNA Gain (in dB) in the 2 RF chains for V_{DD} =1.8V.

are designed in ADS and their behavioral models are used in MATLAB for complete system simulation.

b) Channel Model: The channel is modeled as a non-line- of-sight (NLOS) Rayleigh fading channel with interferers. The modulation used is QPSK with an EVMth,actual of 33%. The interferers are modeled as adjacent OFDM channels. The channel factors that lead to reconfiguration of the front-end are path loss (PL) (and hence signal strength) and interferer strength (I_0). In the setup, we assume that PL can vary between 100 dB to 147 dB and I_0 is between $-40dBm$ and $-55dBm$. Any lower interferer does not significantly affect the circuit EVM performance.

c) Neural network: The complexity of the neural network determines to a large extent the uncertainty in EVM prediction from the neural net model. In Figure 90

we show the uncertainty in prediction of EVM as a function of the number of hidden layers and the number of neurons per layer. However more complex the network is, the more memory it requires and the more number of operations are required for calculating the output from the neural network for a particular input. For a neural network with h hidden layers with d_i being the number of neurons in the i^{th} hidden layer the total number of weights and biases which are needed to be stored in memory is given by:

$$Memory\ required = \sum_{i=0}^{h} [d_i.d_{i+1} + d_{i+1}] \tag{60}$$

Here d_0 and d_{h+1} correspond to the number of inputs and output $(= 1)$ to the neural network. Figure 91 shows the total combined number of weights and bias values needed to be stored for a MLF neural network as a function of the number of hidden layers and the number of neurons in each layer.

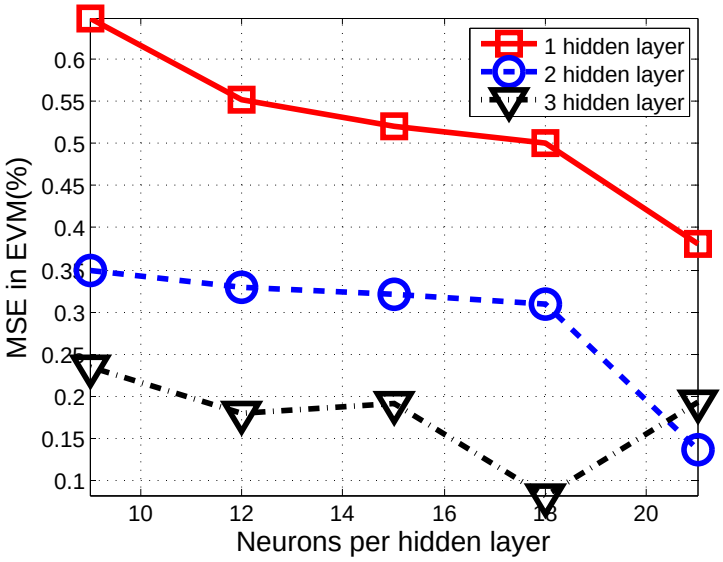

Figure 90: Variation in MSE (of EVM prediction) with neural net complexity.

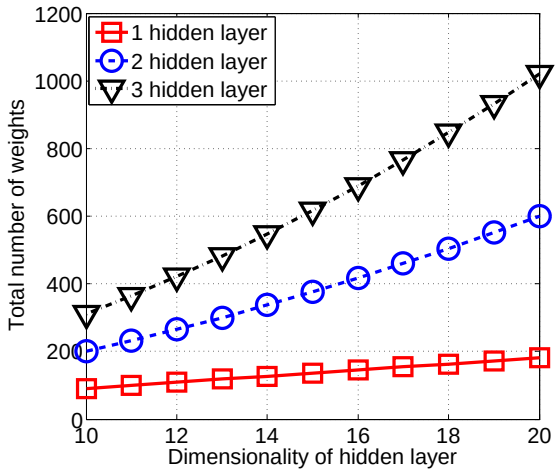

Figure 91: Total number of weights needed to be stored.

Similarly, the speed of output computation of a neural network also decreases with increasing complexity of the neural network. The speed of computation is critical both for faster training as well as a faster prediction capability of the neural network. It can be shown that for the MLF neural- network with h hidden layers the total time taken is given by:

$$Total\ time = \sum_{i=0}^{h} [d_i.d_{i+1} + d_{i+1}.(t_{mult} + t_{add}) + t_{i+1}] \tag{61}$$

Here t_{mult}, t_{add} and t_i are the time taken to execute a multiplication, addition and pass through the i^{th} transfer function (f_i). To estimate the speed of computation we assume a processor of 1 GHz clock frequency. We also assume that in latest processors each floating point multiplication takes 5 clock cycles , each addition takes 3 clock cycles [97] and each pass through the transfer function takes 10 clock cycles (conservative estimate).With this reference processor the time taken for 1 computation is calculated for different neural network topologies as shown in Figure 92.

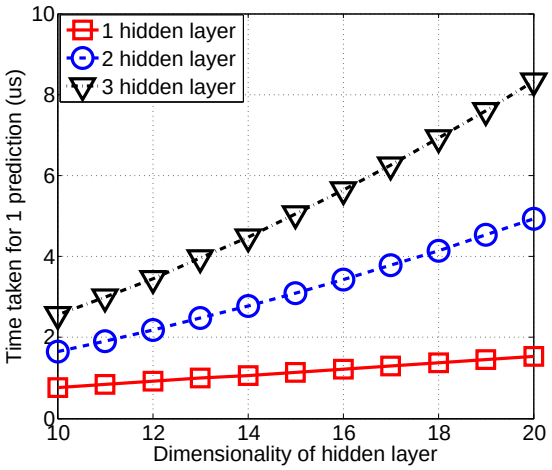

Figure 92: Time taken for single prediction for different neural net configurations.

In our system the weights are stored in a file on the Random access memory (RAM) of the general purpose processor. The number of weights is small and not a bottleneck in modern systems. However since the speed of computation affects both training and prediction, in our system we try to achieve a balance between accuracy and speed. From this study, we found that the neural nets NN_{1a} and NN_{1b} shown in Figure 81 can be best represented by neural networks with 2 hidden layers with 15 neurons in each hidden layer. With such a configuration, the neural net NN_{1a} can produce one output every 3μs.This results in a throughput of more than 300,000 outputs per second. Thus such a neural network will lead to rapid learning and prediction.

d) Simulation results: In order to demonstrate how the set of optimum tuning knob combinations for different channel conditions builds up over time, we would like to illustrate the state of the system at an intermediate time t_{int}. For generating the cluster table using ECM, we need to set the maximum radius of the clusters. For our system we chose a cluster radius of 0.1(normalized over the range of the PL and I_0). The system, at the intermediate time t_{int}, has experienced only a partial set of channel-conditions amongst the totality of channel-conditions possible. The cluster

table tracks this information by storing the cluster centers, radii and effective no. of experiments in each cluster. This cluster table is shown graphically in Figure 93 and maps out the region of the entire channel space already experienced by the front-end. Here, each cluster is represented by a circle with a marked center. This cluster table is used by the system in association with the partially trained neural nets to generate optimum configuration settings for the clustered set of channel conditions. The optimum power consumption thus obtained is shown in Figure 94.

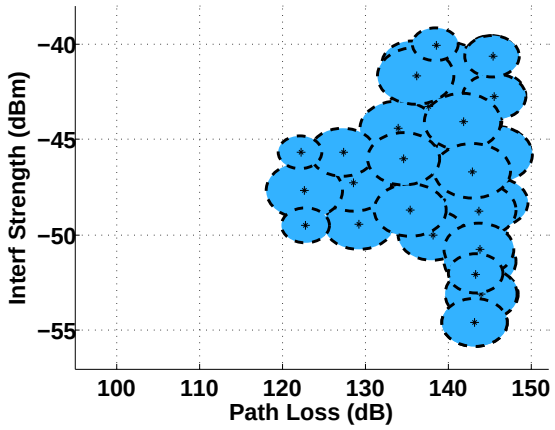

Figure 93: Clusters formed at time t_{int}.

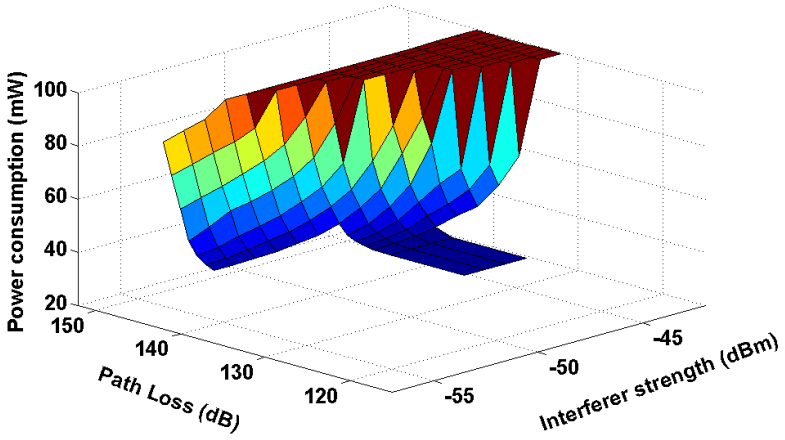

Figure 94: Partially complete optimized power surface at t_{int}.

As is evident, the optimization is partially complete at t_{int}. For channel conditions outside the current set of clusters, the system operates at maximum power consumption (i.e. nominal knob setting). This methodology runs iteratively and after sufficiently time, it can optimize the system performance over the entire channel space. In Figure 95, we see that the cluster circles finally cover the entire channel condition space. The power is also optimized over the entire channel condition space as shown in Figure 96. Here, the red mesh corresponds to the power consumption in a non-adaptive system. We get a maximum power saving of 2.5× over a non-adaptive system.

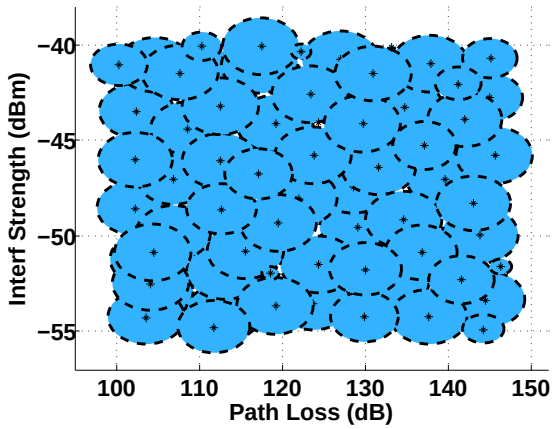

Figure 95: Clusters covering entire channel-space.

Figure97 shows how the number of clusters increases over the number of EXP packets received and the radius of the largest cluster increases to a predefined maximum and then becomes constant. To illustrate the performance of the proposed technique we illustrate in Figure 98 the average power consumption (across the entire gamut of channel conditions) as a function of time. As shown in the figure, there is a 10% overhead due to the presence of the EXP packet required by the technique. As time proceeds progressively optimum tuning knobs are discovered for larger subspaces in the F space and hence the average power consumption (across the gamut of

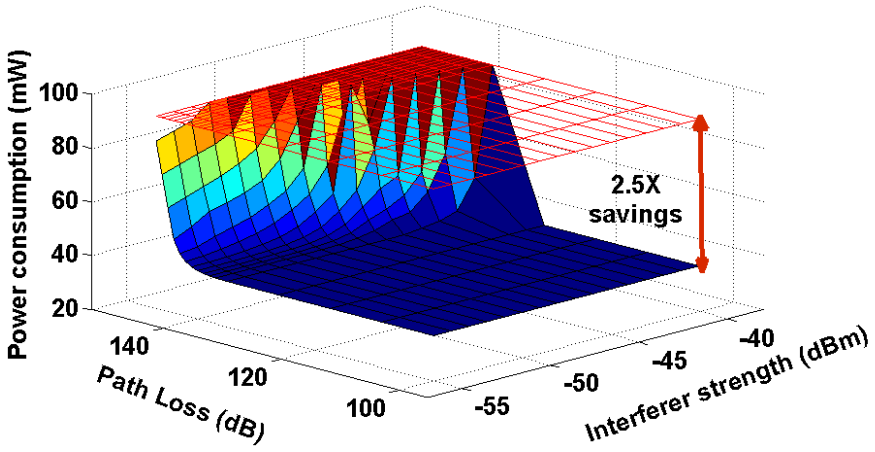

Figure 96: Completely optimized power consumption surface.

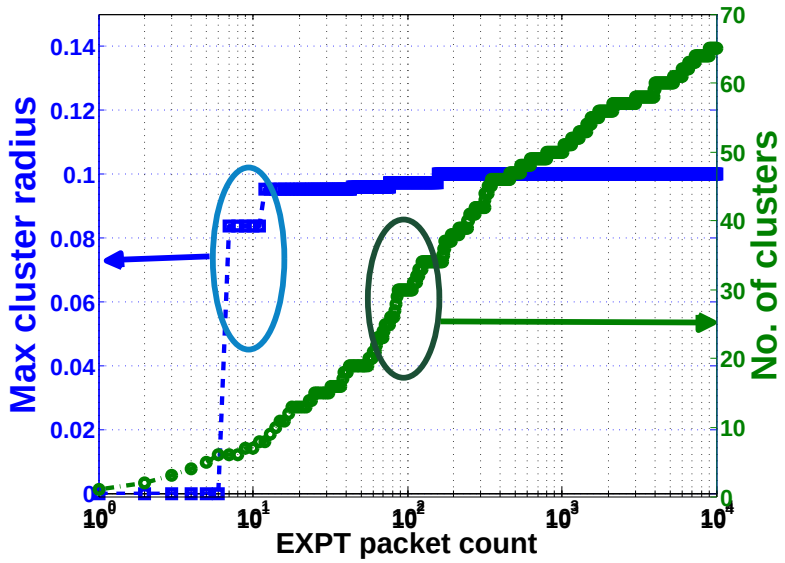

Figure 97: Cluster statistics as a function of the number of EXP packets encountered.

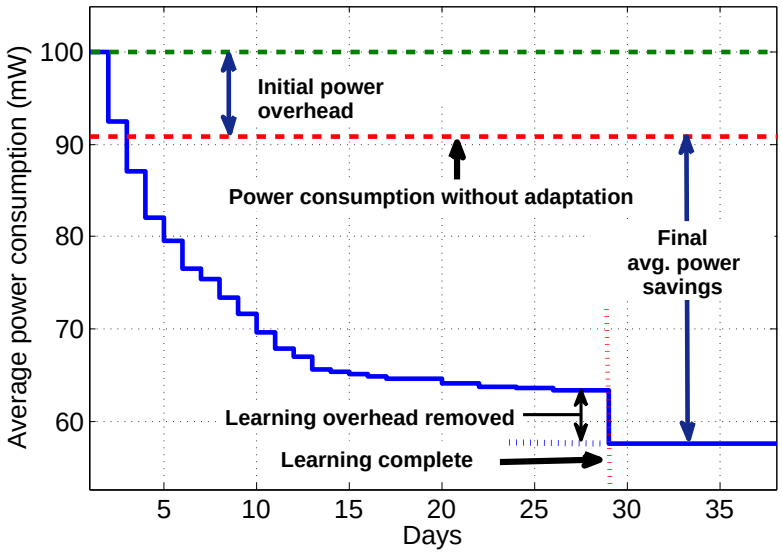

Figure 98: Progressive reduction of average power consumption with time.

channel conditions decreases). When the optimization is complete across the entire channel space, the EXP packet is no longer required and can be switched off at the protocol level. This causes a further savings in average power consumption (10%) due to reduction in protocol overhead. In this particular experiment we have assumed a very slow rate of learning and adaptation. In practice the adaptation rate depends on the usage and is expected to be significantly faster (converging within a few days).

5.8.2 SISO Front-end

A SISO front-end with tunable LNA and mixer is setup to act as a test vehicle for the proposed methodology. The LNA used in the front-end is an orthogonally tunable LNA [35] shown in Figure 99.

The LNA is a 2−stage device with 2 bias knobs, V_{GAIN} and V_{IIP3} that are used to modulate the performance and power- consumption of the LNA. The current consumption variation of the LNA across tuning knobs is shown in Figure 100. The mixer used in the simulation setup is a Gilbert cell mixer with V_{BIAS} and V_{DD} tuning knobs as shown in Figure 101.

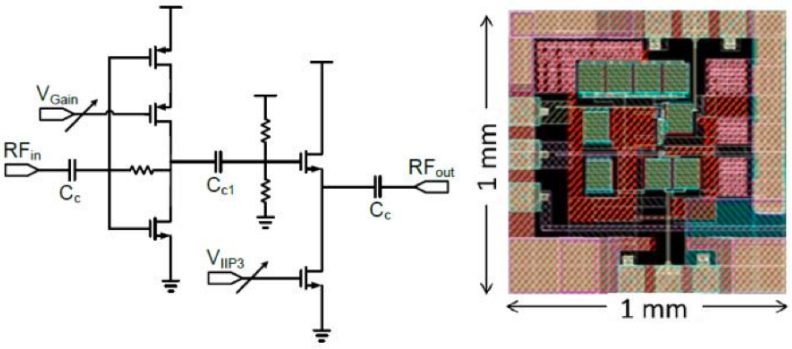

Figure 99: Orthogonally tunable LNA schematic and layout.

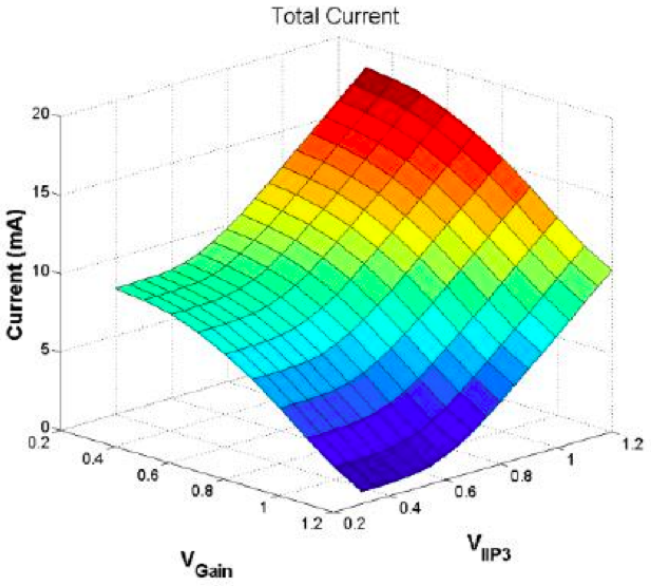

Figure 100: Current consumption of the LNA across tuning knob values.

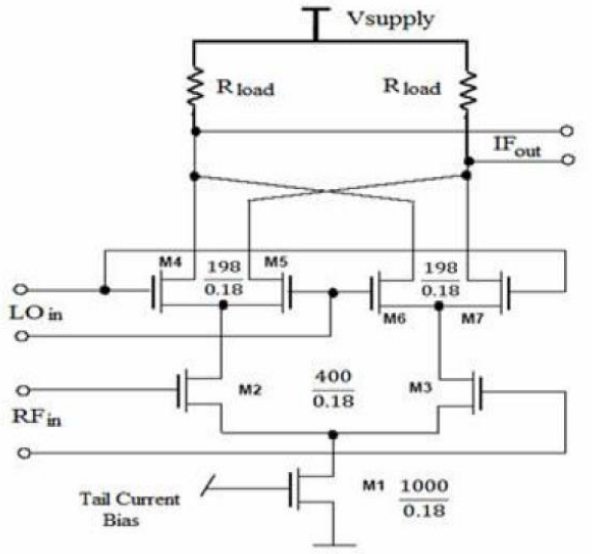

Figure 101: Mixer circuit used in simulation setup.

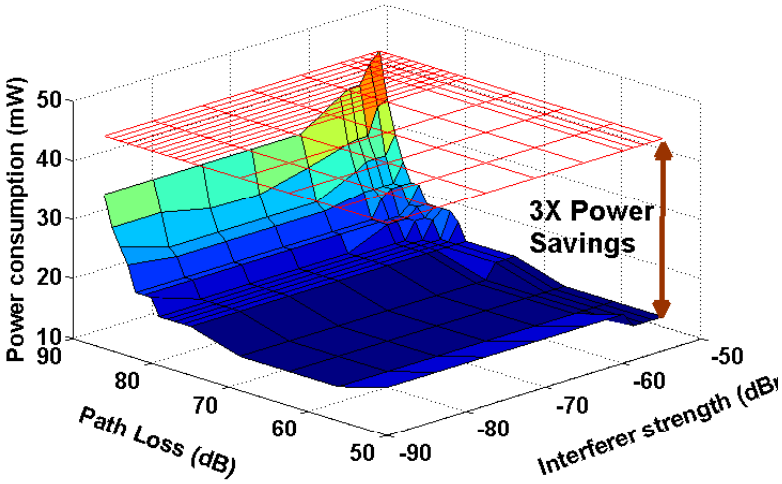

Figure 102: Power consumption across channel conditions for SISO setup.

The power is also optimized over the entire channel condition space as shown in Figure 102. Here, the red mesh corresponds to the power consumption in a non-adaptive system. Thus we get a maximum savings of 3× power consumption through process resilient learning based adaptation.

5.9 Artificial neural net training

The methodology presented in this work relies on artificial neural networks (ANN) to construct the functions f and g (discussed in Section 5.3) in software. These functions are then used to find optimum tuning knob configurations for the mapped channel space F_{sub}. The ANNs are trained using experiment data from the EXP phase. This is done during the MAP phase of operation using supervised learning. The algorithm used to train the ANNs is Levenberg-Marquardt backpropagation [98]. This is an iterative algorithm which adjusts the weights in an ANN to achieve the minimum mean square error (MSE) possible. The performance of the algorithm for the *two* neural networks in Figure 81 is shown in Figure 103. The input dimensionality of NN_{1a} (Figure 81) is less than that of NN_{1b}. Moreover EVM is a much more sharply changing function across the $\{F, T\}$ space compared to P_{DC}. Hence, EVM has a higher (but satisfactory) mean square error as compared to P_{DC}. It may be noted that depending on the dimensionality of the problem and the accuracy required, a more complicated neural network may be chosen to represent the functions f and g.

5.10 Hardware validation

The key contribution of this work is the self-learning methodology presented in earlier sections. In order to validate the proposed methodology, we used the hardware setup shown in Figure 104. Although this hardware setup is demonstrates the methodology on a SISO chain, it can be extended without any modifications to a MIMO front-end. Here, the receiver consists of a down-conversion mixer (ADL 5801) with V_{DD} and V_{BIAS} as tunable knobs. The baseband of the system is implemented in MATLAB

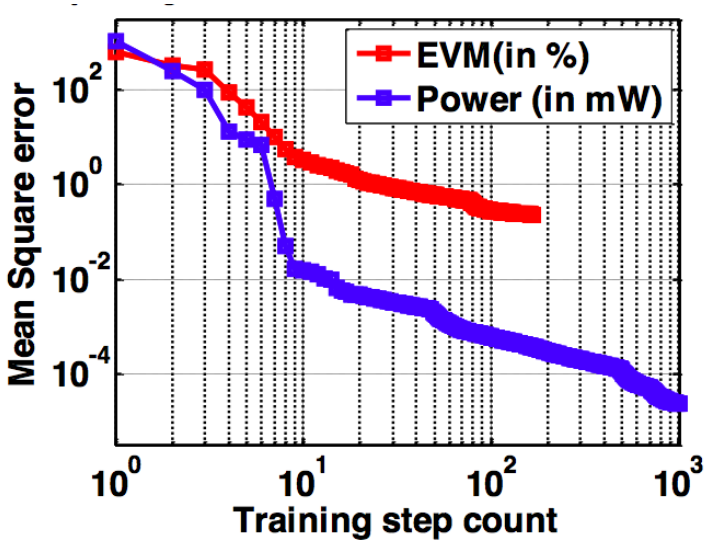

Figure 103: Mean Square Error across training iterations for Power and EVM.

working on a PC. The baseband output of NI DAC (PXI 5412) is upconverted by an upconversion mixer (MAX 2039) and fed to ADL 5801. Figure 105 shows the power profile of the down-conversion mixer ADL5801 across the tuning knobs V_{DD} and V_{BIAS}.

The system is operated at 2 GHz using OFDM modulated data. The channel emulation is done in baseband by adding different amounts of noise to the received signals. A higher amount of noise corresponds to a worse channel.

Using the methodology developed in this work, the system self-learns its characteristics and over time and constructs a table of optimum tuning knob combinations across varying channel conditions. The power consumption across different channel conditions is shown in Figure 106. The different settings of V_{BIAS} and V_{DD} across different channel conditions are shown in Figure 107. We get 3× power savings across varying channel conditions leading to low-power operation.

5.11 Summary

In this work, we have presented a methodology which enables the system to incrementally learn its power consumption characteristics and QoS performance across

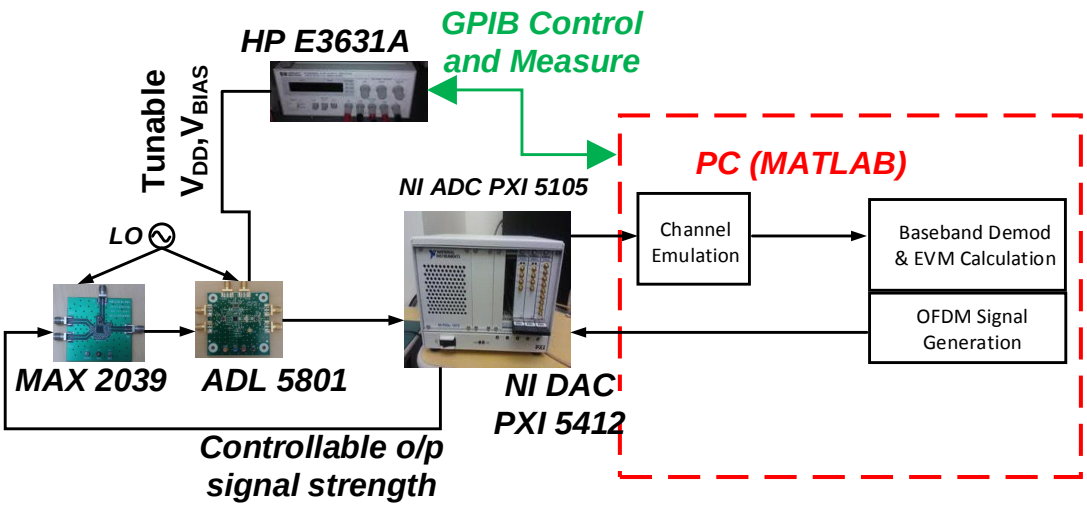

Figure 104: Hardware validation setup schematic.

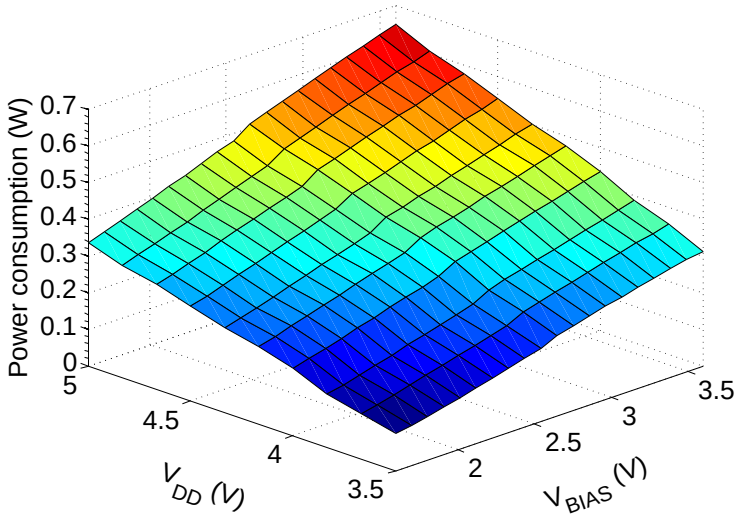

Figure 105: Power profile of ADL 5801 down-conversion mixer across tuning knobs V_{DD} and V_{BIAS}.

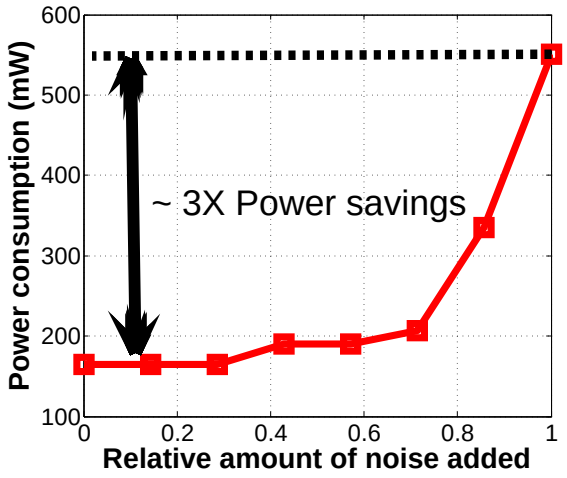

Figure 106: Power consumption across different channels.

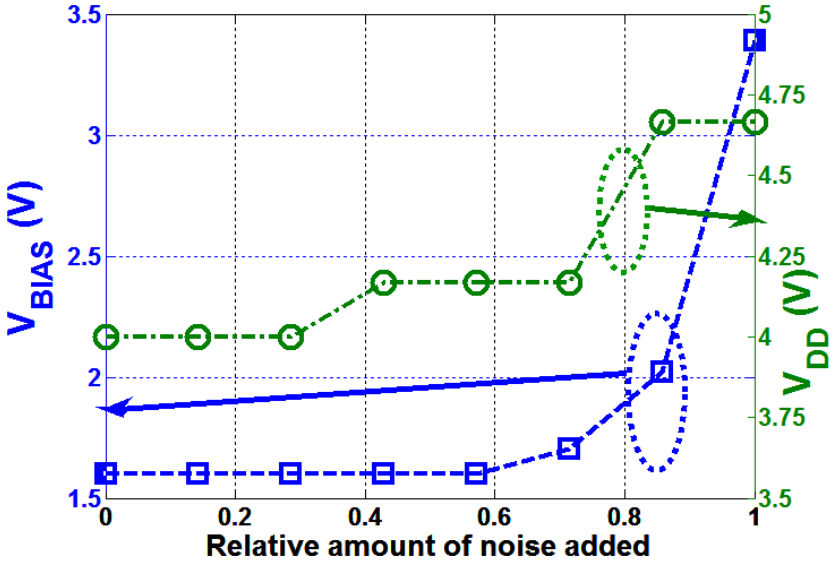

Figure 107: Tuning knob settings across different channels.

different channel and knob configurations. Thereby, the methodology consolidates this knowledge through a neural network and cluster table implemented in software. The trained neural network can then be used in conjunction with the cluster table to generate an optimum reconfiguration strategy on-the-fly. Unlike prior literature, this methodology is inherently process resilient (without the need for process detection and characterization) as it finds the optimum configuration for the device on which it operates. This may be particularly useful for low-power RF systems where the combinations number of process and tuning knob variables may be too high for feasible design phase optimization. Thus, this methodology leads to channel-adaptive process-resilient low-power RF front-ends which are crucial to the success of modern low-power portable devices.

CHAPTER 6

CONCLUSION AND FUTURE WORK

6.1 Conclusion

A key goal in modern wireless system design is to enable the longest operation of the portable communication terminal on a limited amount of battery capacity. This has lead to a significant emphasis on the design of ultra low-power communication systems. Several techniques have been explored to design low-power power wireless systems including protocol level techniques, digital baseband low-power design and low-power RF front-end circuit design. However wireless front-ends are still designed for worst case channel conditions and thus consume more power than required for most of their operational period. Prior work has demonstrated that channel adaptive wireless front-ends can consume significantly reduced power on an average. Prior work has also demonstrated that the reconfiguration settings for the wireless front-end across channel conditions are dependent on the process corner. Hence process dependent adaptation is a key to optimum adaptation across channel conditions. Although prior work has proposed the concept of channel adaptive RF front-ends, several key challenges regarding the implementation of such systems have remained unaddressed so far. This thesis explores the concept of channel adaptive systems in detail and attempts to solve the issues to make practical implementation of such systems feasible.

The techniques presented in prior literature have dealt with LUT based adaptation techniques. LUT based feedback control proposed in prior literature have been demonstrated for uni-dimensional channels. Such adaptation control cannot accommodate multiple independently varying channel parameters. Another drawback of the

LUT based technique is that it requires significant design time computation based on approximate models of the transceiver and channels. Chapter 2 presents a Fuzzy logic and analytical expression based adaptation technique which does not require a pre-computed channel vs tuning knob table while adapting to multiple channel parameters like received signal strength and interferer strength. The Fuzzy logic based adaptation technique mimics an intelligent being who can take decisions based on the current tuning knob combinations, channel conditions and the current EVM. It employs a set of heuristics to determine the dynamics of the systems. The chapter presents a formulation in which proportional control is implemented. However alternate proportional-integral(PI) and proportional-integral-derivative(PID) formulations may be possible. The concept of non-LUT based adaptation is taken a step ahead by attempting to predict the optimum tuning knob settings as a function of channel conditions analytically. Using analytical expressions the performance of the front-end to circuit level parameters to find the optimum tuning knob combinations.

In Chapter 3 the concept of use-aware adaptive RF front-ends is introduced. Traditionally the channel adaptive systems have tried to optimize power consumption while operating at the highest throughput possible for the given channel conditions. However this work demonstrates that when throughput is not the highest priority the adaptation configurations can be tailored to optimize the energy-per-bit. Thus the adaptive system can operate in two possible modes: (i) Data Priority(DP) and (ii) Energy Priority(EP) mode. While DP ensures highest throughput operation (also minimizing power consumption), EP ensures lowest energy-per-bit operation. This results is a trade-off, DP cannot ensure lowest energy-per-bit while EP does not necessarily ensure highest throughput. The benefits and trade-offs are demonstrated for MIMO transmitter and receiver in simulation. Moreover, prior work has not been done while taking into account channel coding for error resilience. The simulation

results presented show the power savings in presence of different MIMO modes, channel coding and modulation techniques. Finally the results are corroborated with the help of hardware demonstration.

In Chapter 4 and 5, the issue of process dependent adaptation is discussed and 2 different techniques are provided to tackle the issue. Firstly, Chapter 4 demonstrates a Simulated Annealing(SA) based learning technique for process aware adaptation. In this technique, the system starts with a table containing the reconfiguration settings for the front-end at nominal process. Over time the system performs perturbations of the nominal settings and records the performance to find the settings optimal for the actual front-end (which might not be at the nominal process corner). Thus over time the system learns better tuning knob settings settings and thus over time the power consumption slowly approaches the optimal power consumption. However there are a few drawbacks of this technique. Firstly, since it starts from a settings corresponding to the nominal process corner, for some devices the quality of service metric would be below the minimum acceptable value. Secondly, the simulated annealing based process adaptation may take a long time to converge and needs to be speeded up. Both of these issues are tackled in Chapter 5 where a better neural network based self-learning technique is proposed. In this technique the system starts off from the highest performance tuning knob combination at the start of its real-time operation, thereby guaranteeing quality of service. Thereafter the device performs random experiments over time and records the results of these experiments in an on-chip buffer. During the time when the device is charging the device can use this stored data to train neural nets to build a map of the performance (EVM) and power consumption (P_{DC}) across tuning knobs and channel conditions. This map is built up incrementally over time. Evolving Clustering Method(ECM) is used to track the region in channel-tuning knob space for which the system has been well-trained. Periodically the neural networks are used to find the optimum tuning knobs for the region in channel space which has

been sufficiently explored. It is shown that this leads to much faster training than the simulated annealing. The technique is demonstrated for MIMO and SISO receiver in simulation. It is also demonstrated in hardware.

To summarize, the key contributions of the thesis are as follows:

1. The thesis introduces non-LUT based control strategies for adaptive low-power front-end operation including Fuzzy logic based control and equation based predictive control.

2. The thesis proposes two low-power adaptation modes with their corresponding benefits and trade-offs in terms of energy-per-bit and throughput.

3. Two learning based techniques are proposed to overcome the problem of process variation in lower technology nodes.

6.2 Future Work

The thesis proposes two low-power adaptation modes, each of which prioritizes either throughput or energy-per-bit. More such modes could be possible which could attempt to maintain a balance of both throughput or energy-per-bit without attempting to maximize one only. The proposed fuzzy logic control concepts in this thesis could be further extended implement proportional-integral (PD) and proportional-integral-derivative (PID) implementations of the control logic. Future work could also include an integrated circuit implementation of the proposed concepts to understand and study the performance and constraints.

REFERENCES

[1] R. Senguttuvan, S. Sen, and A. Chatterjee, "Multidimensional Adaptive Power Management for Low-Power Operation of Wireless Devices," *Circuits and Systems II: Express Briefs, IEEE Transactions on*, vol. 55, no. 9, pp. 867 –871, sept. 2008.

[2] F. Belmas, F. Hameau, and J. Fournier, "A Low Power Inductorless LNA With Double G-m Enhancement in 130 nm CMOS," *Solid-State Circuits, IEEE Journal of*, vol. 47, no. 5, pp. 1094–1103, May 2012.

[3] H. Zhang, X. Fan, and E. Sinencio, "A Low-Power, Linearized, Ultra-Wideband LNA Design Technique," *Solid-State Circuits, IEEE Journal of*, vol. 44, no. 2, pp. 320–330, Feb 2009.

[4] A. Abidi, G. Pottie, and W. Kaiser, "Power-conscious design of wireless circuits and systems," *Proceedings of the IEEE*, vol. 88, no. 10, pp. 1528 –1545, oct. 2000.

[5] B. Perumana, S. Chakraborty, C.-H. Lee, and J. Laskar, "A fully monolithic 260-uW, 1-GHz subthreshold low noise amplifier," *Microwave and Wireless Components Letters, IEEE*, vol. 15, no. 6, pp. 428 – 430, june 2005.

[6] B. Minnis, P. Moore, P. Whatmough, P. Blanken, and M. van der Heijden, "System-Efficiency Analysis of Power Amplifier Supply-Tracking Regimes in Mobile Transmitters," *Circuits and Systems I: Regular Papers, IEEE Transactions on*, vol. 56, no. 1, pp. 268–279, Jan 2009.

[7] H.-I. Pan and G. Rincon-Mora, "Asynchronous Nonlinear Power-Tracking Supply for Power Efficient Linear RF PAs," in *Communications, Circuits and Systems Proceedings, 2006 International Conference on*, vol. 4, June 2006, pp. 2531–2535.

[8] G. Hanington, P.-F. Chen, P. Asbeck, and L. Larson, "High-efficiency power amplifier using dynamic power-supply voltage for CDMA applications," *Microwave Theory and Techniques, IEEE Transactions on*, vol. 47, no. 8, pp. 1471–1476, Aug 1999.

[9] F. Wang, D. Kimball, D. Lie, P. Asbeck, and L. Larson, "A Monolithic High-Efficiency 2.4-GHz 20-dBm SiGe BiCMOS Envelope-Tracking OFDM Power Amplifier," *Solid-State Circuits, IEEE Journal of*, vol. 42, no. 6, pp. 1271–1281, June 2007.

[10] F. Wang, A. Yang, D. Kimball, L. Larson, and P. Asbeck, "Design of wide-bandwidth envelope-tracking power amplifiers for OFDM applications," *Microwave Theory and Techniques, IEEE Transactions on*, vol. 53, no. 4, pp. 1244–1255, April 2005.

[11] N. Singhal and S. Pamarti, "A Digital Envelope Combiner for Switching Power Amplifier Linearization," *Circuits and Systems II: Express Briefs, IEEE Transactions on*, vol. 57, no. 4, pp. 270–274, April 2010.

[12] A. Gil-Garcia, "Output Power-Control Loop Design for GSM Mobile Phones," *Agilent Technologies*, available at http://www.analogzone.com/hft_1206.pdf.

[13] W. Paper, "Control Loop Design for GSM mobile phone applications," *Avago Technologies*, available at http://avagotech.com/docs/AV02-2414EN.

[14] Tutorial, "GSM Power Control and Power Class," *Tutorial*, available at http://www.radio-lectronics.com/info/cellulartelecomms/gsm_technical/power-ontrol-classes-amplifier.php.

[15] P. Malla, H. Lakdawala, K. Kornegay, and K. Soumyanath, "A 28mW Spectrum-Sensing Reconfigurable 20MHz 72dB-SNR 70dB-SNDR DT $\Sigma\Delta$ ADC for 802.11n/WiMAX Receivers," in *Solid-State Circuits Conference, 2008. ISSCC 2008. Digest of Technical Papers. IEEE International*, Feb 2008, pp. 496–631.

[16] D. Gesbert, M. Shafi, D. shan Shiu, P. Smith, and A. Naguib, "From theory to practice: an overview of MIMO space-time coded wireless systems," *Selected Areas in Communications, IEEE Journal on*, vol. 21, no. 3, pp. 281 – 302, apr 2003.

[17] S. Alamouti, "A simple transmit diversity technique for wireless communications," *Selected Areas in Communications, IEEE Journal on*, vol. 16, no. 8, pp. 1451 –1458, oct 1998.

[18] A. He, S. Srikanteswara, K. K. Bae, T. Newman, J. Reed, W. Tranter, M. Sajadieh, and M. Verhelst, "Power Consumption Minimization for MIMO Systems – A Cognitive Radio Approach," *Selected Areas in Communications, IEEE Journal on*, vol. 29, no. 2, pp. 469 –479, february 2011.

[19] L. Wang and N. Shanbhag, "Low-power MIMO signal processing," *Very Large Scale Integration (VLSI) Systems, IEEE Transactions on*, vol. 11, no. 3, pp. 434 –445, june 2003.

[20] E. Kim and N. Shanbhag, "An energy-efficient multiple-input multiple-output (MIMO) detector architecture," in *Signal Processing Systems (SiPS), 2011 IEEE Workshop on*, oct. 2011, pp. 239 –244.

[21] H. Kim, C.-B. Chae, G. de Veciana, and R. Heath, "Energy-efficient adaptive MIMO systems leveraging dynamic spare capacity," in *Information Sciences and Systems, 2008. CISS 2008. 42nd Annual Conference on*, march 2008, pp. 68 –73.

[22] S. Cui, A. Goldsmith, and A. Bahai, "Energy-efficiency of MIMO and cooperative MIMO techniques in sensor networks," *Selected Areas in Communications, IEEE Journal on*, vol. 22, no. 6, pp. 1089 – 1098, aug. 2004.

[23] S. Devarakond, D. Banerjee, A. Banerjee, S. Sen, and A. Chatterjee, "Efficient system-level testing and adaptive tuning of MIMO-OFDM wireless transmitters," in *Test Symposium (ETS), 2013 18th IEEE European*, May 2013, pp. 1–6.

[24] D. Banerjee, A. Banerjee, S. Devarakond, and A. Chatterjee, "Adaptive MIMO RF systems: Post-manufacture and real-time tuning for performance maximization and power minimization," in *Circuits and Systems (MWSCAS), 2013 IEEE 56th International Midwest Symposium on*, Aug 2013, pp. 1095–1099.

[25] R. Heath and A. Paulraj, "Switching between diversity and multiplexing in MIMO systems," *Communications, IEEE Transactions on*, vol. 53, no. 6, pp. 962 – 968, june 2005.

[26] D. Ernst, S. Das, S. Lee, D. Blaauw, T. Austin, T. Mudge, N. S. Kim, and K. Flautner, "Razor: circuit-level correction of timing errors for low-power operation," *Micro, IEEE*, vol. 24, no. 6, pp. 10 –20, nov.-dec. 2004.

[27] T. Burd, T. Pering, A. Stratakos, and R. Brodersen, "A dynamic voltage scaled microprocessor system," *Solid-State Circuits, IEEE Journal of*, vol. 35, no. 11, pp. 1571 –1580, nov. 2000.

[28] A. Tasic, S.-T. Lim, W. A. Serdijn, and J. R. Long, "Design of Adaptive Multimode RF Front-End Circuits," *Solid-State Circuits, IEEE Journal of*, vol. 42, no. 2, pp. 313 –322, feb. 2007.

[29] A. Tasic, W. Serdijn, and J. Long, "Adaptive multi-standard circuits and systems for wireless communications," *Circuits and Systems Magazine, IEEE*, vol. 6, no. 1, pp. 29 – 37, quarter 2006.

[30] B. Brodersen, "Wireless systems-on-a-chip design," in *Quality Electronic Design, 2002. Proceedings. International Symposium on*, 2002, p. 221.

[31] H. Woesner, J.-P. Ebert, M. Schlager, and A. Wolisz, "Power-saving mechanisms in emerging standards for wireless LANs: the MAC level perspective," *Personal Communications, IEEE*, vol. 5, no. 3, pp. 40 –48, jun 1998.

[32] B. Debaillie, B. Bougard, G. Lenoir, G. Vandersteen, and F. Catthoor, "Energy-scalable OFDM transmitter design and control," in *Design Automation Conference, 2006 43rd ACM/IEEE*, 0-0 2006, pp. 536 –541.

[33] R. Senguttuvan, S. Sen, and A. Chatterjee, "VIZOR: Virtually zero margin adaptive RF for ultra low power wireless communication," in *Computer Design, 2007. ICCD 2007. 25th International Conference on*, oct. 2007, pp. 580 –586.

[34] R. Senguttuvan, S. Sen, and A. Chatterjee, "Concurrent Multi-Dimensional Adaptation for Low-Power Operation in Wireless Devices," in *VLSI Design, 2008. VLSID 2008. 21st International Conference on*, jan. 2008, pp. 65 –70.

[35] S. Sen, D. Banerjee, M. Verhelst, and A. Chatterjee, "A Power-Scalable Channel-Adaptive Wireless Receiver Based on Built-In Orthogonally Tunable LNA," *Circuits and Systems I: Regular Papers, IEEE Transactions on*, vol. 59, no. 5, pp. 946–957, 2012.

[36] S. Sen, R. Senguttuvan, and A. Chatterjee, "Environment-Adaptive Concurrent Companding and Bias Control for Efficient Power-Amplifier Operation," *Circuits and Systems I: Regular Papers, IEEE Transactions on*, vol. 58, no. 3, pp. 607 –618, march 2011.

[37] S. Sen, R. Senguttuvan, and A. Chatterjee, "Concurrent PAR and power amplifier adaptation for power efficient operation of WiMAX OFDM transmitters," in *Radio and Wireless Symposium, 2008 IEEE*, jan. 2008, pp. 21 –24.

[38] A. Chatterjee, D. Han, V. Natarajan, S. Devarakond, S. Sen, H. Choi, R. Senguttuvan, S. Bhattacharya, A. Goyal, D. Lee, and M. Swaminathan, "Iterative built-in testing and tuning of mixed-signal/RF systems," in *Computer Design, 2009. ICCD 2009. IEEE International Conference on*, oct. 2009, pp. 319 –326.

[39] D. Han, B. S. Kim, and A. Chatterjee, "Dsp-driven self-tuning of rf circuits for process-induced performance variability," *Very Large Scale Integration (VLSI) Systems, IEEE Transactions on*, vol. 18, no. 2, pp. 305 –314, feb. 2010.

[40] A. Banerjee, S. Sen, S. Devarakond, and A. Chatterjee, "Accurate signature driven power conscious tuning of RF systems using hierarchical performance models," in *Test Conference (ITC), 2011 IEEE International*, sept. 2011, pp. 1 –9.

[41] M. Buhler, J. Koehl, J. Bickford, J. Hibbeler, U. Schlichtmann, R. Sommer, M. Pronath, and A. Ripp, "DATE 2006 Special Session: DFM/DFY Design for Manufacturability and Yield - influence of process variations in digital, analog and mixed-signal circuit design," in *Design, Automation and Test in Europe, 2006. DATE '06. Proceedings*, vol. 1, march 2006, pp. 1 –6.

[42] D. Ghai, S. Mohanty, and E. Kougianos, "Design of Parasitic and Process-Variation Aware Nano-CMOS RF Circuits: A VCO Case Study," *Very Large Scale Integration (VLSI) Systems, IEEE Transactions on*, vol. 17, no. 9, pp. 1339 –1342, sept. 2009.

[43] R. Pratap, P. Sen, C. Davis, R. Mukhophdhyay, G. May, and J. Laskar, "Neurogenetic design centering," *Semiconductor Manufacturing, IEEE Transactions on*, vol. 19, no. 2, pp. 173 – 182, may 2006.

[44] X. Wang, B. Kenfack, E. Silva, and A. Chatterjee, "Built-In Test of Switched-Mode Power Converters: Avoiding DUT Damage Using Alternative Safe Measurements," in *Test Symposium (ATS), 2013 22nd Asian*, Nov 2013, pp. 56–61.

[45] X. Wang, K. Blanchard, S. Estella, and A. Chatterjee, "Alternative "safe" test of hysteretic power converters," in *VLSI Test Symposium (VTS), 2014 IEEE 32nd*, April 2014, pp. 1–6.

[46] X. Wang, K. Blanchard, S. Estela, and A. Chatterjee, "A self-tuning architecture for buck converters based on alternative test," in *Test Conference (ITC), 2014 IEEE International*, Oct 2014, pp. 1–10.

[47] D. Han, B. S. Kim, and A. Chatterjee, "DSP-Driven Self-Tuning of RF Circuits for Process-Induced Performance Variability," *Very Large Scale Integration (VLSI) Systems, IEEE Transactions on*, vol. 18, no. 2, pp. 305 –314, feb. 2010.

[48] T. Das and P. Mukund, "Self-calibration of gain and output match in LNAs," in *Circuits and Systems, 2006. ISCAS 2006. Proceedings. 2006 IEEE International Symposium on*, May 2006, pp. 4 pp.–4986.

[49] R. Senguttuvan and A. Chatterjee, "Alternate Diagnostic Testing and Compensation of RF Transmitter Performance Using Response Detection," in *VLSI Test Symposium, 2007. 25th IEEE*, May 2007, pp. 395–400.

[50] A. Goyal, M. Swaminathan, and A. Chatterjee, "A novel self-healing methodology for RF Amplifier circuits based on oscillation principles," in *Design, Automation Test in Europe Conference Exhibition, 2009. DATE '09.*, April 2009, pp. 1656–1661.

[51] A. Goyal, M. Swaminathan, and A. Chatterjee, "3D-ICs with self-healing capability for thermal effects in RF circuits," in *Quality Electronic Design (ISQED), 2014 15th International Symposium on*, March 2014, pp. 179–183.

[52] A. Goyal, M. Swaminathan, A. Chatterjee, D. Howard, and J. Cressler, "A New Self-Healing Methodology for RF Amplifier Circuits Based on Oscillation Principles," *Very Large Scale Integration (VLSI) Systems, IEEE Transactions on*, vol. 20, no. 10, pp. 1835–1848, Oct 2012.

[53] A. Goyal, M. Swaminathan, A. Chatterjee, D. Howard, and J. Cressler, "A self-testable SiGe LNA and Built-in-Self-Test methodology for multiple performance specifications of RF amplifiers," in *Quality Electronic Design (ISQED), 2012 13th International Symposium on*, March 2012, pp. 7–12.

[54] A. Goyal, M. Swaminathan, and A. Chatterjee, "Self-calibrating embedded rf down-conversion mixers," in *Asian Test Symposium, 2009. ATS '09.*, Nov 2009, pp. 249–254.

[55] A. Chatterjee, H. Wang, A. Banerjee, D. Banerjee, V. Natarajan, S. Sen, and S. Devarakond, "Design of self-healing mixed-signal/RF systems and support CAD tools: A scalable approach," in *Circuits and Systems (MWSCAS), 2014 IEEE 57th International Midwest Symposium on*, Aug 2014, pp. 1065–1068.

[56] T. Schenk, *RF Imperfections in High-rate Wireless Systems Impactand Digital Compensation*. Netherlands: Springer, 2008.

[57] M. Perrott, I. Tewksbury, T.L., and C. Sodini, "A 27-mW CMOS fractional-N synthesizer using digital compensation for 2.5-Mb/s GFSK modulation," *Solid-State Circuits, IEEE Journal of*, vol. 32, no. 12, pp. 2048–2060, Dec 1997.

[58] R. Staszewski, J. Wallberg, S. Rezeq, C.-M. Hung, O. Eliezer, S. Vemulapalli, C. Fernando, K. Maggio, R. Staszewski, N. Barton, M.-C. Lee, P. Cruise, M. Entezari, K. Muhammad, and D. Leipold, "All-digital PLL and transmitter for mobile phones," *Solid-State Circuits, IEEE Journal of*, vol. 40, no. 12, pp. 2469–2482, Dec 2005.

[59] S.-W. Hsiao, X. Wang, and A. Chatterjee, "Analog Sensor Based Testing of Phase-Locked Loop Dynamic Performance Parameters," in *Test Symposium (ATS), 2013 22nd Asian*, Nov 2013, pp. 50–55.

[60] P.-Y. Wang, J. Zhan, H.-H. Chang, and B.-Y. Hsieh, "An analog enhanced all digtial RF fractional-N PLL with self-calibrated capability," in *Custom Integrated Circuits Conference, 2008. CICC 2008. IEEE*, Sept 2008, pp. 749–752.

[61] S. Kim and M. Soma, "An all-digital built-in self-test for high-speed phase-locked loops," *Circuits and Systems II: Analog and Digital Signal Processing, IEEE Transactions on*, vol. 48, no. 2, pp. 141–150, Feb 2001.

[62] V. Natarajan, S. Devarakond, S. Sen, and A. Chatterjee, "BIST Driven Power Conscious Post-Manufacture Tuning of Wireless Transceiver Systems Using Hardware-Iterated Gradient Search," in *Asian Test Symposium, 2009. ATS '09.*, Nov 2009, pp. 243–248.

[63] V. Natarajan, S. Sen, S. Devarakond, and A. Chatterjee, "A holistic approach to accurate tuning of RF systems for large and small multiparameter perturbations," in *VLSI Test Symposium (VTS), 2010 28th*, April 2010, pp. 331–336.

[64] S. Sen, V. Natarajan, R. Senguttuvan, and A. Chatterjee, "Pro-VIZOR: Process tunable virtually zero margin low power adaptive RF for wireless systems," in *Design Automation Conference, 2008. DAC 2008. 45th ACM/IEEE*, june 2008, pp. 492 –497.

[65] D. Banerjee, S. Sen, A. Banerjee, and A. Chatterjee, "Low-power Adaptive RF System Design Using Real-time Fuzzy Noise-distortion Control," in *Proceedings of the 2012 ACM/IEEE International Symposium on Low Power Electronics and Design*, ser. ISLPED '12. New York, NY, USA: ACM, 2012, pp. 249–254. [Online]. Available: http://doi.acm.org/10.1145/2333660.2333719

[66] L. Zadeh, "Fuzzy Sets," *Information Control*, vol. 8, pp. 338–353, 1965.

[67] L. A. Zadeh, "Fuzzy logic and the calculus of fuzzy if-then rules," in *Multiple-Valued Logic, 1992. Proceedings., Twenty-Second International Symposium on*, May, pp. 480–.

[68] S. C. Ciccarelli, "Dynamically programmable receiver," Oct 2006. [Online]. Available: http://www.google.com/patents/US20040142670

[69] H. Muthali and S. Sen, "Wideband Jammer Detector," Sept 2010. [Online]. Available: http://www.google.com/patents/US20100245151

[70] F. Behbahani, A. Karimi-Sanjaani, W.-G. Tan, A. Roithmeier, J. Leete, K. Hoshino, and A. Abidi, "Adaptive analog IF signal processor for a wide-band CMOS wireless receiver," *Solid-State Circuits, IEEE Journal of*, vol. 36, no. 8, pp. 1205–1217, Aug 2001.

[71] D. Banerjee, S. Devarakond, S. Sen, and A. Chatterjee, "Real-time Use-aware Adaptive MIMO RF Receiver Systems for Energy Efficiency Under BER Constraints," in *Proceedings of the 50th Annual Design Automation Conference*, ser. DAC '13. New York, NY, USA: ACM, 2013, pp. 56:1–56:7. [Online]. Available: http://doi.acm.org/10.1145/2463209.2488802

[72] D. Banerjee, S. Devarakond, X. Wang, S. Sen, and A. Chatterjee, "Real-Time Use-Aware Adaptive RF Transceiver Systems for Energy Efficiency under BER Constraints," *Computer-Aided Design of Integrated Circuits and Systems, IEEE Transactions on*, vol. PP, no. 99, pp. 1–1, 2015.

[73] R. Shafik, S. Rahman, R. Islam, and N. Ashraf, "On the error vector magnitude as a performance metric and comparative analysis," in *Emerging Technologies, 2006. ICET '06. International Conference on*, Nov 2006, pp. 27–31.

[74] A. Goldsmith, *Wireless Communications*. Cambridge University Press, 2005.

[75] Y. Yasuda, K. Kashiki, and Y. Hirata, "High-Rate Punctured Convolutional Codes for Soft Decision Viterbi Decoding," *Communications, IEEE Transactions on*, vol. 32, no. 3, pp. 315–319, Mar 1984.

[76] X. Wang, H. W. Choi, T. Moon, N. Tzou, and A. Chatterjee, "Higher than Nyquist test waveform synthesis and digital phase noise injection using time-interleaved mixed-mode data converters," in *Test Conference (ITC), 2012 IEEE International*, Nov 2012, pp. 1–10.

[77] N. Tzou, T. Moon, X. Wang, H. Choi, and A. Chatterjee, "Dual-frequency incoherent subsampling driven test response acquisition of spectrally sparse wideband signals with enhanced time resolution," in *VLSI Test Symposium (VTS), 2012 IEEE 30th*, April 2012, pp. 140–145.

[78] N. Tzou, D. Bhatta, B. Muldrey, T. Moon, X. Wang, H. Choi, and A. Chatterjee, "Low Cost Sparse Multiband Signal Characterization Using Asynchronous Multi-Rate Sampling: Algorithms and Hardware," in *Journal of Electronic Testing*, Feb 2015, pp. 85–98.

[79] T. Moon, N. Tzou, X. Wang, H. Choi, and A. Chatterjee, "Low-cost high-speed pseudo-random bit sequence characterization using nonuniform periodic sampling in the presence of noise," in *VLSI Test Symposium (VTS), 2012 IEEE 30th*, April 2012, pp. 146–151.

[80] I.-W. Lai, G. Ascheid, H. Meyr, and T.-D. Chiueh, "Efficient Channel-Adaptive MIMO Detection Using Just-Acceptable Error Rate," *Wireless Communications, IEEE Transactions on*, vol. 10, no. 1, pp. 73–83, January 2011.

[81] D. Banerjee, S. Sen, A. Banerjee, and A. Chatterjee, "Low-power Adaptive RF System Design Using Real-time Fuzzy Noise-distortion Control," in *Proceedings of the 2012 ACM/IEEE International Symposium on Low Power Electronics and Design*, ser. ISLPED '12. New York, NY, USA: ACM, 2012, pp. 249–254. [Online]. Available: http://doi.acm.org/10.1145/2333660.2333719

[82] S. Kirkpatrick, C. D. Gelatt, and M. P. Vecchi, "Optimization by simulated annealing," *Science*, vol. 220, pp. 671–680, 1983.

[83] V. Černý, "Thermodynamical approach to the traveling salesman problem: An efficient simulation algorithm," *Journal of Optimization Theory and Applications*, vol. 45, no. 1, pp. 41–51, Jan. 1985. [Online]. Available: http://dx.doi.org/10.1007/bf00940812

[84] S. Yoshizawa and Y. Miyanaga, "Tunable word length architecture for low power wireless OFDM demodulator," in *Circuits and Systems, 2006. ISCAS 2006. Proceedings. 2006 IEEE International Symposium on*, May 2006, pp. 4 pp.–.

[85] K. Maharatna, E. Grass, and U. Jagdhold, "A 64-point Fourier transform chip for high-speed wireless LAN application using OFDM," *Solid-State Circuits, IEEE Journal of*, vol. 39, no. 3, pp. 484–493, March 2004.

[86] C.-S. Chen, J.-C. Lo, and T. Xia, "Equivalent IDDQ Tests for Systems with Regulated Power Supply," in *Defect and Fault Tolerance in VLSI Systems, 2006. DFT '06. 21st IEEE International Symposium on*, Oct., pp. 291–299.

[87] W. Chen, W. Che, Z. Bi, J. Wang, N. Yan, X. Tan, J. Wang, H. Min, and J. Tan, "A 1.04 μW Truly Random Number Generator for Gen2 RFID tag," in *Solid-State Circuits Conference, 2009. A-SSCC 2009. IEEE Asian*, Nov., pp. 117–120.

[88] D. Banerjee, B. Muldrey, S. Sen, X. Wang, and A. Chatterjee, "Self-learning MIMO-RF receiver systems: Process resilient real-time adaptation to channel conditions for low power operation," in *Computer-Aided Design (ICCAD), 2014 IEEE/ACM International Conference on*, Nov 2014, pp. 710–717.

[89] S. Sapatnekar, "Overcoming Variations in Nanometer-Scale Technologies," *Emerging and Selected Topics in Circuits and Systems, IEEE Journal on*, vol. 1, no. 1, pp. 5–18, March 2011.

[90] D. Banerjee, A. Banerjee, and A. Chatterjee, "Adaptive RF Front-end Design via Self-discovery: Using Real-time Data to Optimize Adaptation Control," in *VLSI Design and 2013 12th International Conference on Embedded Systems (VLSID), 2013 26th International Conference on*, Jan 2013, pp. 197–202.

[91] T. Kanungo, D. Mount, N. Netanyahu, C. Piatko, R. Silverman, and A. Wu, "An efficient k-means clustering algorithm: analysis and implementation," *Pattern Analysis and Machine Intelligence, IEEE Transactions on*, vol. 24, no. 7, pp. 881–892, Jul 2002.

[92] N. Kasabov and Q. Song, "DENFIS: Dynamic Evolving Neural-Fuzzy Inference System and its application for time-series prediction," *Fuzzy Systems, IEEE Transactions on*, vol. 10, no. 2, pp. 144–154, Apr 2002.

[93] M. Meghdadi and M. Sharif Bakhtiar, "Two-Dimensional Multi-Parameter Adaptation of Noise, Linearity, and Power Consumption in Wireless Receivers," *Circuits and Systems I: Regular Papers, IEEE Transactions on*, vol. 61, no. 8, pp. 2433–2443, Aug 2014.

[94] S. Coleri, M. Ergen, A. Puri, and A. Bahai, "Channel estimation techniques based on pilot arrangement in OFDM systems," *Broadcasting, IEEE Transactions on*, vol. 48, no. 3, pp. 223–229, Sep 2002.

[95] U. Mayer, M. Wickert, and F. Ellinger, "Design of received signal strength indicators for RF-MIMO systems," in *Ph.D. Research in Microelectronics and Electronics (PRIME), 2010 Conference on*, July 2010, pp. 1–4.

[96] D. Svozil, V. Kvasnicka, and J. Pospichal, "Introduction to multi-layer feed-forward neural networks," *Elsevier Chemometrics and Intelligent Laboratory Systems*, vol. 39, no. 1, pp. 43–62, Nov 1997.

[97] "Intel 64 and IA-32 Architectures Optimization Reference Manual," *Intel Corporation*, Mar 2014.

[98] M. Hagan and M. Menhaj, "Training feedforward networks with the Marquardt algorithm," *Neural Networks, IEEE Transactions on*, vol. 5, no. 6, pp. 989–993, Nov 1994.